J Braz. Soc. Mech. Sci. Eng. (2016) 38:1359–1399
DOI 10.1007/s40430-015-0433-2

ORIGINAL PAPER

The persistence of logarithmic solutions in turbulent boundary layer systems

Atila P. Silva Freire[1]

Received: 17 August 2015 / Accepted: 10 September 2015 / Published online: 11 October 2015

Abstract The present work studies the prevalence of logarithmic solutions in the near wall region of turbulent boundary layers. Local solutions for flows subject to such diverse effects as compressibility, wall transpiration, heat transfer, roughness, separation, shock waves, unsteadiness, non-Newtonian fluids or a combination of these factors are discussed. The work also analyzes eleven different propositions by several authors for the near wall description of the mean velocity profile for the incompressible zero-pressure-gradient turbulent boundary layer. The asymptotic structure of the flow is discussed from the point of view of double limit processes. Cases of interest include attached and separated flows for the velocity and temperature fields.

Keywords Law of the wall · Logarithmic solution · Turbulence · Boundary layer · Separation

1 Introduction

To such common fluids as air and water, the basic laws that govern fluid motion are supposed to be known. They stem from the first principles of mechanics and the formalism of a continuous field characterized by density and viscosity.

Thus, the complete absence of a comprehensive theory that can convincingly deal with disordered flows may come to many as a surprise. The crux of the matter, obviously, is the strong non-linear character of the advection terms in the equations of motion. Under certain conditions—in particular, high Reynolds numbers—fluid flows become unstable, growing rapidly to a complicated and confused state that is termed *turbulent* and has a large number of degrees of freedom.

In fact, it can be argued that an exact and detailed description of the manner in which a turbulent flow evolves is physically meaningless due to the inherent difficulty in specifying its boundary and initial conditions for situations that are of interest in practical problems. A microscopic account of the flow behavior is certainly relevant for the understanding of local and instantaneous irregularities, but what is normally of real interest is the behavior of the macroscopic regularities of the flow. Therefore, it seems that the appropriate description of a turbulent flow needs to resort to statistical methods.

Provided the irregular variation of the flow properties can be averaged over, say, some interval of time, the field properties can be decomposed into smoothed out (*mean part*) and rapidly varying quantities (*fluctuating part*). Once this procedure is accepted, substitution of the decomposed field variables into the Navier–Stokes equations results in a new equation for the mean variables, but with additional terms involving double correlations of the fluctuations, quantities that are formally unknown and that, hence, require modeling. The resulting second-order tensor—the Reynolds stress tensor—represents the transport of momentum due to the turbulent fluctuations and has the

Technical Editor: Francisco Ricardo Cunha.

The work is dedicated to Dr. Sergio Luis Villares Coelho, who would have had a brilliant professional carrier, had not departed the planet Earth in October 1989 at the very early age of 32 after a long struggle against cancer. The longer the elapsed time, the more his absence is felt.

✉ Atila P. Silva Freire
atila@mecanica.coppe.ufrj.br

[1] Programa de Engenharia Mecanica (COPPE/UFRJ), Universidade Federal do Rio de Janeiro, C.P. 68503, Rio de Janeiro 21945-970, Brazil

apparent effect of imposing an additional resistance to the flow.

The classical problem of turbulence modeling as introduced by the decomposition of the flow quantities is normally referred to in literature as the "closure problem". The reduction of the Navier–Stokes equations to a new set of equations for the prediction of the mean properties of turbulent flow was essential in the development of quantitative theories. For the least, this ingenious scheme permitted the introduction of analogies, dimensional analysis and phenomenological arguments for the construction of predictive models.

The analysis of turbulent flow has also greatly profited from limiting arguments. The general idea is to explore the properties of a governing equation or boundary and initial conditions in the limit as one or more parameters tend to a designated value, normally zero or infinity. This approach naturally divides the flow domain into characteristic regions with limiting equations that retain the important features of the problem and neglect the secondary (higher order) effects. The simplifications facilitate the development of analytical or numerical solutions and furnish valuable information on the local structure of the flow. The classical approaches consider limits of a single variable (*single limits*). However, a limit process can also be applied to problems that involve asymptotic approximations to solutions valid for small values of a variable and small values of a parameter (*double limits*).

The turbulent boundary layer is a classical problem whose treatment truly benefits from limiting and modeling arguments. For laminar flow, Prandtl had already shown in 1904 that at high Reynolds number the flow adjacent to surfaces tends to squash into layers. His heuristic arguments considered an order of magnitude analysis to formally divide the flow into "inner" and "outer" equations and introduce a method that would later be inspirational to the development of singular perturbation techniques.

Following the derivation of the boundary layer equations for laminar flow, Taylor [1], Prandtl [2] and von Karman [3, 4] further pursued the notion that the near wall flow can be structured into different layers, governed by different leading order effects. For attached flows, a linear solution was advanced for the viscous layer; the fully turbulent layer was associated to a logarithmic solution.

Early arguments for the derivation of the logarithmic solution resorted to similitude and mixing hypotheses for turbulence closure. In fact, further thoughts on the problem showed that none of these somewhat restrictive arguments were necessary. More general reasonings based on the postulate that solutions over the inner (viscous) and outer (inertial) regions must asymptotically match in an overlap domain were successfully introduced by Millikan [5]. The apparent insensitivity of the logarithmic solution to the manner of its derivation certainly played an important role on its wide acceptance among workers in fluid mechanics.

Despite the remarkable good results provided by the logarithmic solution in regard to prediction of skin-friction and mean velocity profiles, certain difficulties soon surfaced. Millikan remarked that certain "constants" appearing in the theories needed be given different values to fit the experimental observations satisfactorily. von Karman also noticed that the similitude arguments applied to a region of vanishing shearing stress would naturally break down.

Of course, an essential element in Prandtl's derivation—the mixing length concept—immediately became a particular source of criticism. Not so much for the simplicity of the formulation, some early experiments clearly realized that the turbulence at any point of the domain cannot be modeled just in terms of local properties (production and dissipation) but must consider transport processes from other parts of the flow. The exaggerated criticism on the adequacy of mixing length theories was disputed by Townsend [6], who argued that near a rigid wall the balance of turbulent kinetic energy is virtually unaffected by the flow in the adjacent regions.

The objective of the present work is not to praise or condemn the logarithmic solution for fully turbulent boundary layer flows, or the arguments that led to its derivation. Rather, we show how the simple set of arguments introduced by Taylor, Prandtl, von Karman and Millikan based on similitude, mixing theories and limit processes can be used to find useful approximate solutions to very intricate problems. Instances that include compressibility, wall transpiration, heat transfer, roughness, shock wave interaction, separation and non-Newtonian fluids are all discussed. In particular, the developments indicate the prevalence of logarithmic solutions to all discussed cases in a characteristic near wall region where turbulent effects can be considered the dominant effects. Irrespective of the flow complexity, the work shows that adequate mathematical transformations can be defined to reduce the mean velocity profiles to logarithmic solutions.

For flows near to a separation point, the logarithmic solution has been shown by Stratford [7] to reduce to a power-law solution of the type $y^{1/2}$. In the context of the above statement, it is demonstrated that a general local solution can be obtained which under the appropriate limit process tends to the logarithmic solution on one side and to the $y^{1/2}$-solution on the other.

Wall functions have been used to test new theories, calibrate measuring instruments and validate numerical schemes, having become one of the great paradigms of turbulence theory. In particular, they have been a great relief to the numerical computation of turbulent flows. As pointed out by Launder and Spalding [8], they are economic in terms of computer time and storage and can be often

specialized to account for different physical effects. Alternative formulations, notably low Reynolds number models have been proposed. However, this latter approach usually requires dense computational grids and introduces additional non-linearity and numerical stiffness. The enduring usefulness of wall-function methods has been illustrated in the recent works of Craft el at. [9] and Popovac and Hanjalic [10]. One difficulty with wall-function methods is the introduction of the wall boundary condition explicitly, which naturally results in numerical instability. This drawback can be solved with the introduction of unconditionally unstable numerical procedures. This is a common problem that is rarely discussed in literature, but is given a detailed treatment in Fontoura Rodrigues et al. [11].

Here, some early expressions proposed for the description of the mean velocity behavior in the near wall region are discussed in a separate section. The lack of a unique approach means that some of the proposed equations can be more effective than others to some particular conditions and that, in particular, they differ in simplicity of formulation, the extent of phenomenological domain covered and esthetic form. Two sets of experimental data were selected for theory validation, the data presented in Andersen et al. [12] and Purtell et al. [13].

The arguments invoked by Millikan [5] are also shortly revisited in a separate section, but given a different development so that a new insight into the derivation of the log-law is introduced and the skin-friction equation follows from differentiating arguments.

The asymptotic structure of the turbulent boundary layer is discussed through the rationale introduced by Yajnik [14]. Deliberately avoiding similarity, dimensional or modeling arguments, Yajnik used matched asymptotic expansions to demonstrate that the unclosed Reynolds equations lead to a double-layered structure. Here, we show that the application of limit processes directly to the equations rather than to the anticipated solutions results in a different interpretation of the flow structure. The new explanation is consistent with some elements of the work of Sychev and Sychev [15].

2 Equations of motion

The equations of motion are here introduced for the sake of completeness. In the following developments, any differences observed in notation are particularly highlighted.

In turbulent flows, the parameters in the Navier–Stokes equations are decomposed into mean and fluctuating quantities. The continuity, momentum and energy equations obtained through *mass-weighted-averaging* can be written in the following form (Cebeci and Smith [16]):

(a) Continuity

$$\partial_t \bar{\rho} + \partial_i(\bar{\rho}\tilde{u}_i) = 0 \tag{1}$$

(b) Momentum

$$\partial_t(\bar{\rho}\tilde{u}_i) + \partial_j(\bar{\rho}\tilde{u}_j\tilde{u}_i) = -\partial_i\bar{p} + \partial_j(-\overline{\rho u_i' u_j'} + \overline{\tau_{ij}}) \tag{2}$$

(c) Energy

$$\partial_t(\bar{\rho}\tilde{H}) + \partial_j(\bar{\rho}\tilde{u}_j\tilde{H}) = \partial_t\bar{p} + +\partial_j(-\bar{q}_j - \overline{\rho u_j' H'} + \tilde{u}_i\overline{\tau_{ij}} + \overline{u_i'\tau_{ij}}) \tag{3}$$

where the stress tensor and the heat flux tensor are given, respectively, by

$$\tau_{ij} = \lambda\delta_{ij}\partial_k u_k + \mu(\partial_j u_i + \partial_i u_j) \tag{4}$$

and

$$q_j = K\partial_j T \tag{5}$$

and the total enthalpy by

$$H = h + \frac{u_i u_i}{2} \tag{6}$$

In the above equations, x_i, u_i, p, ρ, h and H have their classical meaning, λ is the bulk viscosity ($=-(2/3)\mu$), μ the dynamic viscosity, K the thermal conductivity and δ_{ij} the Kronecker delta operator. The tilde denotes mass-weighted averaging and the over line conventional time averaging; fluctuations are denoted with the dashes.

3 The law of the wall

In the early arguments, the flow in the wall layer was postulated to depend on the wall shear stress τ_w, on the distance y to the wall, on a roughness parameter k_s, and on the fluid properties ρ and μ. Then, from dimensional considerations, it follows that the functional dependence of the mean velocity u (in the following, an over line is omitted to represent a mean quantity) on the flow parameters can be expressed as

$$\frac{u}{u_\tau} = f\left(\frac{u_\tau y}{\nu}, \frac{y}{k_s}\right) \tag{7}$$

where $u_\tau (=\sqrt{\tau_w/\rho})$ denotes the wall friction velocity and $\nu = \mu/\rho$.

This equation was referred to by Millikan as the "Prandtl Wall Velocity Law". For the flow over a smooth wall, it reduces to

$$\frac{u}{u_\tau} = f\left(\frac{u_\tau y}{\nu}\right) = f\left(y^+\right) \tag{8}$$

For the outer flow region, von Karman suggested the solution to be independent of Reynolds number or wall roughness, but dependent on a gross property of the flow, say, the boundary layer thickness, δ. The "Velocity Defect Law" was written as

$$\frac{u_o - u}{u_\tau} = g\left(\frac{y}{\delta}\right) = g(\eta) \tag{9}$$

where u_o stands for the outer flow velocity.

Of course, the solutions specified by Eqs. (8) and (9) are not expected to hold in the viscous region. However, it is plausible to consider that there exists a finite region where both equations are valid and undistinguished. In this region of overlap,

$$f(y^+) = u_o^+ - g(\eta), \quad u_o^+ = u_o/u_\tau \tag{10}$$

so that

$$\frac{\partial u^+}{\partial y^+} = \frac{\mathrm{d}f}{\mathrm{d}y^+} = -\frac{\mathrm{d}g}{\mathrm{d}\eta}\frac{\mathrm{d}\eta}{\mathrm{d}y^+} \tag{11}$$

with $u^+ = u/u_\tau$.

Since $\mathrm{d}\eta/\mathrm{d}y^+ = \nu/\delta u_\tau = \eta/y^+$, it follows immediately that

$$y^+\frac{\mathrm{d}f}{\mathrm{d}y^+} = -\eta\frac{\mathrm{d}g}{\mathrm{d}\eta} = \text{constant} = \mathrm{A} \tag{12}$$

implying

$$u^+ = f(y^+) = A\ln y^+ + B \tag{13}$$

and

$$u_o^+ - u^+ = g(\eta) = -A\ln\eta + C \tag{14}$$

The integration parameters in the above equations need to be determined experimentally. Parameter A is normally written as $\varkappa^{-1}$, with $\varkappa = 0.4$. In fact, in his 1930 classical paper, von Karman suggested $\varkappa = 0.36$. Many subsequent works have quoted $\varkappa$ to vary between 0.36 and 0.44. The value $\varkappa = 0.4$ has been specially suggested by Coles [17], who also recommends $A = 5$ (smooth wall).

For a slight different derivation of the logarithmic law, consider again Eq. (10). Differentiation with respect to x yields

$$\begin{aligned} u_o' = u_\tau &\left[\frac{u_\tau'}{u_\tau}y^+f'(y^+) - \frac{\delta'}{\delta}\eta g'(\eta)\right] \\ &+ u_\tau'\left[f(y^+) + g(\eta)\right] \end{aligned} \tag{15}$$

where the dashes indicate differentiation.

A further differentiation with respect to y gives,

$$\begin{aligned} &0 = u_\tau\left[\tfrac{u_\tau}{\nu}f'(y^+) + \tfrac{1}{\delta}g'(\eta)\right], \text{ that is} \\ &g'(\eta) = -\tfrac{u_\tau\delta}{\nu}f'(y^+) \end{aligned} \tag{16}$$

Substitution of Eqs. (10) and (16) into (15) results

$$u_o' = u_\tau\left[\frac{u_\tau'}{u_\tau}y^+f'(y^+) + \frac{\delta'}{\delta}y^+f'(y^+)\right] + u_\tau'\frac{u_o}{u_\tau} \tag{17}$$

or still,

$$\frac{\frac{u_o'}{u_\tau} - u_o\frac{u_\tau'}{u_\tau^2}}{\frac{u_\tau'}{u_\tau} + \frac{\delta'}{\delta}} = y^+f'(y^+) \tag{18}$$

The left and right sides of the above equation are functions of different variables. This equality is only satisfied provided they are equal to the same constant, so that

$$y^+f'(y^+) = A, \qquad f(y^+) = A\ \ln y^+ + B \tag{19}$$

The left side of Eq. (18) furnishes

$$\begin{aligned} \frac{u_o'}{u_\tau} - u_o\frac{u_\tau'}{u_\tau^2} &= A\left[\frac{u_\tau'}{u_\tau} + \frac{\delta'}{\delta}\right] \\ \frac{d}{\mathrm{d}x}\left[\frac{u_o}{u_\tau}\right] &= A\,\frac{d}{\mathrm{d}x}[\ln u_\tau + \ln\delta] \\ \frac{u_o}{u_\tau} &= A\ \ln u_\tau\delta + B \end{aligned} \tag{20}$$

an expression that can easily be recognized as the law of resistance for turbulent flow.

4 Further formulations for the law of the wall

Following the developments of the original authors, numerous alternative formulations for the $u^+(y^+)$ relation were proposed. The main motivation was to advance single expressions valid in the whole range of the non-dimensional distance y^+ and, in some cases, for the complete velocity profile. New formulations introduced a modified mixing length hypothesis or even arguments in favor of a power-type law.

Some of the theories are reviewed next.

4.1 The theory of Reichardt [18]

The equation of continuity implies that for the very near wall region, $v \sim y^2$. Then, as shown by Reichardt [18], it results from the momentum equation that $\nu_t \sim y^3$. On the other hand, for large values of y^+ the eddy viscosity must present a linear behavior. Thus, it was only natural to Reichardt to assume that

$$\frac{\nu_t}{\nu} = k\left(y^+ - \delta_l^+\ \tanh\frac{y^+}{\delta_l^+}\right) \tag{21}$$

The velocity profile can then be obtained from

$$(\mu + \rho\nu_t)\,\partial_y u = \tau_w. \tag{22}$$

Unfortunately, this equation cannot be solved analytically. An approximated solution is given by

$$u^+ = \frac{1}{\varkappa}\ln(1+\varkappa y^+) + c\left[1-\exp(-y^+/\delta_l^+) - \frac{y^+}{\delta_l^+}\exp(-0.33y^+)\right] \tag{23}$$

where $\varkappa = 0.41$, $\delta_l^+ = 11$ and $c = 7.4$.

4.2 The theory of Rotta [19]

Rotta [19] assumed that, for the flow in the region $5.0 < y^+$, the total shear stress is determined through both viscous and turbulence effects. Thus, a direct application of the mixing length hypothesis leads to

$$\rho\left(\nu + I_m^2\left|\partial_y u\right|\right)\partial_y u = \tau_w \tag{24}$$

where $I_m = \varkappa(y-\delta_l)$.

The solution to the above equation can be written as

$$u^+ = \frac{1}{2\varkappa I_m^+}\left(1-\sqrt{1+4I_m^{+2}}\right) + \frac{1}{\varkappa}\ln\left(2I_m^+ + \sqrt{1+4I_m^{+2}}\right) + \delta_l^+ \tag{25}$$

with $I_m^+ = u_\tau I_m/\nu$ and $\delta_l^+ = u_\tau \delta_l/\nu$.

The main difficulty with this formulation is that it requires the correct specification of the value of the thickness of the viscous sub-layer δ_l^+. The abrupt distinction made between the viscous sub-layer and the turbulent region, however, does not reflect the true physics of the flow where the turbulent fluctuations are continuously damped by viscous effects. In the present implementation of Eq. (25), we initially considered $\delta_l^+ = 5.0$. That hypothesis resulted in a very low level for the logarithmic part of the profile. A purely empirical choice based on the experimental data of Andersen et al. [12] and Purtell et al. [13] suggests $\delta_l^+ = 7.0$.

4.3 The theory of Van Driest [20]

Van Driest [20] was the first to consider the inclusion of a damping function into the mixing length theory of Prandtl. As a result, he wrote

$$\nu_t = \varkappa^2 y^2\left(1-\exp(-y^+/a)\right)^2\left|\partial_y u\right| \tag{26}$$

The rate at which the flow velocity approaches zero at the wall is now controlled by the damping exponential function. In this case, $\nu_t \sim y^4$ as $y \to 0$.

An integration of Eqs. (22) and (26) gives

$$u^+ = 2\int_0^{y^+} \frac{\mathrm{d}y^+}{1+[1+4\,\varkappa^2\,y^{+2}(1-\exp(-y^+/a))^2]^{1/2}} \tag{27}$$

where Van Driest considered $a = 26$.

4.4 The theory of Rannie [21]

As the wall is approached, all previous expressions for the non-dimensional eddy viscosity show a functional behavior with either the form y^{+3} or y^{+4}. However, for finite values of y^+ a more appropriate behavior would be of the form y^{+2}. To satisfy this requirement, Rannie [21] proposed for the region $y^+ \le 27.5$ the following expression

$$\frac{\nu_t}{\nu} = \sinh^2(\sigma y^+) \tag{28}$$

The resulting mean velocity profile is then given by

$$u^+ = \frac{1}{\sigma}\tanh(\sigma\, y^+) \tag{29}$$

where $\sigma = 0.0688$.

4.5 The theory of Spalding [22]

The motivation for Spalding [22] was to find a good formula for the representation of the velocity profile which presented at the same time a simpler form than the expressions of Reichardt and Van Driest. This formula should fit the experimental data closely, contain a sufficient number of constants to permit modification in the light of the experimental data, and have a simple analytical form. He then proposed a formula that satisfied the following conditions:

1. passes through the point: $y^+ = 0, u^+ = 0$;
2. is tangential at this point to: $u^+ = y^+$;
3. is asymptotic at large y^+ to: $u^+ = 2.5\ln y^+ + 5.5$;
4. fits the experimental points at intermediate y^+ values.

The equation introduced as a candidate was

$$y^+ = u^+ + C\left[\exp(\varkappa u^+) - 1 - \varkappa u^+ - \frac{(\varkappa u^+)^2}{2!} - \frac{(\varkappa u^+)^3}{3!} - \frac{(\varkappa u^+)^4}{4!}\right] \tag{30}$$

where $C = \exp(-\varkappa A)$, with A the standard constant in the law of the wall. For $A = 5.5$ (the value suggested by Spalding), C becomes 0.1108.

Expression (30) furnishes, for large values of y^+, the asymptotic behavior $\nu_t/\nu \sim y^{+4}$.

4.6 The theory of Rasmussen [23]

Following the same line of thought of Spalding, Rasmussen [23] introduced a similar expression, but with fewer terms. In his formulation, we have

$$y^+ = u^+ + \exp^{-A}\left[2\ \cosh(\varkappa u^+) - (\varkappa u^+)^2 - 2\right] \tag{31}$$

The above equation satisfies the two boundary conditions specified by Spalding at the wall. In addition, conditions $(y = \delta, u = u_o)$ and $(y = \delta, \partial_y u = 0)$ are satisfied. Only the requirement $(y = \delta, u = u_o)$ is not satisfied exactly. However, it is easily shown that the error becomes vanishingly small for $u^+ > 20$.

4.7 The theory of Musker [24]

Observing the limiting behavior of the eddy viscosity for small and large values of y^+, Musker [24] proposed the following interpolating formula

$$\frac{1}{\nu_t/\nu} = \frac{1}{C\,y^{+3}} + \frac{1}{\varkappa\, y^+} \tag{32}$$

where C (=0.001093) is a proportionality constant.

Using Eq. (22), it follows

$$\frac{\mathrm{d}u^+}{\mathrm{d}y^+} = \frac{\varkappa + Cy^{+2}}{\varkappa + Cy^{+2} + C\varkappa y^{+3}}. \tag{33}$$

An integration of this equation gives

$$\begin{aligned} u^+ = 5.454\ \tan^{-1}&\left[\frac{2y^+ - 8.15}{16.7}\right] \\ &+ \log_{10}\left[\frac{(y^+ + 10.6)^{9.6}}{(y^{+2} - 8.15y^+ + 86)^2}\right] \\ &- 3.52 + 2.44 \end{aligned} \tag{34}$$

4.8 The theory of Haritonidis [27]

In the sixties, some authors, notably Kline et al. [25] and Kovasznay [26], associated the structure of the turbulent boundary layer to a sequence of "events" dominated by two features: wall layer streaks and the bursting phenomenon. The streaks are elongated in the flow direction, typically have a length of the order of $1000\nu/u_\tau$ and can be observed over a large characteristic time, the quiescent period. The resulting set organized large-scale motions was shown to be responsible for the bulk of turbulence production.

In an attempt to incorporate the bursting process into a simple algebraic model for the eddy viscosity, Haritonidis [27] considered a two-dimensional mean flow with randomly distributed bursts. In the analysis, the transverse velocity fluctuation was modeled in accordance with a modified mixing length hypothesis.

The resulting expression for the eddy viscosity was written as

$$\nu_t = \frac{1}{2} n\, l_m^2 f \tag{35}$$

where n is the number of ejections of equal strength and duration over the period Δt_b between bursts, $f = 1/\Delta t_b$ is the bursting frequency, and l_m (=my) is the distance traveled by the bursts.

An integration of Eqs. (22) and (35) gives

$$u^+ = \lambda^{-1}\tan^{-1}(\lambda y^+) - 2^{-1}a\lambda^{-2}\ln(1 + \lambda^2 y^{+2}) \tag{36}$$

where $\lambda^2 = \alpha f^+$, $\alpha = 2^{-1}nm^2$, $a = (h^+)^{-1}$ and h^+ is the half height of a channel or pipe. For a zero-pressure gradient boundary layer $a = 0$.

A relation between m and $\varkappa$ was found to be $m = \varkappa n^{-1}(\Delta t_e/\delta t_b)^{-1}$ and Δt_e is the duration of the ejections.

In the calculations of Haritonides, λ^2 was considered equal to 0.00877.

4.9 The theory of Yakhot et al. [28]

A new formulation for an algebraic eddy viscosity model based on a renormalization group approach (RNG) was developed by Yakhot et al. [28]. Through a systematic elimination of the small scales of motion from the Navier–Stokes equation in a given wave-number interval, say, $\Lambda_f < k < \Lambda_0$, the following expression follows:

$$\frac{\nu_t}{\nu} = \left[1 + H\left(a\frac{\epsilon\Lambda_f^{-4}}{\nu^3} - C\right)\right]^{1/3} \tag{37}$$

where H is the ramp function defined by $H(x) = \max(x, 0)$, $a = 0.12$, and $C = 160$.

The RNG eddy viscosity is expressed in terms of the mean dissipation rate, ϵ, and the length scale, $\Delta = 2\pi\Lambda_f^{-1}$, corresponding to the smallest fluctuating scales retained in the system. Appealing to well known correlations for the k-ϵ transport model of turbulence, to an equilibrium hypothesis between production and dissipation near the wall and to mixing length type arguments, Eq. (37) becomes:

$$\frac{\nu_t}{\nu} = \left[1 + H\left(\varkappa^4\frac{u_\tau^4\, l^4}{\nu_t\, \nu^3} - C\right)\right]^{1/3} \tag{38}$$

Assuming that $H(x) = x$, Eq. (38) can be written as

$$Q4(\hat{\nu}) = \hat{\nu}^4 + (C-1)\hat{\nu} - \hat{\nu}_m^4 = 0, \tag{39}$$

where, $\hat{\nu} = \nu_t/\nu$, $\hat{\nu}_m = \varkappa l^+$, $l^+ = u_\tau l/\nu$.

The quartic Eq. (39) is solved under the constraint $\hat{\nu} = \max(\hat{\nu}, 1)$, $l = \min(y, \gamma\delta^*)$, $\gamma = \gamma_0(1 - H^{-1})^{-1}$; $\gamma_0 = 0.3$,

H is the shape factor ($=\delta^*/\theta$), δ^* = displacement thickness, θ = momentum thickness.

In the fully turbulent region, the flow is governed by Eq. (22) with $\nu = 0$. An integration of this equation together with Eq. (39) gives

$$u^+(y^+) = \frac{1}{3k}\left[4C^{1/4} - z + \ln\left(\frac{z+1}{z-1}\right) + 2\,\tan^{-1}(z) - \ln\left(\frac{C^{1/4}+1}{C^{1/4}-1}\right) - 2\,\tan^{-1}(C^{1/4})\right], \tag{40}$$

where $z = (\hat{v}^3 - 1 + C)^{1/4}/\hat{v}^{3/4}$ and $\hat{v} = \hat{v}(y^+)$ is the solution of the quartic Eq. (39).

4.10 The theory of Barenblatt [29]

Starting with early studies, two different propositions were advanced for the description of the mean velocity distribution.

The logarithmic law was derived on the assumption that for "sufficiently large *local* Reynolds number and sufficiently large *flow* Reynolds number, the dependence of the velocity gradient on the molecular viscosity disappears completely" [29]. In mathematical terms that is to say that $y^+\partial_{y^+}u^+$ tends to a finite value as y^+ and R_e tend to infinity. It follows immediately that $\varkappa$ and B are universal constants.

In the alternative approach, the velocity gradient dependence on molecular viscosity is considered not to disappear regardless of how big y^+ and R_e may be. In this approach, the velocity gradient is assumed to possess a power-type asymptotic behavior, where the exponent and the multiplying parameter are supposed to depend on the R_e. The form of the power-scaling law yields a family of curves whose parameter is the Reynolds number. The resulting envelop of curves is shown to be very close to the universal log-law.

The derivations of both laws are generally considered equally consistent and rigorous. They are, however, based on entirely different assumptions. Based on arguments related to general fractal properties of vortex dissipative structures in turbulent flow and on the experimental data of Nikuradze [30] for pipe flow, Barenblatt [29] proposes

$$u^+ = C\,(y^+)^\alpha, \tag{41}$$

where

$$C = \frac{1}{\sqrt{3}}\ln R_e + \frac{5}{2} = \frac{\sqrt{3}+5\alpha}{2\alpha}, \qquad \alpha = 3/(2\ln R_e). \tag{42}$$

4.11 An alternative expression

As we shall see next, the results provided by most of the above formulations are generally in good agreement with experimental data, despite the quite different underlying hypotheses in the derivation of the equations. In fact, their derivations have appealed to such diverse arguments as dimensional analysis, mixing length theories, heuristics, RNG theory, asymptotic limits, or even a combination of these.

All formulations, however, present shortcomings. The theories of Reichardt and Van Driest propose modifications in the mixing length theory which lead to quadratures requiring numerical integration. The theories of Spalding and Rasmussen present solutions in an inverse form. Rotta, Rannie and Haritonidis present solutions with a limited range of validity. The theory of Yakhot requires the solution of a quartic equation. Barenblatt's solution has been developed for pipe flow. The theory of Musker is the easiest to implement and provides a solution with a wide range of validity and good accuracy.

To find an alternative solution, we combine some of the ideas of Rotta, Spalding and Van Driest. First, identify a specific region of the flow where Eq. (22) holds. Next, the mixing length theory is evoked to perform a first integration and obtain

$$u^+(y^+) = \frac{1}{\varkappa}\left(\frac{1-\sqrt{1+4\,\varkappa^2\,y^{+2}}}{2\,\varkappa\,y^+} + \ln\left(2\,\varkappa\,y^+ + \sqrt{1+4\,\varkappa^2\,y^{+2}}\right)\right) \tag{43}$$

This exact result is similar to the one found by Rotta, Eq. (25). The only difference here is the omission of the thickness of the viscous sub-layer, δ_l^+. The asymptotic behavior of Eq. (43) is

$$u^+ \to y^+, \quad y^+ \to 0 \tag{44}$$

$$u^+ \to 2.5\,\ln y^+ - 1.325, \quad y^+ \to \infty \tag{45}$$

The result is that the single-variable profile, Eq. (43), fails in the high y^+ limit. To ensure a good curve fitting for the whole range of inner scales, we add the function

$$D_A(y^+) = \frac{d}{2}\left[1 + \tanh\left(\frac{2\,\varkappa\,y^+ - y^c}{y^r}\right)\right] \tag{46}$$

to Eq. (43), where $d = 6.7$ and $y^c = y^r = 8$.

This function substitutes the need for the specification of δ_l^+ in Rotta's theory, adjusting the asymptotic behavior of Eq. (43) as $y^+ \to \infty$.

4.12 Discussion

The theories are compared with the data of Andersen [12] and Purtel et al. [13]. Curves corresponding to the first three theories are plotted in Fig. 1.

The main comments are: (1) the theory of Reichardt overshoots the experimental data; (2) the solution of Rannie is good but limited to $y^+ < 27.5$; (3) Rotta's solution clearly suffers from the ill definition of δ_l^+ (here, we have used $\delta_l^+ = 7$); (4) the agreement with the experimental data provided by Van Driest's solution is very good, the same is true to Spalding's expression; (5) the theory of Rasmussen undershoots the data; (6) the agreement with the data yielded by Musken's expression is very good; (7) Haritonidis'solution is good but limited to $y^+ < 27.5$; (8) the results provided by the RGN theory are not good in the transition region; (9) the theory of Barenblatt developed for pipe flows needs a better definition of the Reynolds number for boundary layer flows, in the present comparison we have used R_e based on the external flow velocity u_o and the boundary layer thickness, δ; (10) the present formulation compares well with the data, being also comparable with the solutions of Van Driest and of Musker.

5 The asymptotic structure of turbulent flows

The early ideas upon which the boundary layer theory rests were systematically generalized and formalized in the first-half of the last century to give birth to what has normally been referred to in literature as *singular perturbation methods*. The heart of these methods is to divide the problem into global and local domains, find the approximate solutions and use some accepted working rule for their unification into a single composite solution that is expectedly asymptotic to the exact solution in the limit as a small parameter tends to zero.

A critical aspect of the described methodology refers to the process of unification, commonly referred to as matching. Two are the main possibilities: *intermediate variables* and the *asymptotic matching principle*. The former leans its results on *extension theorems* and *overlap hypotheses* to produce intermediate matching (Eckhaus [31, 32]). The latter appeals to the *asymptotic matching principle*, that is, to assumptions regarding the structure of the uniform expansions.

The interrelations between the two procedures were investigated by Eckhaus [31], who showed that the existence of an overlap domain assures the validity of the

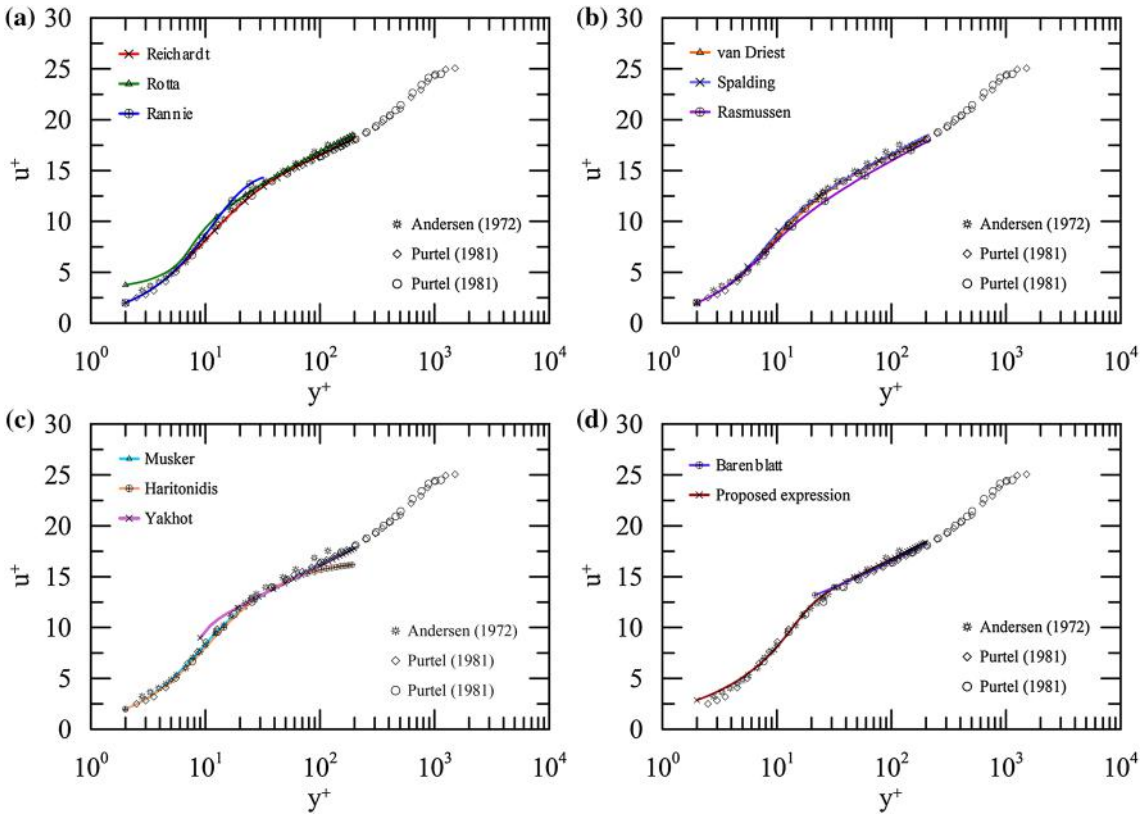

Fig. 1 Formulations for the law of the wall according to the several authors

asymptotic matching principle, but the nonexistence of an overlap does not preclude the validity of the principle. Matching based on an intermediate limit and the corresponding intermediate variable is an idea closely related—but not identical—to the original notion advanced by Prandtl of a "limit matching principle" whereby it suffices the local limit of the global equation to be equal to the global limit of the local equation.

Precise definitions and exact results can be enunciated to determine uniform approximations and perform the matching of functions. However, the determination of the domain of validity of an approximation is a difficult matter. Two important results in perturbation theory are the intermediate matching lemma and the extension theorem of Kaplun. These results are of fundamental importance for the definition of matching, but say nothing about the domain of validity of the approximations. To circumvent this difficulty, Kaplun [33] applied the concept of limit processes directly to the equations rather than to the solutions and enunciated an Ansatz about domains of validity to relate the domain of validity of solutions with the formal domain of validity of equations (a concept which is easily defined). For some difficult problems, e.g., the Stokes paradox of fluid mechanics, only consideration of these ideas can clarify the conceptual structure of the problem.

The notions on perturbation methods introduced by Kaplun were particularly discussed by Lagerstrom and Casten [34] and Lagerstrom [35]. Further discussions can be found in Silva Freire and Hirata [36], Silva Freire [37] and Silva Freire [38]. The next section highlights some of the results introduced in these works.

Most of Kaplun's ideas were developed in connection with boundary value problems. In the present work, some formal properties of the turbulent boundary layer equations are investigated through the concepts introduced by Kaplun and relate them to the actual problem of determining the overlap domain and local approximations.

The asymptotic structure of the turbulent boundary layer was extensively investigated by many authors in the past. Using only the hypothesis that the order of magnitude of the Reynolds stresses does not change throughout the boundary layer, Yajnik [14] and Mellor [39] have described the structure of the turbulent boundary layer through the matched asymptotic expansions method. They modeled the flow by a two-deck structure, consisting of a wall region and a defect region. Other authors using closure conditions in terms of eddy viscosity (Bush and Fendell [40]) or κ–ϵ (Deriat and Guiraut [41]) models have reached the same conclusion, making the two-deck asymptotic structure of the turbulent boundary layer the basis of most subsequent work. Sychev and Sychev [15], however, used the same method to find a three-layered structure.

In this work, the asymptotic structure of the turbulent boundary layer is investigated through a direct application of Kaplun ideas to the Navier–Stokes equation.

5.1 Kaplun limits

The following topology is introduced on the collection of order classes (Meyer [42]).

For positive, continuous functions of a single variable ϵ defined on (0, 1], let *ord* η denote the class of equivalence

$$\operatorname{ord}\eta = \{\theta(\epsilon) \,/\, \lim \theta(\epsilon)/\eta(\epsilon),\ \epsilon \to 0, \text{ exists and is } \neq 0\}. \tag{47}$$

A partial ordering is constructed on these functions by defining

$$\operatorname{ord}\eta_1 < \operatorname{ord}\eta_2 \quad \Leftrightarrow \quad \lim \frac{\eta_1}{\eta_2} = 0, \quad \epsilon \to 0. \tag{48}$$

A set D of order classes is said to be convex if $\operatorname{ord}\delta_1, \operatorname{ord}\delta_2 \in D$ and $\operatorname{ord}\delta_1 < \operatorname{ord}\theta < \operatorname{ord}\delta_2$ together imply $\operatorname{ord}\theta \in D$. A set D is said to be open if it is converse and if $\operatorname{ord}\theta \in D$ implies the existence of functions γ, δ such that $\operatorname{ord}\theta > \operatorname{ord}\gamma \in D$ and $\operatorname{ord}\theta < \operatorname{ord}\delta \in D$. A set D, on the other hand, is said to be closed if it is convex and has particular elements $\operatorname{ord}\delta_1, \operatorname{ord}\delta_2$ such that $\operatorname{ord}\delta_1 \leq \operatorname{ord}\theta \leq \operatorname{ord}\delta_2$ for every $\operatorname{ord}\theta \in D$. Two order sets, D and D' are said adjacent if: (1) $D' > D$ and (2) $\eta < D'$ and $\eta' > D \to \eta' > \eta$. We may refer to D' as being the upper adjacent region of D. Analogously, D is said to be the lower adjacent region of D'.

Definition (Lagerstrom [35]) We say that $f(x, \epsilon)$ is an approximation to $g(x, \epsilon)$ uniformly valid to order $\delta(\epsilon)$ in a convex set D (f is a δ-approximation to g), if

$$\lim \frac{f(x,y) - g(x,y)}{\delta(\epsilon)} = 0, \quad \epsilon \to 0, \text{ uniformly for } x \text{ in } D. \tag{49}$$

The function $\delta(\epsilon)$ is called a gauge function.

The essential idea of η-limit process is to study the limit as $\epsilon \to 0$ not for fixed x near the singularity point x_d, but for x tending to x_d in a definite relationship to ϵ specified by a stretching function $\eta(\epsilon)$. Taking without any loss of generality $x_d = 0$, we define

$$x_\eta = \frac{x}{\eta(\epsilon)}, \quad G(x_\eta; \epsilon) = F(x; \epsilon), \tag{50}$$

with $\eta(\epsilon)$ a function defined in Ξ, the space of all positive continuous functions in (0, 1].

Definition (Meyer [42]) If the function $G(x_\eta; +0) = \lim G(x_\eta; \epsilon)$, $\epsilon \to 0$, exists uniformly on $\{x_\eta / |x_\eta| > 0\}$; then, we define $\lim_\eta F(x; \epsilon) = G(x_\eta; +0)$.

Thus, if $\eta \to 0$ as $\epsilon \to 0$, then, in the limit process, $x \to 0$ also with the same speed of η, so that x/η tends to a

non-zero limit value. One of the central results of Kaplun's work is the extension theorem, which is here presented in the following version (Meyer [42]).

Kaplun's extension theorem If $f(x;\epsilon)$ is a $\xi(\epsilon)$-approximation to $g(x;\epsilon)$ uniformly in a closed interval D_0, then it is so also in an open set $D \supset D_0$.

The above theorem was first published in Kaplun and Lagerstrom [43] in connection with the Stokes paradox for flow at low Reynolds number. The theorem needs to be complemented by an Axiom and by an Ansatz to relate the formal domain of validity of an equation with the actual domain of validity of its solution. The idea of Kaplun was to shift the emphasis to applying limit processes directly to the equations rather than to the solutions, establishing some rules to determine the domain of validity of solutions from the formal domain of validity of an equation.

The set of equations that will result from passage of the limit is referred to by Kaplun as the "splitting" of the differential equations. The splitting must be seen as a formal property of the equation obtained through a "formal passage of the η-limit process". To every order of η a correspondence is induced, $\lim_\eta \rightarrow$ associated equation, on that subset of Ξ for which the associated equation exists.

Definition The formal limit domain of an associated equation E is the set of orders η such that the η-limit process applied to the original equation yields E.

Passage of the η-limit will give equations that are distinguished in two ways: (1) they are determined by specific choices of η, and (2) they are more complete, or in Kaplun's words, "richer" than the others, in the sense that, application of the η-limit process to them will result in other associated equations, but neither of them can be obtained from any of the other equations.

Limit processes which yield "rich" equations are called principal limit processes. The significance of principal limit processes is that the resulting equations are expected to be satisfied by the corresponding limits of the exact solution. The notion of principal equation will be formalized below.

The above concepts and ideas can be given a more rigorous interpretation if we introduce Kaplun's concept of equivalent in the limit for a given set of equations for a given point (η, δ) of the (Ξ, Σ) product space.

Given any two associated equations E_1 and E_2, we define the remainder of E_1 with relation to E_2 as

$$\mathbb{R}(x_\eta;\epsilon) = E_1(x_\eta;\epsilon) - E_2(x_\eta;\epsilon), \tag{51}$$

where ϵ denotes a small parameter.

According to Kaplun [33], $\mathbb{R}$ should be interpreted as an operator giving the "apparent force" that must be added to E_2 to yield E_1.

Definition (of equivalence in the limit) (*Kaplun* [33]) Two equations E_1 and E_2 are said to be *equivalent in the limit* for a given limit process, $\lim_\eta$, and to a given order, δ, if

$$\frac{\mathbb{R}(x_\eta;\epsilon)}{\delta} \rightarrow 0, \quad \text{as } \epsilon \rightarrow 0,\ x_\eta \text{ fixed.} \tag{52}$$

The following propositions are important; they can be found in Kaplun [33]. The symbol $\sim$ is used to indicate equivalent in the limit whereas $\not\sim$ indicates not equivalent in the limit.

Proposition 1 *If $E \sim E'$ for the point (η', δ') of the product space $\Xi \times \Sigma$, then $E \sim E'$ for all points (η, δ) such that $\eta = \eta'$ and $\delta \gg \delta'$.* Conversely, if $E \not\sim E'$ for the point (η', δ'), then $E \not\sim E'$ for all points (η, δ) such that $\eta = \eta'$ and $\text{ord}\,\delta \ll \text{ord}\,\delta'$.

Proposition 2 *If $E \sim E'$ for the point (η, δ) of the product space $\Xi \times \Sigma$, and if associated equations for that point exist for E, then they exist also for E' and are identical for both.*

Proposition 3 *If associated equations exist for E and E', respectively, corresponding to $\eta = \eta'$ and the sequence $\delta = \delta'_0, \delta'_1, \ldots, \delta'_n, \delta'$ where $\delta'_n > \delta' > \delta'_{n+1}$, and are identical for both, then $E \sim E'$ for the point (η', δ').*

We can make the following definition.

Definition (of formal domain of validity) The formal domain of validity to order δ of an equation E of formal limit domain D is the set $D_e = D \cup D'_i s$, where $D'_i s$ are the formal limit domains of all equations E'_i such that E and E'_i are equivalent in D'_i to order δ.

Definition (of principal equation) An equation E of formal limit domain D is said to be principal to order δ if:

(1) one can find another equation E', of formal limit domain D', such that E and E' are equivalent in D' to order δ;
(2) E is not equivalent to order δ to any other equation in D.

An equation which is not principal is said to be intermediate.

To relate the formal properties of equations to the actual problem of determining the uniform domain of validity of solutions, Kaplun [33] advanced two assertions, the Axiom of Existence and the Ansatz about domains of validity. These assertions constitute primitive and unverifiable assumptions of perturbation theory.

Axiom (*of existence*) (Kaplun [33]) If equations E and E' are equivalent in the limit to the order δ for a certain region, then given a solution S of E which lies in the region of

equivalence of E and E', there exists a solution S' of E' such that as $\epsilon \to 0, |S - S'|/\delta \to 0$, in the region of equivalence of E and E'.

In other words, the axiom states that there exists a solution S' of E' such that the "distance" between S and S' is of the same order of magnitude of that between E and E'.

In using perturbation methods, the common approach is to consider the existence of certain limits of the exact solution or expansions of a certain form. This is normally a sufficient condition to find the associated equations and to assure that the axiom is satisfied (Kaplun [33]). Equivalence in the limit, however, is a necessary condition as shown by Propositions (1)–(3).

To the axiom of existence there corresponds an Ansatz; namely that there exists a solution S of E which lies in the region of equivalence of E and E'. More explicitly, we write.

Ansatz (*about domains of validity*) (Kaplun [33]) An equation with a given formal domain of validity D has a solution whose actual domain of validity corresponds to D.

The word "corresponds to" in the Ansatz was assumed by Kaplun to actually mean "is equal to"; this establishes the link we needed between the "formal" properties of the equation and the actual properties of the solution.

The Ansatz can always be subjected to a *canonical test* which consists in exhibiting a solution S' of E' which lies in the region of equivalence of E and E' and is determined by the boundary conditions that correspond to S.

Because the heuristic nature of the Axiom and of the Ansatz, comparison to experiments will always be important for validation purposes. The theory, however, as implemented through the above procedure, is always helpful in understanding the matching process and in constructing the appropriate asymptotic expansions.

5.2 The asymptotic structure of the zero-pressure gradient turbulent boundary layer

For an incompressible two-dimensional turbulent flow over a smooth surface in a prescribed pressure distribution, the time averaged motion equations, Eqs. (1) through (2), can be written as

$$\partial_j u_j = 0, \tag{53}$$

$$u_j \partial_j u_i = -\partial_j p - \epsilon^2 \partial_j \left(\overline{u_j' u_i'} \right) + R_e^{-1} \partial_{jj}^2 u_i, \tag{54}$$

where the notation is classical. Thus, $(x_1, x_2) = (x, y)$ stand for the coordinates, $(u_1, u_2) = (u, v)$ for the velocities, p for pressure and R_e for the Reynolds number. The dashes are used to indicate a fluctuating quantity. In the fluctuation terms, an overbar is used to indicate a time average.

The small parameter ϵ is defined through Eq. (56) below.

All mean variables are referred to some characteristic quantity of the external flow. The velocity fluctuations, on the other hand, are referred to a characteristic velocity u_R, first introduced in Cruz and Silva Freire [44].

The correct assessment of the characteristic velocity is fundamental for the determination of the boundary layer asymptotic structure. For unseparated flows the characteristic velocity is known to be the friction velocity; for separating flows it reduces to $(\nu(\mathrm{d}p/\mathrm{d}x)/\rho)^{1/3}$. For the moment, we will consider attached flow so that we can write

$$\mathrm{ord}\,(u_i') = \mathrm{ord}\,(u_\tau). \tag{55}$$

This result is valid for incompressible flows as well as for compressible flows (see, e.g., Kistler [45] and Kistler and Chen [46]).

The small parameter ϵ is, therefore, defined by

$$\epsilon = \frac{u_R}{u_o} = \frac{u_\tau}{u_o} \tag{56}$$

where, again, u_τ is the friction velocity and u_o the external flow velocity.

To find the asymptotic structure of the boundary layer, we consider the following stretching transformation

$$\hat{y} = y_\eta = \frac{y}{\eta(\epsilon)}, \quad \hat{u}_i(x, y_\eta) = u_i(x, y) \tag{57}$$

with $\eta(\epsilon)$ defined on Ξ.

Passage of the η-limit process onto the motion equation results:

x-momentum equation:

$$\mathrm{ord}\,\eta = \mathrm{ord}\,1: \qquad \hat{u}\partial_x \hat{u} + \hat{v}\partial_{y_\eta} \hat{u} = -\partial_x \hat{p} \tag{58}$$

$$\mathrm{ord}\,\epsilon^2 < \mathrm{ord}\,\eta < \mathrm{ord}\,1: \qquad \hat{u}\partial_x \hat{u} + \hat{v}\partial_{y_\eta} \hat{u} = -\partial_x \hat{p} \tag{59}$$

$$\mathrm{ord}\,\epsilon^2 = \mathrm{ord}\,\eta: \qquad \hat{u}\partial_x \hat{u} + \hat{v}\partial_{y_\eta} \hat{u} = -\partial_x \hat{p} - \partial_{y_\eta} \overline{\hat{u}'\hat{v}'} \tag{60}$$

$$\mathrm{ord}\,(\epsilon R_e)^{-1} < \mathrm{ord}\,\eta < \mathrm{ord}\,\epsilon^2: \qquad \partial_{y_\eta} \overline{\hat{u}'\hat{v}'} = 0 \tag{61}$$

$$\mathrm{ord}\,(\epsilon R_e)^{-1} = \mathrm{ord}\,\eta: \qquad \partial_{y_\eta} \overline{\hat{u}'\hat{v}'} + \partial^2_{y_\eta y_\eta} \hat{u} = 0 \tag{62}$$

$$\mathrm{ord}\,(\epsilon R_e)^{-1} < \mathrm{ord}\,\eta: \qquad \partial^2_{y_\eta y_\eta} \hat{u} = 0 \tag{63}$$

Passage of the η-limit process onto the y-momentum equation shows the dominance of the pressure term in all regions

of the domain. All information regarding the asymptotic structure of the boundary layer is, therefore, contained in the x-momentum equation.

In respect to the determination of Eq. (62), please, refer to further arguments presented in Loureiro and Silva Freire [47]. The matching process that involves the inner and outer solutions presents a peculiar difficulty, sometimes referred to in literature as "generation gap" (Mellor [39]). When this happens, an inspection of formally higher order terms leads to "switchback" and to a change in the leading order of the inner solution.

Equations (60) and (62) are distinguished in two ways: (1) they are determined by specific choices of η, and (2) they are "richer" than the others in the sense that, application of the limit process to them yields some of the other equations, but neither of them can be obtained from passage of the limit process to any of the other equations. Thus, according to the definitions introduced in the previous sections, these equations are the principal equations. We have seen that principal equations are important since they are expected to be satisfied by the corresponding limits of the exact solution.

A complete solution to the problem should then according to the Axiom of Existence and Kaplun's Ansatz, be obtained from the principal equations located at points $\mathrm{ord}(\eta) = \mathrm{ord}(\epsilon^2)$ and $\mathrm{ord}(\eta) = \mathrm{ord}((\epsilon R_e)^{-1})$. The formal domains of validity of these equations cover the entire domain and overlap in a region determined according to the definition of equivalent in limit.

To find the overlap region of Eqs. (60) and (62), we must show these equations to have a common domain where they are equivalent. A direct application of the definition of equivalence in the limit to Eqs. (60) and (62) yields

$$\mathbb{R} = \frac{\hat{u}\partial_x\hat{u} + \hat{v}\partial_{y_\eta}\hat{u} + \partial_x\hat{p} - \partial^2_{y_\eta y_\eta}\hat{u}}{\epsilon^\alpha} \tag{64}$$

Noting that the leading order term in region $\mathrm{ord}(1/\epsilon R_e) < \mathrm{ord}(\eta) < \mathrm{ord}(\epsilon^2)$ is the turbulent term, of $\mathrm{ord}(\epsilon^2/\eta)$, we normalize the above equation to order unity to find

$$\overline{\mathbb{R}} = \frac{\eta}{\epsilon^2}\mathbb{R} \tag{65}$$

The overlap domain is the set of orders such that the η-limit process applied to $\overline{\mathbb{R}}$ tends to zero for a given α. Then, since $\mathrm{ord}(\partial_y) = \epsilon$ and $\mathrm{ord}(\partial_x) = 1$, the formal overlap domain is given by

$$D_{\mathrm{overlap}} = \{\eta / \mathrm{ord}(\epsilon^{1+\alpha}R_e)^{-1} < \mathrm{ord}\eta < \mathrm{ord}(\epsilon^{2+\alpha})\} \tag{66}$$

According to Kaplun's Ansatz about domains of validity, the approximate equations, Eqs. (60) and (62), only overlap if set (66) is a non-empty set, that is, if

$$0 \le \alpha \le -\frac{1}{2}\left(\frac{\ln R_e}{\ln \epsilon} + 3\right) \tag{67}$$

The implication is that the two-deck turbulent boundary layer structure given by the two principal equations, Eqs. (60) and (62), provides approximate solutions which are accurate to the order of $\epsilon^{\alpha_{\max}}$, where $\alpha_{\max}$ is the least upper bound of the interval (67). This fundamental result can only be reached through the application of Kaplun's concepts and ideas to the problem.

6 Logarithmic solutions for generalized flows

Variations of the arguments used in the early research for the determination of local solutions of the turbulent boundary layer have led to the development of some complex expressions for the near wall treatment of yet more complex problems. The examples are many, but perhaps a very good illustration may be provided by that of the wall shear stress prediction for the interaction of a shock wave and a turbulent boundary layer at high transonic speeds (Liou and Adamson [48]).

Solutions for the interaction between a shock wave and a boundary layer are very complex since they must account not only for the geometry of the problem but also for the nature of the boundary layer, i.e., whether it is laminar or turbulent, and for the strength of the shock. If the pressure rise across the shock is moderate, the boundary layer remains attached through the interaction, giving rise to a flow configuration that can be treated analytically. Once separation occurs, however, the flow pattern changes drastically and analytical solutions become difficult to obtain. Three-dimensional effects further complicate the problem.

To apply perturbation methods to the interaction problem, authors in the past separated the flow field into a region of strong interaction and regions of weak interaction upstream and downstream of the shock wave. Particular solutions for every region of the flow were developed in terms of three small parameters: the friction velocity, the global Reynolds number and the strength of the shock. A composite solution for the whole field is found from the asymptotic matching of the various solutions in the x- and y-directions.

Silva Freire [49, 50] showed how perturbation methods could also be used to study passive flow control when a plenum chamber in fitted underneath an interacting shock wave.

In the following subsections, several near wall solutions are constructed for different flow conditions. The combination of the several effects is made in such a way as to lead to conditions with an increasing order of complexity.

6.1 The compressible turbulent boundary layer

In turbulent compressible flow, the transport mechanisms associated with the fluctuations in density, temperature and viscosity do not alter the asymptotic structure of the flow as shown by Silva Freire [51]. In fact, this discussion is not trivial.

Afzal [52] extended the theories of Yajnik [14] and Mellor [39] to compressible flow. His theory was formulated for a perfect gas with constant specific heats when $(\gamma-1)M_o^2$ and the molecular Prandtl number are of order unity; he also worked with an underdetermined system of equations. However, Melnik and Grossman [53], Adamson and Feo [54] and Liou and Adamson [48] argued that Afzal had not showed that the flow properties in the inner and outer regions actually matched. Their main objection was related to the matching of the density profiles. Because the density varied by order unity from one region to the other, the solution presented by Afzal was not capable of dealing with this behavior. Of course, the failure in achieving matching depended on the choice of the asymptotic expressions.

In Silva Freire [51], the matched asymptotic expansion method is applied to the compressible turbulent boundary layer. Local equations and solutions for the defect and wall regions disclose the existence of first-order logarithmic and second-order bi-logarithmic terms. The bi-logarithmic terms appearing in the second-order solutions for the velocity, temperature and density solutions are shown to make matching viable. The analysis shows how important it is the consideration of bi-logarithmic terms in the compressible flow problem. The analysis further applies the theory of Kaplun [33] to the equations of momentum, energy and state to show that double limits also indicate the existence of an overlap domain.

For a compressible flow, Morkovin [55] showed that

$$\frac{t'}{T}=-\frac{\rho'}{\rho}=-(\gamma-1)M^2\frac{u'}{u}, \tag{68}$$

where M stands for Mach number.

This equation indicates that the fluctuations in density are small as compared to the mean value, not exceeding values over 0.1 for Mach numbers less than 5. The conclusion is that the fluctuations in temperature and density do not exert a significant influence on the turbulent field for $M\leq 5$. Therefore, part of the knowledge of the turbulent structure obtained for subsonic flow may be extended to supersonic flow.

Under certain conditions, the energy equation for a turbulent flow exhibits an analytical solution. For the specific case of constant wall temperature, Crocco [56] shows that

$$\frac{T}{T_o}=-\frac{T_w}{T_o}+\frac{T_r-T_w}{T_o}\frac{u}{u_o}-r\frac{\gamma-1}{2}M_o^2\left(1-\left(\frac{u}{u_o}\right)\right), \tag{69}$$

where, $\gamma=c_p/c_v$, r = recovery factor (=0.896), T_w = wall temperature, T_o = outer flow temperature, T_r = recovery temperature, and

$$T_r=T_o\left(1+r\frac{\gamma-1}{2}M_o^2\right). \tag{70}$$

For adiabatic flow, Eq. (69) becomes

$$\frac{T}{T_o}=1+r\frac{\gamma-1}{2}M_o^2\left(1-\left(\frac{u}{u_o}\right)\right), \tag{71}$$

The above remarks suggest that the compressible turbulent boundary layer may be divided into two regions, an inner (wall) layer and an outer (defect) layer. In the region adjacent to the wall, viscous effects dominate so that

$$\partial_y u=\frac{u_\tau^2}{\nu_w}\left(\frac{T_w}{T}\right)^{\omega}, \tag{72}$$

where the changes in viscosity have been considered through

$$\mu=\mu_w\left(\frac{T_w}{T}\right)^{\omega}. \tag{73}$$

Substitution of Eq. (69) into Eq. (72) with $\omega=1$ results

$$\frac{u^c}{u_\tau}=\frac{u_\tau y}{\nu_w}, \tag{74}$$

where

$$\begin{aligned} u^c&=u\left[1+\frac{1}{2}a^*\frac{u}{u_o}-\frac{1}{3}b^{*2}\left(\frac{u}{u_o}\right)^2\right],\\ a^*&=\frac{T_o}{T_w}\left(1+r\frac{\gamma-1}{2}M_o^2\right)-1,\\ b^{*2}&=r\frac{\gamma-1}{2}M_o^2\frac{T_o}{T_w} \end{aligned} \tag{75}$$

and the superscript c has been used to remind the reader that the flow is compressible.

In the limit $M_\delta\longrightarrow 0$, the incompressible flow law of the wall is recovered.

On top of the region dominated by viscous effects, there exists a region where the fully turbulent effects prevail. In this region, the local velocity gradient is

$$\partial_y u^c=\frac{u_\tau}{\varkappa y}\left(\frac{T}{T_w}\right)^{1/2} \tag{76}$$

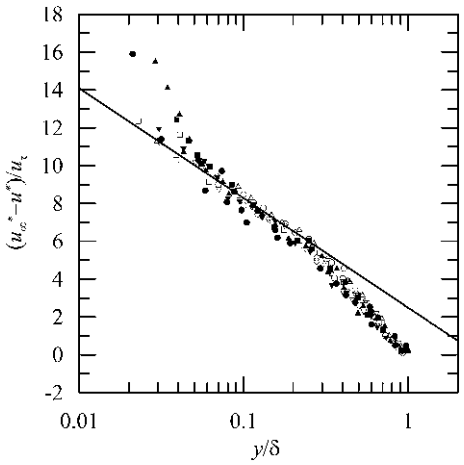

Fig. 2 Van Driet's transformation applied to compressible, adiabatic, turbulent boundary layers. Data shown in Maise and McDonald [58]. The experiments cover a Mach number range of 1.47–4.93 and a Reynolds number (based on the momentum thickness) range of 2,640–702,000

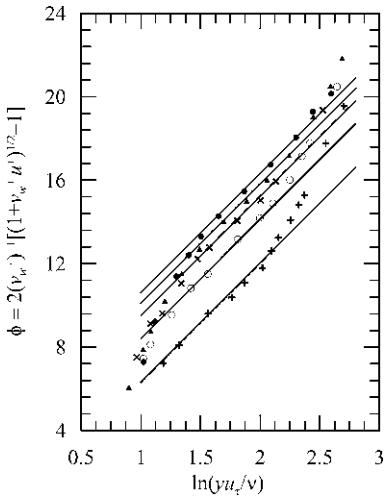

Fig. 3 Mean velocity profiles for transpired incompressible flow. Data of Andersen [12]. The injection rate ($F = v_w/u_o$) varies according to $F = 0.0, 0.001, 0.002, 0.00375, 0.008$

An integration of the above equation results

$$\frac{u^*}{u_\tau} = \frac{1}{\varkappa} \ln \frac{y u_\tau}{\nu} + C_1^*, \tag{77}$$

where

$$u^* = \frac{u_o}{b^*} \operatorname{sen}^{-1}\left[\frac{2b^{*2}\frac{u^c}{u_o^c} - a^*}{(a^{*2} + 4b^{*2})^{1/2}}\right]. \tag{78}$$

The above transformation is known as Van Driest's transformation [57]. Equation (78) transforms a compressible velocity profile, u^c, into a corresponding incompressible profile, u^*. All the compressible effects are incorporated to the transformation through coefficients a^* and b^*. Constant C_1^* takes on the classical value 5.

An extension of Eq. (78) to the outer part of the flow is easily carried out with the addition of a wake function. For details see Maise and McDonald [58]. Figure 2 shows the application of Eq. (78) to the outer region of the compressible turbulent boundary layer.

6.2 Transpired incompressible turbulent boundary layer

For flow subject to wall transpiration, the asymptotic structure of the turbulent boundary layer does not change. Since the wall injection enters the problem as a regular perturbation parameter (Silva Freire [59]), the flow structure remains double layered.

In fact, the result of the injection or suction of fluid into an oncoming flow is to modify the velocity distribution throughout the boundary layer so that drag is either reduced or increased. Any expression advanced with the purpose of determining the friction coefficient should, therefore, reflect this fact.

Regarding the inner layer equations of motion, the effects of flow injection can be account for through consideration of contributions by the inertia term, through equation

$$v_w \partial_y u = \nu \partial_{yy}^2 u + \partial_y(-\rho \overline{u'v'}) \tag{79}$$

In Silva Freire [59], the matched asymptotic expansions method was applied to the equations of motion to find a law of the wall in which the additive parameter A varied with transpiration. The resulting expression is

$$\begin{aligned} u^+ = {} & \varkappa^{-1} \ln\left(y^+\right) + A + \Pi \varkappa^{-1} W\left(y\delta^{-1}\right) \\ & + v_w^+ \left((2\varkappa)^{-1} \ln\left(y^+\right) + 2^{-1}A\right)^2 \\ & + \tilde{\Pi} \varkappa^{-1} W\left(y\delta^{-1}\right) \end{aligned} \tag{80}$$

where $u^+ = u u_\tau^{-1}$, $y^+ = y u_\tau \nu^{-1}$, $v_w^+ = v_w u_\tau^{-1}$, v_w = normal velocity at the wall, and A is given by:

$$A = 5 - 512(v_w u_o^{-1}) \tag{81}$$

The parameters Π and $\tilde{\Pi}$ and function W are related to the universal wake function.

Figure 3 shows the logarithmic behavior of the transpired incompressible turbulent boundary layer, provided the velocity profile is plotted according to the transformation given by Eq. (82),

$$\begin{aligned} \Phi &= 2(v_w^+)^{-1}\left[\left(v_w^+ (u^+)^2 + 1\right)^{1/2} - 1\right] \\ &= \varkappa^{-1} \ln y^+ + A \end{aligned} \tag{82}$$

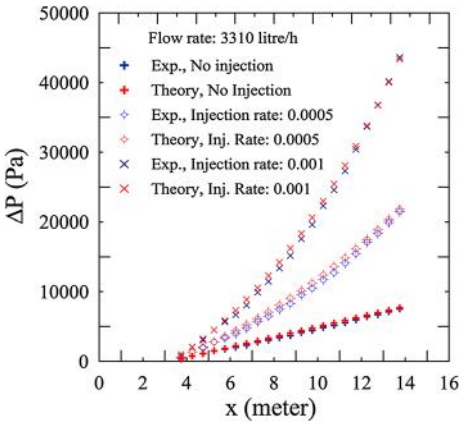

Fig. 4 Pressure drop for three flow conditions in a transpired pipe

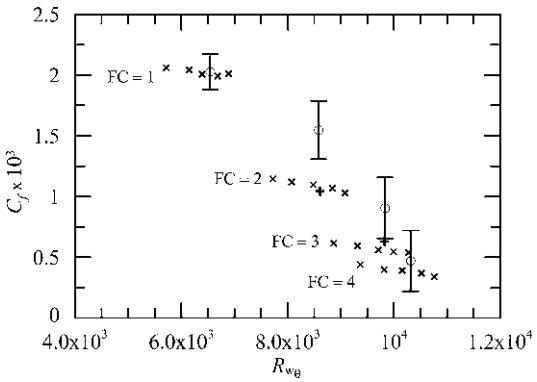

Fig. 5 Predictions of C_f for a compressible turbulent boundary layer with air injection for $M = 1.8$. *multiplication symbols* Silva Freire [63]; *open circles* Squire [62]; *plus symbols* experiments. ($FC = \rho_w v_w / \rho_o u_o$); $FC = 0.0$ (1), $FC = 0.0013$ (2), $FC = 0.0025$ (3), $FC = 0.0031$ (4)

The validation data are the data of Andersen [12].

The above equations are valid for incompressible, isothermal flows over smooth surfaces. They have been derived for external flows, but can be easily specialized to describe pipe flows. This has been made in Loureiro and Silva Freire [60], where a resistance law is proposed for pipe flows with wall transpiration.

The resistance formula for flow in a rough transpired pipe can be obtained by extending Eq. (82) to flow over a rough surface. Some further algebraic manipulation and an integration of Eq. (82) over the cross-sectional area of a pipe result

$$1 = \frac{\sqrt{\lambda}}{2\sqrt{2}}(2.5\ln(R/k_s) + A_k - 3.75) + v_w^+(1.56\ln^2(R/k_s) + (1.25A_k - 4.68)\ln(R/k_s) + \frac{A_k^2}{4} + 1.86A_k + 5.47). \tag{83}$$

where

$$\lambda = \frac{2D}{\rho U_m^2}\frac{\mathrm{d}p}{\mathrm{d}x}, \quad v_w^+ = \frac{v_w}{u_\tau}, \quad v_w^{++} = \frac{v_w}{U_m} \tag{84}$$

D denotes the pipe diameter, U_m is the mean flow velocity, $A_k = B - 512v_w^{++}$, k_s is a characteristic length of the roughness and $B = 8.5$ (completely rough regime).

In the limiting case, $v_w^+ \to 0$, Eq. (83) reduces to the law of resistance of Nikuradze.

The pressure losses for three experimental conditions are shown in Fig. 4 (Bandeira et al. [61]). The straight line for the unblown case indicates that the flow is in a completely developed state. In external flows, an increase in v_w^{++} always results in a decrease of u_τ. In transpired pipe flows, the local acceleration provoked by the wall transpiration increases the pressure drop. In fact, as shown in Fig. 4, the highest injection rate yields an increase in pressure drop of about 5.5 as compared with the unblown case.

6.3 Transpired compressible turbulent boundary layer

The question to be discussed concerns the appropriate use of the transformation defined in Sect. 6.1 to the results of Sect. 6.2. The answer is not easy due to the strong variation in density and temperature throughout the boundary layer. To account for the normal velocity local change with temperature, a quadratic expression (Squire [62]) can be used which leads to a compressible law of the wall with air injection that involves an elliptic integral. The derivation of Squire appeals to the mixing length theory and considers a constant $\varkappa$, independent of Mach number and injection velocity.

An extension of Eq. (82) to the compressible case through the transformation defined by Eq. (78) was proposed in Silva Freire [63]. One distinct modification was the use of a characteristic normal velocity v_{wo}, the normal velocity in the overlap region. For the numerical implementation of the velocity profiles and the skin-friction equation, it was considered that $v_{wo} = v(y/\delta) = v(0.1)$.

Predictions of the friction coefficient C_f with the formulation of Silva Freire [63] are shown in Fig. 7 for one Mach number (=1.8). A comparison with two other flow conditions ($M = 2.5$, 3.6) is further discussed in Silva Freire [63]. Results are presented for predictions of C_f and the mean velocity profile (Fig. 5).

6.4 Transpired near wall solution for the κ–ϵ model

The above results for the transpired turbulent boundary layer have been achieved with the specification of algebraic turbulent models. A more general formulation that is likely to work better for flows with high injections rates is that provided by the κ–ϵ model.

In this Section, we show how perturbation methods can be used to find closed analytical solutions for the flow velocity,

u, turbulent kinetic energy, κ, and turbulent energy dissipation rate per unit mass, ϵ, in the near wall fully turbulent region. These analytical solutions offer a convenient set of boundary conditions for a numerical computation of the flow field that avoids the complexities of the sub-layer region. In this case, the outer region numerical solution is matched to the analytical solutions rather than to the conditions at the wall itself.

The approaches that resort to a near wall analytical solutions normally consider the velocity profile to be given by universal logarithmic laws. In this case, the turbulent kinetic energy is made directly proportional to u_τ^2 and the dissipation rate directly proportional to $u_\tau^3/\varkappa y$. For transpired flows, these approximations are reasonable provided the transpiration rate is small and the changes in the friction velocity are not large. For high injection rates, modifications in the classical formulation must be made so as to correctly capture the strong explicit dependence of the wall region flow solution on the injection or suction velocity. In fact, for high injection rates the dominance of the term which explicitly depends on the injection velocity on the flow solution is complete.

In the κ–ϵ model, dimensional arguments are invoked to give

$$\nu_t = c_\nu \frac{\kappa^2}{\epsilon}, \tag{85}$$

where c_ν is a model constant.

The turbulence parameters, κ and ϵ, are determined through the following transport equations

$$\frac{D\kappa}{Dt} = P - \epsilon + \frac{\partial}{\partial x_i}\left(\frac{\nu_t}{\sigma_\kappa}\frac{\partial \kappa}{\partial x_i}\right), \tag{86}$$

$$\frac{D\epsilon}{Dt} = \frac{\partial}{\partial x_i}\left(\frac{\nu_t}{\sigma_\epsilon}\frac{\partial \epsilon}{\partial x_i}\right) + c_{\epsilon 1}\frac{\epsilon}{\kappa}P - c_{\epsilon 2}\frac{\epsilon^2}{\kappa}, \tag{87}$$

$$P = \nu_t \frac{\partial u_i}{\partial x_i}\left(\frac{\partial u_i}{\partial x_j} + \frac{\partial u_j}{\partial x_i}\right), \tag{88}$$

where all the c's and σ's are model constants. Typical values of the empirical constants are shown in Table 1.

As we have seen before, the region where the turbulent effects dominate is defined by the domain

$$D = \{\eta/\mathrm{ord}(1/u_\tau R_e) < \mathrm{ord}(\eta) < \mathrm{ord}({u_\tau}^2)\}. \tag{89}$$

Passing the η-limit with $\mathrm{ord}(\eta) = \mathrm{ord}({u_\tau}^2)$ onto the momentum equation and Eqs. (85)–(88), we get

$$\nu_w \frac{\partial u}{\partial y} = \frac{\partial}{\partial y}\left[c_\nu \frac{\kappa^2}{\epsilon}\frac{\partial u}{\partial y}\right], \tag{90}$$

$$\nu_w \frac{\partial \kappa}{\partial y} = \nu_t\left(\frac{\partial u}{\partial y}\right)^2 - \epsilon + \frac{\partial}{\partial y}\left(\frac{\nu_t}{\sigma_\kappa}\frac{\partial \kappa}{\partial y}\right), \tag{91}$$

Table 1 Model constants

c_ν	$c_{\epsilon 1}$	$c_{\epsilon 2}$	σ_κ	σ_ϵ
0.09	1.44	1.92	1.0	1.30

$$\nu_w \frac{\partial \epsilon}{\partial y} = c_{\epsilon_1}\frac{\epsilon}{\kappa}\nu_t\left(\frac{\partial u}{\partial y}\right)^2 - c_{\epsilon_2}\frac{\epsilon^2}{\kappa} + \frac{\partial}{\partial y}\left(\frac{\nu_t}{\sigma_\epsilon}\frac{\partial \epsilon}{\partial y}\right). \tag{92}$$

These are the intermediate equations, in the sense of Kaplun, that hold in the fully turbulent region. The wall functions for u, κ and ϵ are constructed on their basis.

To find the solutions to Eqs. (90)–(92), we consider the flow quantities to be given by the following asymptotic expansions

$$u(x,y) = u_\tau u_1(x,y) + \nu_w u_2(x,y), \tag{93}$$

$$\kappa(x,y) = u_\tau^2 \kappa_1(x,y) + u_\tau \nu_w \kappa_2(x,y) + \nu_w^2 \kappa_3(x,y), \tag{94}$$

$$\epsilon(x,y) = u_\tau^3 \epsilon_1(x,y) + u_\tau^2 \nu_w \epsilon_2(x,y) + u_\tau \nu_w^2 \epsilon_3(x,y). \tag{95}$$

The first- and second-order approximate equations can be found if we substitute Eqs. (93)–(95) into Eqs. (90)–(92) and collect the terms of same order. The result is:

(a) first-order equations,

$$0 = \frac{\partial}{\partial y}\left[c_\nu \frac{\kappa_1^2}{\epsilon_1}\frac{\partial u_1}{\partial y}\right], \tag{96}$$

$$0 = c_\nu \frac{\kappa_1^2}{\epsilon_1}\left(\frac{\partial u_1}{\partial y}\right)^2 - \epsilon_1 + \frac{\partial}{\partial y}\left[\frac{c_\nu}{\sigma_K}\frac{\kappa_1^2}{\epsilon_1}\frac{\partial \kappa_1}{\partial y}\right], \tag{97}$$

$$0 = c_{\epsilon_1} c_\nu \kappa_1\left(\frac{\partial u_1}{\partial y}\right)^2 - c_{\epsilon_2}\frac{\epsilon_1^2}{\kappa_1} + \frac{\partial}{\partial y}\left[\frac{c_\nu}{\sigma_\epsilon}\frac{\kappa_1^2}{\epsilon_1}\frac{\partial \epsilon_1}{\partial y}\right]; \tag{98}$$

(b) second-order equations,

$$\frac{\partial u_1}{\partial y} = \frac{\partial}{\partial y}\left[\left(c_\nu \frac{\kappa_1^2}{\epsilon_1}\frac{\partial u_2}{\partial y} + \frac{1}{\epsilon_1}\left(2\kappa_1\kappa_2 - \frac{\epsilon_2}{\epsilon_1}\kappa_1^2\right)\frac{\partial u_1}{\partial y}\right)\right], \tag{99}$$

$$\frac{\partial \kappa_1}{\partial y} = 2\,c_\nu \frac{\kappa_1^2}{\epsilon_1}\frac{\partial u_1}{\partial y}\frac{\partial u_2}{\partial y} + \frac{c_\nu}{\epsilon_1}\left(2\kappa_1\kappa_2 - \frac{\epsilon_2}{\epsilon_1}\kappa_1^2\right) \times \left(\frac{\partial u_1}{\partial y}\right)^2 - \epsilon_2 + \frac{c_\nu}{\sigma_K}\frac{\partial}{\partial y} \times \left[\left(\frac{\kappa_1^2}{\epsilon_1}\frac{\partial \kappa_2}{\partial y} + \frac{1}{\epsilon_1}\left(2\kappa_1\kappa_2 - \frac{\epsilon_2}{\epsilon_1}\kappa_1^2\right)\frac{\partial \kappa_1}{\partial y}\right)\right], \tag{100}$$

$$\frac{\partial \epsilon_1}{\partial y} = c_\nu\, c_{\epsilon_1}\left(2\kappa_1\frac{\partial u_1}{\partial y}\frac{\partial u_2}{\partial y} + \left(2\kappa_2 - \frac{\epsilon_2}{\epsilon_1}\kappa_1\right) \times \left(\frac{\partial u_1}{\partial y}\right)^2\right) c_{\epsilon_2}\frac{1}{\kappa_1}\left(2\epsilon_1\epsilon_2 - \frac{\kappa_2}{\kappa_1}\epsilon_1^2\right) + \frac{c_\nu}{\sigma_\epsilon}\frac{\partial}{\partial y}\left[\left(\frac{\kappa_1^2}{\epsilon_1}\frac{\partial \epsilon_2}{\partial y} + \frac{1}{\epsilon_1}\left(2\kappa_1\kappa_2 - \frac{\epsilon_2}{\epsilon_1}\kappa_1^2\right)\frac{\partial \epsilon_1}{\partial y}\right)\right]. \tag{101}$$

The solutions of the above equations are:

(a) first-order solutions,

$$u_1 = \frac{1}{\varkappa}(\ln y^+ + A_0), \quad \kappa_1 = A, \quad \epsilon_1 = \frac{B}{ky} \tag{102}$$

(b) second-order solutions,

$$u_2 = \frac{1}{4\varkappa^2}(\ln y^+ + A_0)^2, \quad \kappa_2 = C\ln y^+ + D, \quad \epsilon_2 = E\frac{\ln y^+}{y} + \frac{F}{y}; \tag{103}$$

where $y^+ = yu_\tau/\nu$, $\varkappa$ is the Von Karman constant and A_0 is a parameter that was shown to vary with the transpiration rate (Silva Freire [59]).

The constants A, B, C, D, E and F are given by $A = (\sqrt{c_\nu})^{-1} = 3.3$, $B = 1$, $C = (\varkappa\sqrt{c_\nu})^{-1} = 8.1$, $D = (\varkappa\sqrt{c_\nu})^{-1}((17/2) - \sigma_\epsilon) = 58.3$, $E = 3\varkappa^{-2} = 17.9$, $F = (49 - 2\sigma_\epsilon)(4\varkappa^2) = 69.6$.

Please note that the values of these constants are determined exactly from the standard κ–ϵ model constants.

To verify the logarithmic form of κ, we re-write Eq. (93) as

$$\Gamma = C\ln y^+ + D, \quad \Gamma = \frac{\kappa - {u_\tau}^2 A}{u_\tau v_w}. \tag{104}$$

The experimental results plotted as Γ against y^+ are shown in Fig. 6. The presence of a logarithmic region is clearly illustrated, thus confirming the solution obtained for Eq. (104). An observation of the experimental data shows that the uncorrected expressions cannot provide a good description for the boundary conditions. The difficulty here is that κ is seen to increase with an increase in injection rate whereas u_τ is seen to decrease. When suction is applied to the flow, the inverse behavior is observed. The conclusion is that consideration of the higher order correction term is crucial for a good representation of the flow field.

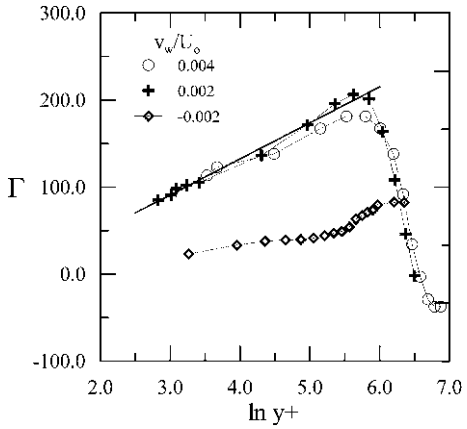

Fig. 6 The logarithmic behavior of Γ according to the data of Andersen [12] for three different injection rates

In Avelino et al. [64], a full account on the implementation of Eqs. (102) and (103) for the numerical simulation of flows with very high injection rates is presented. The results obtained with the modified equations are clearly better than those obtained with the standard approach.

6.5 The thermal incompressible turbulent boundary layer

The temperature boundary layer exhibits an asymptotic structure identical to that of the velocity boundary layer. Distinct flow regions can be identified where conductive and convective effects dominate separately. These two regions overlap in the region where fully turbulent diffusive effects prevail. The overlap domain is upper limited by a characteristic length of the order of the fluctuations $\mathrm{ord}(t') \approx \mathrm{ord}(v') \approx \mathrm{ord}(u_\tau) \approx \mathrm{ord}(t_\tau)$, where t_τ is the temperature friction. The lower limit defines the thickness of the conduction region and depends on the Reynolds and Prandtl numbers. The analysis of Cruz and Silva Freire [44] shows that the overlap region to the leading order is given by

$$D_{\text{overlap temperature}} = \{\mathrm{ord}\,(\epsilon P_r R_e)^{-1} < \mathrm{ord}\,\eta < \mathrm{ord}\,(\epsilon^2),\ \epsilon = u_\tau u_o^{-1}\}. \tag{105}$$

Thus, a logarithmic law of the wall naturally appears for the temperature boundary layer. Much in the same way, be outer flow region can be described by a "law of the wake".

Consider the problem of a given incompressible fluid flowing over a smooth, heated surface under a steady-state condition. In the following analysis, for the sake of

completeness, the mean velocity and temperature fields are discussed together. The purpose is to show how simple analogies can be drawn between the two transfer processes.

The governing equations, Eqs. (1) through (3), reduce:
Continuity:

$$\partial_x u + \partial_y v = 0, \tag{106}$$

x-Momentum:

$$\rho u \partial_x u + \rho v \partial_y u = \mu \partial^2_{yy} u - \rho \partial_y \overline{u'v'}, \tag{107}$$

Energy:

$$\rho c_p u \partial_x T + \rho c_p v \partial_y T = k \partial^2_{yy} T - \rho c_p \partial_y \overline{v't'}, \tag{108}$$

where the notation is classical and the boundary layer hypotheses apply.

These equations must be solved under appropriate boundary conditions at the wall. For the velocity field, the no-slip condition and the permeability condition can be used. For the temperature field, a number of different possible boundary conditions can be specified. Basically, one can prescribe the wall temperature, the wall heat flux or a combination of these two.

Consider next that, as shown before, the turbulent boundary layer has a two-layered structure, and that, furthermore, in one of the existing layers the turbulence effects dominate. Thus, in the fully turbulent region, the governing equations reduce to:
x-Momentum:

$$\partial_y \overline{u'v'} = 0, \tag{109}$$

Energy:

$$\partial_y \overline{v't'} = 0. \tag{110}$$

So that the above equations can be solved, a relation has to be established between the mean and the turbulent quantities. Previously, we showed how similitude arguments can be used. Here, the concepts of eddy diffusivity for momentum and heat, together with the mixing length hypothesis are invoked. This results in the following algebraic equations for the turbulent quantities

$$-\partial_y \overline{u'v'} = \partial_y \left[\nu_t \partial_y u \right] = \partial_y \left[l^2 \left(\partial_y u \right)^2 \right] = 0, \tag{111}$$

$$-\partial_y \overline{v't'} = \partial_y \left[a_t \partial_y u \right] = \partial_y \left[\left(l \partial_y u \right) \left(l_t \partial_y T \right) \right] = 0 \tag{112}$$

where ν_t and a_t denote the eddy diffusivities for momentum and heat.

We further incorporate into our analysis two extra hypotheses:

1. von Karman's hypothesis that the mixing length can be considered proportional to the wall distance, i.e., $l = \varkappa y$ and $l_t = \varkappa_t y$, where $\varkappa$ and $\varkappa_t$ are constants.
2. Prandtl's hypothesis that in the near wall region the total shear stress and the heat flux are constant.

A simple integration results that in the fully turbulent region the local solutions are given by:

$$u^+ = \varkappa^{-1} \ln y + A, \tag{113}$$

and

$$T^+ = \varkappa_t^{-1} \ln y + B, \tag{114}$$

where $u_+ = u/u_\tau$, $u_\tau = \sqrt{(\tau_w/\rho)}$ and $T^+ = (T_w - T)/t_\tau$, $t_\tau = q_w/(\rho c_p u_\tau)$.

The implication of Eqs. (113) [previously shown as Eq. (13)] and (114) is that, provided $\varkappa$ and $\varkappa_t$ are known, the skin-friction coefficient and the heat transfer coefficient can be evaluated, respectively, from the slope of semi-log graphs of y vs u and y vs T.

If a turbulent Prandtl number is defined, it follows that

$$Pr_t = \frac{\nu_t}{a_t} = \frac{\varkappa}{\varkappa_t}. \tag{115}$$

A common sense in literature is that Pr_t varies across the boundary layer in a way that depends on both the molecular properties of the fluid and the flow field. In the logarithmic region, however, several authors have shown that Pr_t is approximately 0.9 which results in a value of 0.44 for $\varkappa_t$.

6.6 The thermal incompressible turbulent boundary layer with wall transpiration

Flow transpiration is an effective means of promoting the thermal protection of walls. For the velocity field, a local solution of the momentum equation resulted in logarithmic and bi-logarithmic terms. To study the effects of transpiration on the temperature boundary layer we again split the flow region into distinct parts where certain dominant effects can be used to derive simplified equations. The formulation of the transpiration problem basically differs from the solid surface problem in the sense that the inertia effects near the wall can no longer be neglected (Eq. 79). Therefore, for the near wall dominated part of the flow, the approximate energy equation becomes

$$\rho c_p v_w \partial_y T = k \partial^2_{yy} T + \rho c_p \partial_y (-\overline{v't'}) \tag{116}$$

In the fully turbulent region, the mixing length hypothesis can be considered and the molecular diffusivity neglected. Hence, a double integration of Eq. (116) gives (Medeiros and Silva Freire [65])

$$\phi = \frac{1}{\varkappa_t} \ln \frac{y^+}{y_b^+} \tag{117}$$

where

$$\phi = \frac{\varkappa_m}{\varkappa_t}\frac{2}{v_w^+}\left[\left(\frac{v_w^+ t^+ + 1}{v_w^+ t_b^+ + 1}\right)^{\varkappa_t/2\varkappa_m}\left[\frac{v_w^+}{2}\left(\frac{1}{\varkappa_m}\ln\frac{y_a^+}{y_b^+ P_r}\right) + \sqrt{1 + v_w^+ u_a^+}\right] - \sqrt{1 + v_w^+ u_a^+}\right] \tag{118}$$

here, $v_w^+ = v_w u_\tau^{-1}$, the pair (y_b^+, u_b^+) is a constant of integration and parameters $\varkappa_m$ and $\varkappa_t$ are characteristic of the turbulence modeling.

The analytical solution of the near wall conductive layer gives

$$y_b^+ = \frac{\ln v_w^+ t_b^+ + 1}{v_w^+ P_r} \tag{119}$$

with $t_b^+ = 10$.

A comparison of Eq. (117) with the data of Whitten et al. [66] is shown in Fig. 7.

The above equation can be used to determine a Stanton number equation. This has been discussed in Medeiros and Silva Freire [65].

The above formulation can be given an alternative solution provided the following flow similarity variables are considered

$$t^* = \frac{T - T_w}{(T_o - T_w)\sqrt{S_t}}, \quad y^* = \frac{y u_o \sqrt{S_t}}{\nu} \tag{120}$$

These parameters do not include u_τ in their definition, thus allowing an immediate evaluation of Stanton number. The alternative law of the wall is thus given by

$$\frac{2}{v_w^*}\left[\sqrt{(1 + t^* v_w^*)} - \sqrt{(1 + t_b^* v_w^*)}\right] = \varkappa_t^{-1}\ln(y^*/y_b^*) \tag{121}$$

with $v_w^* = v_w/u_o\sqrt{S_t}$.

Figure 7 compares Eq. (121) with the data of Whitten et al. [66]).

6.7 The thermal compressible turbulent boundary layer with wall transpiration

To find a local solution for the temperature transpired turbulent boundary layer in a compressible flow, we consider (Silva Freire et al. [67]) that the flow parameters can be expressed by

$$u(x, y) = u_\tau u_1 + v_w u_2 \tag{122}$$

$$v(x, y) = (u_\tau R_e)^{-1}[u_\tau v_1 + v_w v_2] \tag{123}$$

$$p(x, y) = p_1 + u_\tau p_2 + v_w p_3 \tag{124}$$

$$h_c(x, y) = h_1 + h_\tau h_2 + v_w h_3 \tag{125}$$

$$\rho(x, y) = \rho_1 + u_\tau \rho_2 + v_w \rho_3 \tag{126}$$

where h denotes the enthalpy, h_t the friction enthalpy, and

$$h_c = \frac{h}{h_o - h_w} \tag{127}$$

An asymptotic expansion for the viscosity is derived by expanding μ in a Taylor series around h_1, i.e.,

$$\mu = \mu(h_1) + h_\tau(\partial_h \mu(h_1))h_2 + v_w(\partial_h \mu(h_1))h_3 \tag{128}$$

Substitution of Eqs. (122) through (128) into the equations of motion (continuity, momentum, energy and state) together with an eddy viscosity/mixing length hypothesis, and collection of the terms with the same order of magnitude furnishes a set of equations (Silva Freire et al. [67]) for the determination of u_1, u_2, h_1, h_2 and h_3 (Fig. 8).

The result is

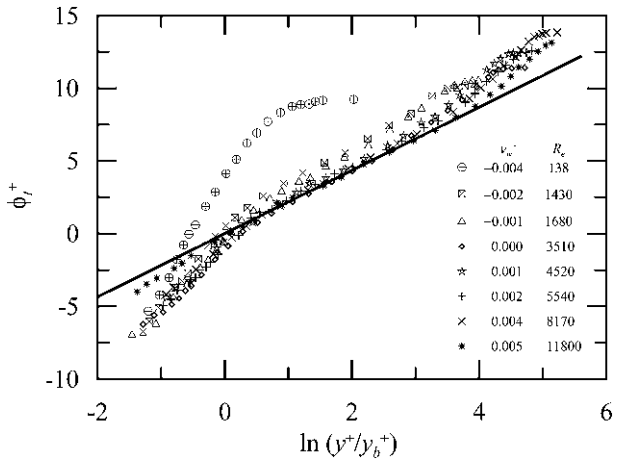

Fig. 7 Temperature law of the wall for transpired incompressible flow. Data from Whitten et al. [66]. $v_w^+ = v_w/u_\tau$

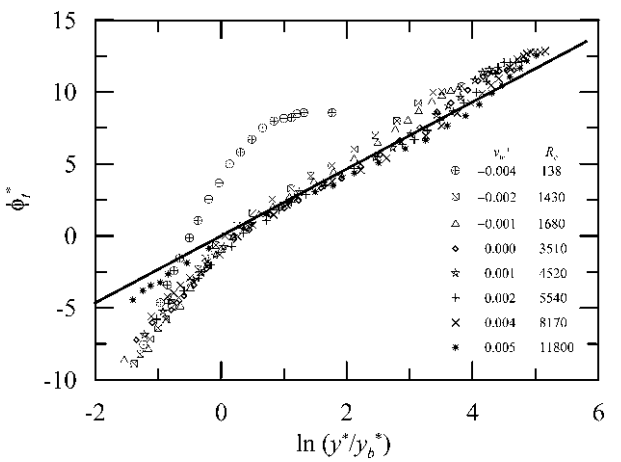

Fig. 8 Temperature law of the wall for transpired incompressible flow, alternative approach. Data from Whitten et al. [66]

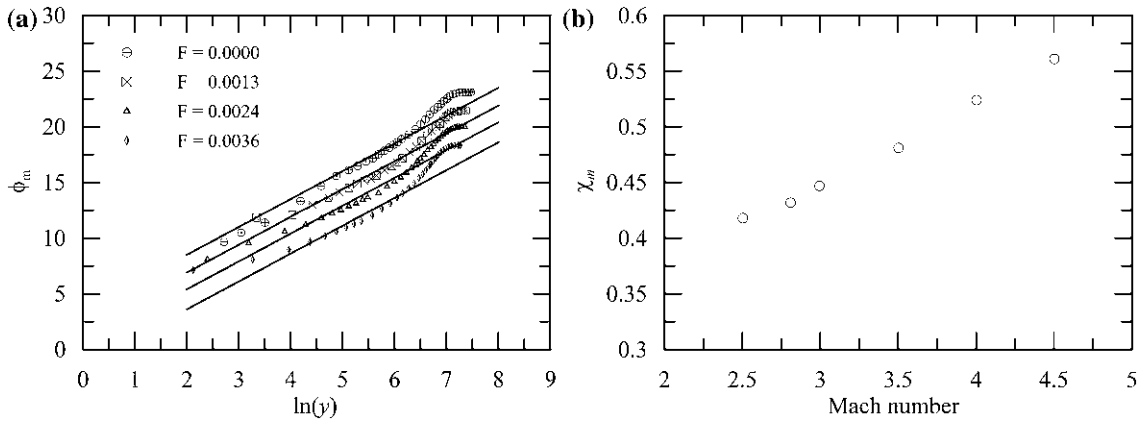

Fig. 9 Typical mean velocity profiles and the behavior of $\varkappa_m$ for transpired compressible flows. Data from Squire [69]. *F* stands for the injection rate ($=\rho_w v_w/\rho_o u_o$)

$$u_1 = \varkappa_m^{-1} \ln y + A \tag{129}$$

$$u_2 = 4^{-1}[\varkappa_m^{-1} \ln y + A]^2 \tag{130}$$

$$h_1 = h_w(h_o - h_w)^{-1} \tag{131}$$

$$h_2 = \varkappa_t^{-1} \ln P_r y + B + Eu_\tau^3 S_t^{-1} (\varkappa_m \varkappa_t)^{-1} \ln^2 P_r y \tag{132}$$

$$\begin{aligned} h_3 = {} & 4^{-1} \varkappa_t^{-2} (\varkappa_m A + 2) h_B^2 \\ & + [6^{-1} + 3^{-1} Eu_\tau^3 S_t^{-1} (\varkappa_m \varkappa_t^2)^{-1}] \\ & \times \ln^3 P_r y - 12^{-1} Eu_\tau \varkappa_m \varkappa_t^{-1} u_1^3 \end{aligned} \tag{133}$$

where parameters κ_m, κ_t, A and B are in general a function of E ($= u_o^2/(c_p(T_o - T_w))$, Eckert number) and

$$h_B = \varkappa^{-1} \ln P_r y^+ B \tag{134}$$

The asymptotic results of Eqs. (129)–(133) are leading order results in the sense that they have been obtained with the leading order terms of the density and temperature solutions.

The influence of the Eckert number and the injection velocity on the problem solution is clearly characterized through Eqs. (129)–(133). For the solid surface case, it was shown that the dissipation contributes to the leading order solution with a bi-logarithmic term. For flows with transpiration, however, the dissipation also contributes with a trilogarithmic higher order correction.

To validate Eqs. (129)–(133) the experimental data of Danberg [68], Squire [69] and Mabey et al. [70] were used. The velocity profiles are plotted with the transformation defined by Eq. (82). The enthalpy behavior is tested with the following transformation

$$\Phi_t = \frac{h_t}{v_w}\left(-1 + \sqrt{\left(1 - 2\frac{v_w}{h_t}\left[\frac{\Phi_e}{h_t} - \frac{h}{h_\tau}\right]\right)}\right) \tag{135}$$

with

$$\begin{aligned} \Phi_e = {} & -\frac{Eu_\tau^2}{2\varkappa_m \varkappa_t} \ln^2 P_r y \\ & + v_w \left[-\frac{Eu_\tau^3}{6 S_t \varkappa_m \varkappa_t^2} \ln^3 P r y \right. \\ & \left. - \left(\frac{\varkappa_m}{4\varkappa_t} + \frac{A}{2}\right) u_1^2 + \frac{Eu_\tau \varkappa_m}{6\varkappa_t}\left(\frac{u_2^2}{S_t} - \frac{1}{2}\right) u_1^3 \right] \end{aligned} \tag{136}$$

Compressible mean velocity profiles and the behavior of $\varkappa_m$ are shown in Fig. 9.

Following the tendency observed by Squire and by Mabey et al., $\varkappa_m$ shows an appreciable dependence on Mach number (M), being apparently invariant with the injection rate. For the lowest Mach number, $\varkappa_m$ is equal to 0.43; an increase in Mach number provokes an increase in $\varkappa_m$ (=0.6 for $M = 6.5$). The value of $\varkappa_m$ (=0.6) found for the data of Danberg is about l0 % lower than the theoretical value given by the correlation of Winter and Gaudet [71].

Silva Freire et al. [67] show that A varies with M and the injection rate. This is in accordance with previous observations for incompressible and compressible flows. It is now generally recognized in literature that A decreases with the increase in injection rate.

Typical temperature profiles, plotted under the appropriate coordinate defined by Eq. (135), are shown in Fig. 10. The linear, logarithmic and wake regions of the flow are clearly visible.

The theoretical values of S_t are normally higher than the experimental values by a margin of 10–30 %. This is acceptable since the error found in literature for skin-friction and Stanton number data on transpired compressible turbulent boundary layer flows normally ranges, even for very low injection rates, from 20 to 50 %.

In Silva Freire et al. [67], the near wall solutions were extended to the defect region by adding Coles' function to

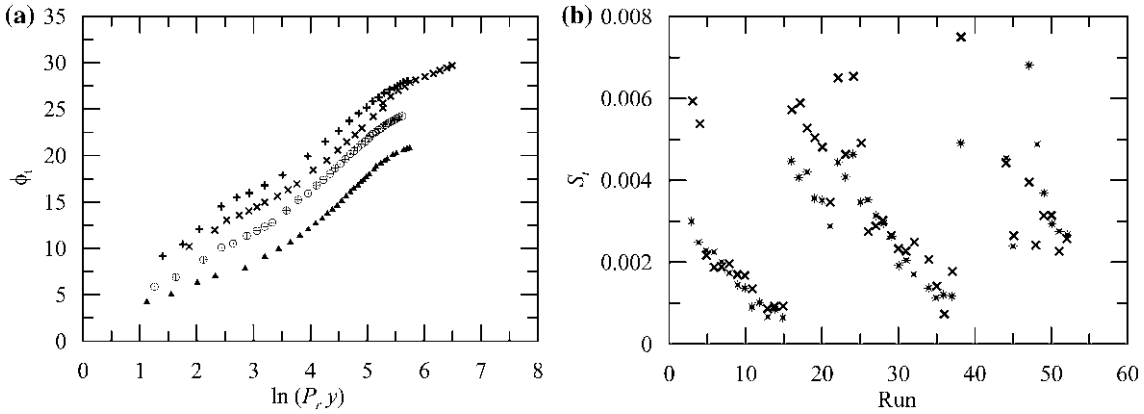

Fig. 10 Typical mean temperature profiles and the behavior of S_t for transpired compressible flows. Data from Danberg [68]. **b** *multiplication symbols* theory; *asterisks* experiments

the logarithmic terms. With arguments similar to those of Medeiros and Silva Freire [65], a Stanton number equation was developed.

6.8 Turbulent boundary layers over rough surfaces

The effects of roughness on the flow in the near wall region of a turbulent boundary layer are significant. Provided the characteristic size of the roughness elements is large enough, a regime can be established where the flow is turbulent right down to the wall (fully rough flow) (Fig. 11). One important consequence is that the viscous sub-layer may be completely removed so that local purely viscous solutions do not apply anymore. The roughness also distorts the logarithmic profile acting as if the entire flow is displaced downwards. The differences between flows over smooth and rough walls are illustrated in Fig. 11. The linear region in the smooth wall flow is easily identified. For the rough surface, only the logarithmic and defect regions are observed. The origin for the rough profile is set on the top of the protuberances.

Schlichting [72] offers a physical interpretation of the flow regimes in the following terms: (1) a regime is said to be hydraulically smooth provided "the size of the roughness is so small that all protrusions are contained within the laminar sub-layer" ($0 \leq k_s^+ \leq 5$, $k_s^+ = (k_s u_\tau)/\nu$, k_s = sand grain roughness), (2) in the transition regime, "protrusions extend partly outside the laminar sub-layer and the additional resistance, as compared with a smooth pipe, is mainly due to the form drag experienced by the protrusions in the boundary layer" ($5 \leq k_s^+ \leq 70$); (3) in the fully rough regime, "all protrusions reach outside the laminar sub-layer and by far the largest part of the resistance to flow is due to the form drag which acts on them" ($k_s^+ \geq 70$).

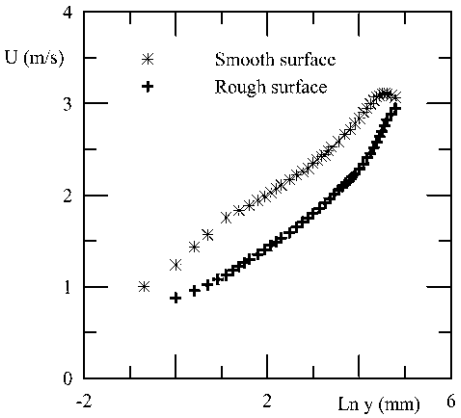

Fig. 11 Mean velocity profiles for smooth and rough surfaces

The classification intervals defined above are reminded by Schlichting [72] to have been obtained with maximum density sand. In practical applications, the typical roughness density is much smaller, so that roughness cannot be described by the indication of the height of a protrusion, k. Thus, k_s^+ is not directly related to the geometry of the surface, but to the dynamic properties of the flow.

The manner in which the logarithmic law is expressed to describe flow over a rough surface depends on the field of application. In meteorology, a common practice is to write

$$u^+ = \varkappa^{-1} \ln((y - d)/y_0), \tag{137}$$

where y is the distance above the actual ground surface.

The specification of the lower boundary condition on rough walls depends thus on two unknown parameters: the aerodynamic surface roughness, y_0, and the displacement height, d. Many works have attempted to relate the magnitude of d and y_0 to geometric properties of the surface.

To find u_τ, d and y_0, two methods can be used: the graphical method of Perry et al. [73] and the hypothesis of

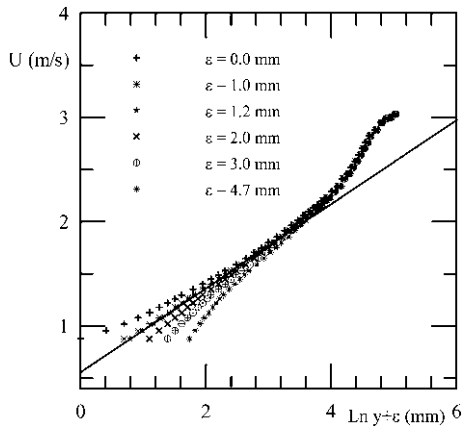

Fig. 12 Illustration of the velocity gradient method

Prandtl [2] that across the wall layer the total shear stress deviates just slightly from the wall shear stress.

In the first method, the raw undisturbed velocity profiles are subtracted by a small value (e.g., 0.1 mm) from their distance to the wall. Then, a global optimization algorithm is used to find the best logarithmic fit. This process is progressively repeated—using the same subtraction step—until the curve with the best statistics can be identified. The slope of the determined curve, α, furnishes u_τ (since $\alpha = u_\tau \varkappa^{-1}$). The level of the curve gives y_0.

In the second method, the Reynolds shear stress considered to be the dominant part of the total shear stress in the fully turbulent region. Then, by introducing the hypothesis that in the neighborhood of the wall the shear stress remains constant, we have

$$\tau_w = -\rho \overline{u'v'}. \tag{138}$$

The logarithmic law for flow over a rough surface is sometimes written in terms of the distance from the top of the rough elements. The distance to which the velocity profile is referred below the crest of the roughness elements is called the error in origin, ε (Perry et al. [73], Perry and Joubert [74], Antonia and Luxton [75], Avelino and Silva Freire [76], Loureiro and Silva Freire [77]).

Thus, Eq. (137) is re-written as

$$\frac{u}{u_\tau} = \frac{1}{\varkappa} \ln \left[\frac{(y_T + \varepsilon) u_\tau}{\nu} \right] + A - \frac{\Delta u}{u_\tau} \tag{139}$$

where,

$$\frac{\Delta u}{u_\tau} = \frac{1}{\varkappa} \ln \left[\frac{\varepsilon u_\tau}{\nu} \right] + C; \tag{140}$$

the subscript T is used to indicate that the origin is to be taken at the top of the protuberances, $\varepsilon =$ error in origin, $\varkappa = 0.4$, $A = 5.0$, and C is a parameter characteristic of the roughness.

Of course, the simple geometrical relation holds $k = d + \varepsilon$, $k =$ height of protuberances.

Figure 12 illustrates the velocity gradient method when applied to Eq. (139).

Loureiro et al. [78] discusses six different methods that can be used for the determination of u_τ in flows over smooth and rough surfaces. The work comments in detail the behavior of the logarithmic profile and of the second- and third-order moments in regions of non-equilibrium provoked by the changes from a rough to a smooth surface.

The Reynolds shear stress, the velocity gradient and the Preston tube methods consider that close to the wall in the fully turbulent region there the flow is primarily determined by the wall shear stress. In other words, they rely their estimates on the existence of the logarithmic law. The first two methods are based on estimates obtained from local data. The Preston tube readings correspond to pressure data averaged over the entire tube diameter. This integral character of the Preston tube makes its readings less sensitive to measurements off equilibrium condition. The conclusion of Loureiro et al. [78] is that the Reynolds shear stress and the velocity gradient method fail in regions of non-equilibrium flow, but the Preston tube still furnishes useful results.

6.9 Thermal turbulent boundary layers over rough surfaces

The increase in the heat transfer rate provoked by the exposition of a turbulent flow to a rough wall is known to be considerably less than the corresponding increase in skin-friction. The matter is clearly discussed in Owen and Thomson [79]. As a simple argument, the transport of heat in the vicinity of a wall is controlled solely by a molecular property of the fluid, its thermal conductivity, whereas the shear stress is observed to depend on the form drag of individual protuberances. In other words, the pressure mechanism for the transfer of momentum finds no counterpart for the transfer of heat in flows over rough surfaces. The different transfer mechanisms for momentum and heat imply that characteristic parameters for the velocity and temperature profiles must behave distinctly, including the roughness effective length and the error in origin. For this reason, the Reynolds analogy between transfer processes must be modified to consider the local influence of the Reynolds and Prandtl numbers.

To extend Eq. 139 to the temperature turbulent boundary layer (Avelino and Silva Freire [76]), we simply postulate the momentum and heat transfer processes for turbulent

flows to be similar in the fully turbulent flow region. The result is

$$\frac{T_w - T}{t_\tau} = \frac{1}{\varkappa_t} \ln\left[P_r \frac{(y_T + \varepsilon_t)u_\tau}{\nu}\right] + B - \frac{\Delta t}{t_\tau} \tag{141}$$

with,

$$\frac{\Delta t}{t_\tau} = \frac{1}{\varkappa_t} \ln\left[P_r \frac{\varepsilon_t u_\tau}{\nu}\right] + D \tag{142}$$

and D is a constant characteristic of the roughness.

Equations (141) and (142) are the law of the wall formulation for flows over rough surfaces with transfer of heat.

As discussed in the previous Section, two key concepts for the interpretation of turbulent boundary layers over rough walls are the roughness length and the error in origin (also known as the displacement in height or the zero-plane displacement). While a clear distinction is made in the literature regarding the behavior of the roughness lengths for the velocity and temperature fields (see, e.g., the works of Malhi [80]) and Sun [81]), the position of the error in origin (ε) for both fields is normally considered identical or even not considered in the investigations. In fact, Raupach [82] argues that the error in origin is normally considered property independent for the pragmatic reason that independent assessments of ε and ε_T are not available.

Loureiro and Silva Freire [77] show that d and d_T are different quantities, which take on different values. Parameter d_T $(k - \varepsilon_T)$ is argued to depend only on the molecular heat flux coming from the roughness elements. Thus, it is clear that both d $(k - \varepsilon)$ and d_T depend on different physical parameters, and hence are unrelated quantities. Loureiro and Silva Freire [77] also show that the physical interpretation of d presented in Jackson [83] is not consistent. Jackson [83] interprets the displacement in height as the level at which the mean drag on the surface appears to act. In particular, he considers the displacement height to be identical to the displacement thickness for the shear stress. Three distinct experimental data sets analyzed by Loureiro and Silva Freire [77] support the notion that d and d_T are different.

The temperature gradient method is shown in Fig. (13).

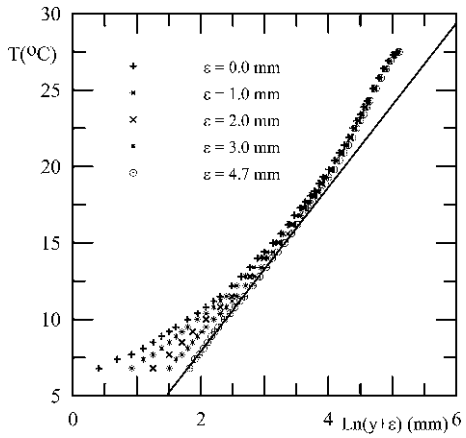

Fig. 13 Illustration of the temperature gradient method

6.10 Transient convection in turbulent boundary layer over smooth and rough surfaces

Consider now the transient convection in turbulent boundary layers over smooth, flat surfaces. The velocity field remains unaltered so that the velocity local solution in the fully turbulent region can still be approximated by a logarithmic profile. The thermal problem, however, suffers an important modification since the surface boundary conditions have to change to accommodate a time varying imposed heat flux.

Thus, it results that the energy governing equation becomes

$$\partial_t T = -\partial_y \overline{v't'}. \tag{143}$$

In view of the results of Sect. 2, the above equation can be re-written as

$$\partial_t T = \partial_y\left(u_\tau \varkappa_t y \partial_y T\right). \tag{144}$$

A solution to Eq. (144) can be found (Loureiro and Silva Freire [77]) through the method of variables separation and some asymptotic arguments, to give

$$T(y,t) = Je^{-\sigma t}[(C\ \ln y + D) + (\sigma/(\varkappa_t u_\tau)) \times (E\ \ln y + R\, y\ \ln y + S\, y + Q)], \tag{145}$$

where all constants must be determined experimentally.

For flow over a rough surface, Eq. (145) reduces to

$$T(y,t) = Je^{-\sigma t}[(C \ln y^+ + D) + (\sigma/(\varkappa_t u_\tau)) \times (E \ln y^+ + R y^+ \ln y^+ + S y^+ + Q)], \tag{146}$$

where $y^+ = (y_T + \varepsilon_t)u_\tau/\nu$ and the parameters to be determined may now be a function of the roughness.

The error in origin for the temperature, ε_t, is now time dependent.

Equation (146) provides a good means to measure the heat flux at the wall. Provided we can evaluate the error in origin through one of the classical techniques, the slope of the temperature profile plotted in a semi-log graph furnishes the friction temperature and, thus, the heat transfer coefficient.

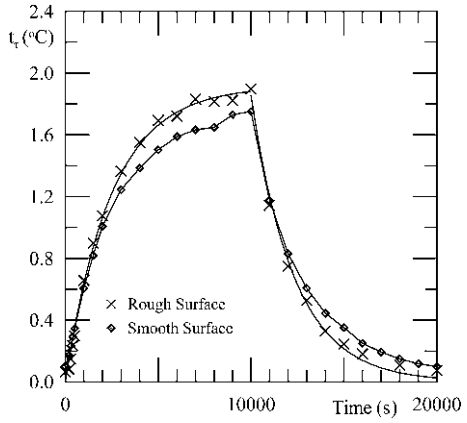

Fig. 14 Friction temperature for flow over smooth and rough wall

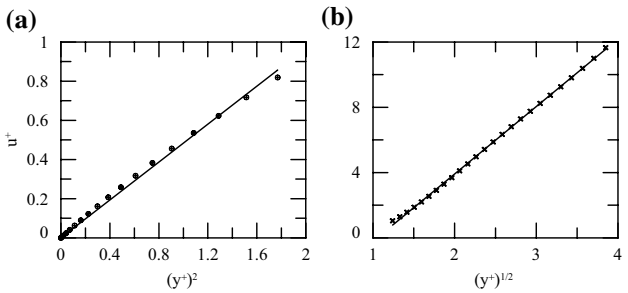

Fig. 15 Velocity profiles at the point of zero wall shear stress for the DNS data of Na and Moin [86]. **a** Solution of Goldstein ($u^+ = 0.484(y^+)^2$); **b** solution of Stratford ($u^+ = 4.125(y^+)^{1/2} - 4.332$)

The behavior of the friction temperature for a time varying wall heat flux is shown in Fig. 14. Stanton number follows from $S_t = (u_\tau/u_o)(t_\tau/(T_w - T_o))$.

6.11 Near wall approximate solutions for attached and separated flows over smooth surfaces

The structure of the separate turbulent boundary layer has been studied in Cruz and Silva Freire [44], Loureiro et al. [84], Loureiro et al. [85] and Loureiro and Silva Freire [47]. This section and the next summarize some of the results.

The action of an arbitrary pressure rise in the inner layers of a laminar or turbulent flow is to distort the velocity profile until it is balanced by the gradient of shear stress. At the wall, inertia forces are zero so that the momentum balance is expressed through the viscous and pressure terms.

For laminar flow, at a point of zero skin-friction the velocity profile must follow a y^2-profile at the wall. For turbulent flow, the fact that the local leading order equations must be dominated by viscous and pressure gradient effects implies immediately that this result remains valid.

In fact, in the viscous region the local governing equation can be written as:

$$\nu \partial^2_{yy} u = \rho^{-1} \partial_x p. \tag{147}$$

Two successive integrations of Eq. (147) and the fact that $\tau_w = 0$, give

$$u^+ = (1/2)\, y^{+2}, \tag{148}$$

with $u^+ = u/u_{pv}$, $y^+ = y/(\nu/u_{pv})$, $u_{pv} = ((\nu/\rho)\partial_x p)^{1/3}$.

In Eq. (148) the term $\partial_x p$ must be evaluated at $y = 0$. Hence, wall similarity solutions cannot be expressed in terms of the external pressure gradient.

For the turbulence dominated region, Stratford [7] wrote

$$\partial_y \tau_t = \partial_x p. \tag{149}$$

Two successive integrations of Eq. (149) together with the mixing length hypothesis and, again, the fact that at a separation point $\tau_w = 0$, give

$$u^+ = (2\varkappa^{-1})\, y^{+1/2}, \tag{150}$$

with u^+ and y^+ defined as in Eq. (148).

To find his solution Stratford used the condition $y = 0$, $u = 0$. Strictly speaking, this condition should not have been used since Goldstein's y^2-expression is the solution that is valid at the wall. Stratford also incorporated an empirical factor—β (=0.66)—to Eq. (150) to correct pressure rise effects on $\varkappa$.

Thus, we may conclude that, at a separation point, $\mathrm{ord}(u') = \mathrm{ord}(v') = \mathrm{ord}(u_{pv})$.

The DNS data of Na and Moin [86] are used in Fig. 15 to illustrate the solutions of Goldstein and Stratford. These solutions are given, respectively, by $u^+ = 0.484(y^+)^2$ and $u^+ = 4.125(y^+)^{1/2} - 4.332$ in the ranges $0.028 << y^+ << 1.33$ and $1.54 << y^+ << 14.82$.

The relevant velocities and length scales in the wall region for flows away and close to a separation point are then $(u_\tau, \nu/u_\tau)$ and $(u_{pv}, \nu/u_{pv})$, respectively.

An important result is that both relevant velocity scales—u_τ and u_{pv}—are contained in

$$\nu \partial^2_{yy} u + \partial_y(-\rho \overline{u'v'}) = \rho^{-1} \partial_x p. \tag{151}$$

In the limiting cases $\tau_w >> (y/\rho)(\partial_x p)$ and $\tau_w << (y/\rho)(\partial_x p)$, the scaling velocity tends to u_τ and $((\nu/\rho)\partial_x p)^{1/3}$, respectively, where $\partial_x p$ is to be considered at the wall.

To propose a characteristic velocity that is valid for the whole domain, Cruz and Silva Freire [44, 87] suggested to reduce Eq. (153) to an algebraic equation by considering $\mathrm{ord}(u') = \mathrm{ord}(v') = \mathrm{ord}(u_R)$ and $\mathrm{ord}(y) = ord(\nu/u_R)$, where the reference velocity, u_R, is to be determined from

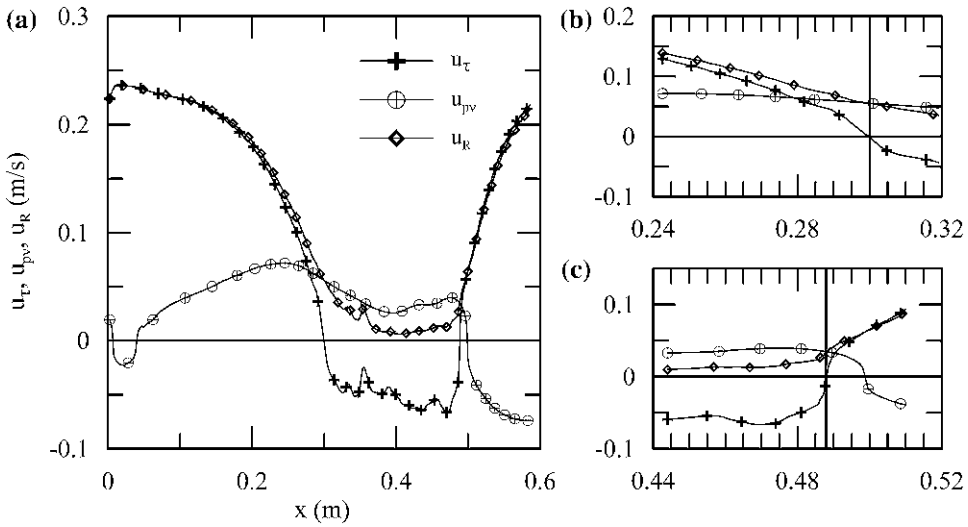

Fig. 16 Characteristic behavior of u_τ, u_{pv} and u_R for the flow of Na and Moin [86]. **a** Global behavior; **b** behavior near to the separation point; **c** behavior near to the re-attachment point

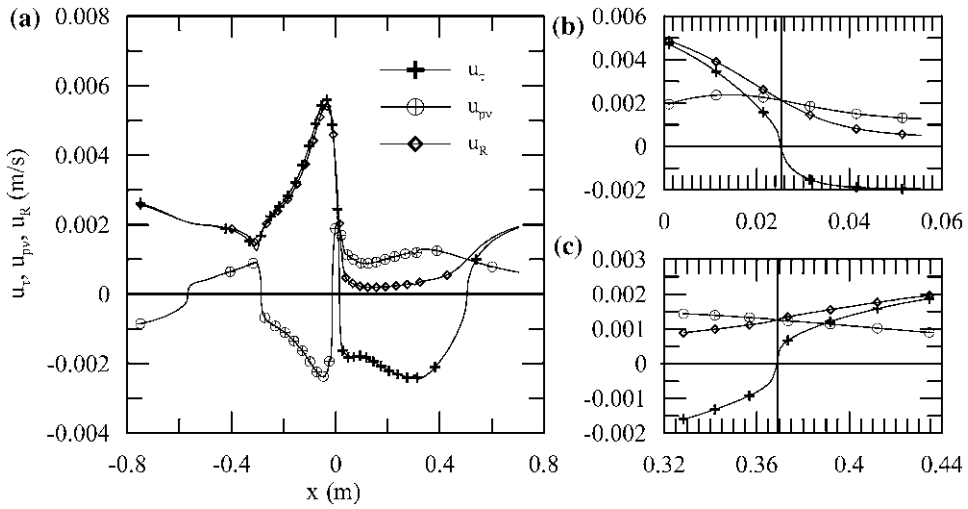

Fig. 17 Characteristic behavior of u_τ, u_{pv} and u_R for the flow of Loureiro et al. [85]. **a** Global behavior; **b** behavior near to the separation point; **c** behavior near to the re-attachment point

$$u_R^3 - (\rho^{-1}\tau_w)\, u_R - (\rho^{-1}\nu)\partial_x p = 0. \tag{152}$$

Equation (152) always presents, at least, one real root. When three real roots are obtained, the highest root must be considered.

Figures 16 and 17 show the variation of u_τ, u_{pv} and u_R according to the data of Na and Moin [86] and Loureiro et al. [85]. A negative value of u_τ indicates a region of reverse flow whereas a negative u_{pv} indicates that this parameter has been evaluated in a region of favorable pressure gradient. The results show the dominance of u_τ in regions of attached flow. Close to the separation and re-attachment points and in the region of reverse flow u_{pv} dominates. The ponderation furnished by u_r captures the relevant effects in all regions of the flow.

To find a solution over the entire viscous sub-layer, for attached as well as detached flow, we consider

$$\nu\partial^2_{yy}u + \partial_y(-\rho\overline{u'v'}) = \rho^{-1}\partial_x p. \tag{153}$$

The global solution of Eq. (153) should reduce, under the relevant limiting processes, to the local approximate solutions in the viscous and turbulent regions.

A double integration of Eq. (153) in the fully turbulent region ($\mu\partial^2_{yy}u \approx 0$) gives (see, e.g., Cruz and Silva Freire [44])

$$u = 2\varkappa^{-1}\sqrt{\Delta_w} + \varkappa^{-1}u_\tau \times \ln\left((\sqrt{\Delta_w} - u_\tau)/(\sqrt{\Delta_w} + u_\tau)\right) + C, \tag{154}$$

with $\Delta_w = \rho^{-1}\tau_w + (\rho^{-1}\partial_x p)y$.

Equation (154) can be used indistinctly in all flow regions—including regions of reverse flow—provided its domain of validity is respected and appropriate integration constants are determined. Many other different treatments of the lower boundary condition can be appreciated in literature. Loureiro et al. [84], for example, have investigated the numerical prediction of flows over two-dimensional,

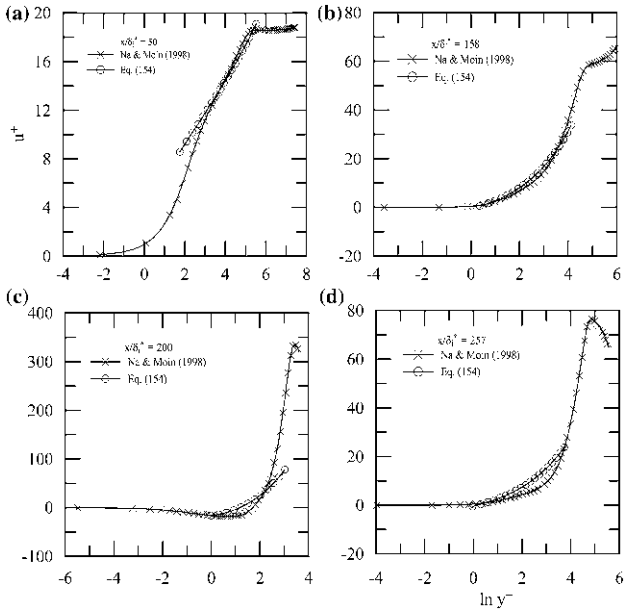

Fig. 18 Mean velocity profiles in wall coordinates according to the data of Na and Moin [86]. **a** $x/\delta_i^* = 50$; **b** 158 (position of flow separation); **c** 200; **d** 257 (position of flow re-attachment). δ_i^* = inlet displacement thickness

smooth, steep hills according to the above formulation and the formulations of Mellor [88] and of Nakayama and Koyama [89]. The standard κ–ϵ model was then used to close the averaged Navier–Stokes equations. The results were shown to vary greatly.

In general, however, Eq. (154) can be seen as a generalization of the classical law of the wall for separating flows. In the limiting case $(\partial_x p)y \ll \tau_w$, Eq. (154) reduces to the logarithmic expression

$$u^+ = \varkappa^{-1} \ln y^+ + b_m, \tag{155}$$

$$b_m = 2\varkappa^{-1} + \varkappa^{-1} \ln((u_{pv}^3/4u_\tau^3)e^{\varkappa C}). \tag{156}$$

Near a point of separation Stratford's solution is recovered.

Figure 18 shows the behavior of Eq. (154) in the several flow regions according with the DNS data of Na and Moin [86].

6.12 The separating thermal turbulent boundary layer

The similarity dependence of the thermal field for the inner layers of a turbulent flow can be generally expressed as (Cruz and Silva Freire [44])

$$\partial_y T = g(y, \rho, c_p, q_w, \partial_y u), \tag{157}$$

where c_p and q_w stand for the specific heat at a constant pressure and the local flux of heat at the wall.

Further dimensional considerations give

$$\partial_y T = B \frac{q_w}{\rho c_p} \frac{1}{(y^2 \partial_y u)} \tag{158}$$

where B is a constant still to be determined.

These equations lead to three different integration functions depending on the relative values of τ_w and $\mathrm{d}p_w/\mathrm{d}x$ (Cruz and Silva Freire [44]). The resulting equations (not shown here) are the law of the wall for the temperature boundary layer in separating flows. Under the appropriate limit processes the equations meet the expected behavior near and far away from a separation point. In fact, for the limit case, $|\tau_w/\rho| >> |(\mathrm{d}p_w/\mathrm{d}x)(y/\rho)|$, they reduce to the classical law of the wall logarithmic profile given by

$$\frac{T - T_w}{t_\tau} = \frac{1}{\varkappa_t} ln y^+ + c_t(P_r). \tag{159}$$

In the limit case $\tau_w \to 0$, they reduce to

$$\frac{T_w - T}{t_\tau} = \frac{1}{\varkappa_t} \frac{q_w}{\rho c_p} \frac{2}{\sqrt{\frac{1}{\rho}\frac{\mathrm{d}p_w}{\mathrm{d}x} y}} + c_t(x, P_r). \tag{160}$$

This equation has a functional form different from Stratford's law of the wall; this clearly characterizes the break down of the Reynolds analogy near to a separation point.

6.13 The asymptotic structure of a separating flow

The asymptotic structure of a separating turbulent boundary layer has been discussed in Cruz and Silva Freire [44] and Loureiro and Silva Freire [47]. The main discussion for the velocity field is shortly reproduced here. The discussion for the thermal field can be seen in Cruz and Silva Freire [44].

As the flow approaches a separation point the classical structure must break down since $u_\tau \to 0$. To account for the changes in the flow, we must consider Kaplun limits in x-direction.

Define

$$\begin{aligned} \hat{x} &= x_\Delta = x/\Delta(\epsilon), \\ \hat{y} &= y_\eta = y/\eta(\epsilon), \\ \hat{u}_i(x_\Delta, y_\eta) &= u_i(x, y) \end{aligned} \tag{161}$$

with $\Delta(\epsilon)$ and $\eta(\epsilon)$ defined on Ξ.

The idea is to approach the separation point by taking simultaneously the η- and Δ-limits at a fixed rate $\zeta = \Delta/\eta = \mathrm{ord}(1)$. Note that in regions where $\mathrm{ord}(\Delta) = \mathrm{ord}(\epsilon)$, $\mathrm{ord}(u_\tau) = \mathrm{ord}(u_{pv})$; under this condition, $\mathrm{ord}(\epsilon^2) = \mathrm{ord}(1/\epsilon R_e)$.

The resulting flow structure is given by continuity equation:

$$\mathrm{ord}(\hat{v}_i(x, y_\eta)) = \mathrm{ord}(\hat{u}_i(x, y_\eta)). \tag{162}$$

x-momentum equation:

$$\mathrm{ord}\Delta = \mathrm{ord}1 : \ \hat{u}_1 \partial_{x_\Delta} \hat{u}_1 + \hat{v}_1 \, \partial_{y_\eta} \hat{u}_1 + \partial_{x_\Delta} \hat{p}_1 = 0 \tag{163}$$

$$\mathrm{ord}\epsilon^2 < \mathrm{ord}\Delta < \mathrm{ord}1 : \ \hat{u}_1 \partial_{x_\Delta} \hat{u}_1 + \hat{v}_1 \, \partial_{y_\eta} \hat{u}_1 + \partial_{x_\Delta} \hat{p}_1 = 0 \tag{164}$$

$$\begin{aligned} \mathrm{ord}\epsilon^2 = \mathrm{ord}\Delta : \ & \hat{u}_1 \partial_{x_\Delta} \hat{u}_1 + \hat{v}_1 \partial_{y_\eta} \hat{u}_1 + \partial_{x_\Delta} \hat{p}_1 \\ & = -\partial_{x_\Delta} \overline{u_1'^2} - \partial_{y_\eta} \overline{u_1' v_1'} + \partial^2_{x_\Delta} \hat{u}_1 + \partial^2_{y_\eta} \hat{u}_1 \end{aligned} \tag{165}$$

$$\mathrm{ord}\Delta < \mathrm{ord}\epsilon^2 : \ \partial^2_{x_\Delta} \hat{u}_1 + \partial^2_{y_\eta} \hat{u}_1 = 0 \tag{166}$$

y-momentum equation:

$$\mathrm{ord}\Delta = \mathrm{ord}1 : \ \hat{u}_1 \, \partial_{x_\Delta} \hat{v}_1 + \hat{v}_1 \, \partial_{y_\eta} \hat{v}_1 + \partial_{y_\eta} \hat{p}_1 = 0 \tag{167}$$

$$\mathrm{ord}\epsilon^2 < \mathrm{ord}\Delta < \mathrm{ord}\,1 : \ \hat{u}_1 \partial_{x_\Delta} \hat{v}_1 + \hat{v}_1 \partial_{y_\eta} \hat{v}_1 + \partial_{y_\eta} \hat{p}_1 = 0 \tag{168}$$

$$\begin{aligned} \mathrm{ord}\epsilon^2 = \mathrm{ord}\Delta : \ & \hat{u}_1 \partial_{x_\Delta} \hat{v}_1 + \hat{v}_1 \, \partial_{y_\eta} \hat{v}_1 + \partial_{y_\eta} \hat{p}_1 \\ & = -\partial_{x_\Delta} \overline{u_1' v_1'} - \partial_{y_\eta} \overline{u_1'^2} + \partial^2_{x_\Delta} \hat{v}_1 + \partial^2_{y_\eta} \hat{v}_1 \end{aligned} \tag{169}$$

$$\mathrm{ord}\Delta < \mathrm{ord}\epsilon^2 : \ \partial^2_{x_\Delta} \hat{v}_1 + \partial^2_{y_\eta} \hat{v}_1 = 0 \tag{170}$$

The principal equations are Eqs. (165) and (169). They show that near to a separation point the two principal equations that were found for attached flow merge giving rise to a new structure dominated basically by two regions: a wake region (ord(η), ord(Δ) $> \epsilon^2$) and a viscous region (ord(η), ord(Δ) $< \epsilon^2$). These are regions governed by intermediate equations. Thus, matching between them cannot be achieved directly. The disappearance of the region dominated by the turbulence effects is noted. The principal equations recover the full Reynolds averaged Navier–Stokes equations.

The system of Eqs. (163)–(170) indicates that the pressure gradient effects become leading order effects for orders higher than ord(ϵ^2) = ord(Δ). Thus, at about ord(x / l) = ord(Δ) = ord(ϵ) we should have ord(u_τ) = ord(u_{pv}), so that these terms furnish first-order corrections to the mean velocity profile.

The asymptotic structure of the flow is illustrated through Fig. 19, where the thickness scalings $(\epsilon R_e)^{-1}$ and ϵ^2 are shown in semi-log form for the data of Na and Moin [86]. Far upstream of the separation point a classical two-layered structure is found with thickness $(\epsilon R_e)^{-1}$ representing a leading order balance between the laminar and turbulent stresses. Thickness ϵ^2 represents the balance between the turbulent stress and inertial effects. As the separation point is approached, $(\epsilon R_e)^{-1}$ and ϵ^2 exhibit opposed variations. The steady increase of $(\epsilon R_e)^{-1}$ together with the steady decrease of ϵ^2 provokes a continuous narrowing of the turbulence dominated region up to the point where it becomes completely extinguished. This happens exactly at the position of flow separation. The implication is that at this position the near wall flow solution is viscous dominated so that a Goldstein solution prevails up to $y \approx (\epsilon R_e)^{-1}$. On the other hand, the region ord(η) = ord(y / l) = ord(ϵ^2) defines the flow position where Stratford's solution is supposed to hold. Above this point, an inertia dominated solution is to be found.

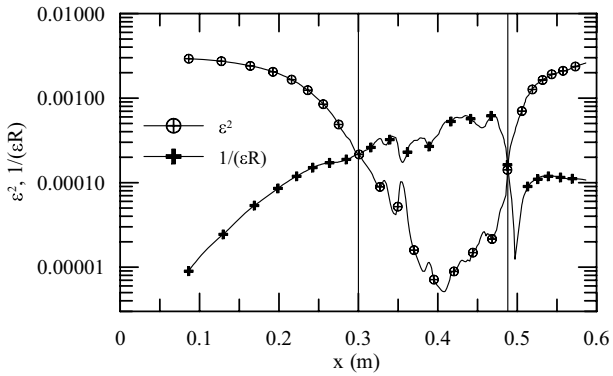

Fig. 19 Diagram of the asymptotic structure of the turbulent boundary layer for separating and reattaching flows; DNS data of Na and Moin [86]

6.14 Near wall approximate solutions for attached and separated flows over rough surfaces

The arguments that lead to Stratford's law are based on the fundamental hypothesis that near a separation point a fully turbulent region can be identified in the flow. This consideration remains valid for flow over a rough surface. The direct implication is that the procedure that resulted in the derivation of Eq. (150) can be repeated for flow over rough surface but with $y^p = (y - d)/y_0$ and $u_{pv} = ((y_0/\rho)\partial_x p)^{1/2}$. The integration constant must also be determined so as to correctly account for the roughness effects.

The derivation of Eq. (154) has disregarded any detail of the wall roughness. This equation is, in fact, supposed to be valid not in the region adjacent to the wall where the complicated flow around the individual roughness elements is apparent, but, instead, in a region where the flow statistics are spatially homogeneous. Hence, inasmuch as for the classical law of the wall, the characteristics of the rough surface must enter the problem through the integration constant C. In addition, the coordinate system must be displaced by d. The immediate conclusion is that Eq. (154) can be used to model separating flow over a rough surface provided d and C are adequately modeled.

Parameter C is a general function of τ_w, $\partial_x p$ and y_0 that must be determined by a consistent analysis of experimental data. However, an estimate of its functional form might be obtained by considering the limiting behavior of Eq. (154) as $\tau_w \gg (\partial_x p)y$. The resulting expression is

$$C = \varkappa^{-1} u_\tau \left[\ln \left(4u_\tau^2 / ((\rho^{-1} \partial_x p) y_0) \right) - 2 \right]. \tag{171}$$

This parametrization scheme was first presented in Loureiro et al. [90]. A detailed comparison with experimental data has been presented in Loureiro et al. [91] and Loureiro and Silva Freire [92].

The mean velocity profile at a point of zero wall shear stress for turbulent flow over a rough surface is shown in Fig. 20.

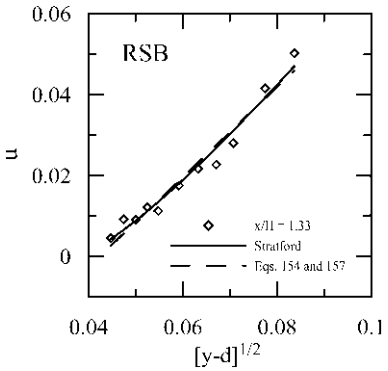

Fig. 20 Stratford profiles. y is plotted in m; u in ms^{-1}. Data of Loureiro et al. [90, 91]. *RSB* indicates the type of rough surface [90]

Equation (154) together with the parametrization scheme provided by Eq. (171) is tested in Fig. 21.

6.15 Interaction between shock waves and transpired turbulent boundary layers

The general configuration of the flow around transonic aerofoil has been discussed by Nieuwland and Spee [93]. For M_o slightly higher than the critical Mach number (M_{cr}), a weak shock wave develops on the aerofoil and a small supersonic region forms ahead of the shock. As M_o increases the strength of the shock increases inducing eventually boundary layer flow separation.

To prevent flow separation—and consequently the occurrence of large wave drag increase—the shapes of conventional aerofoils have been modified. One suggestion is to make the surface in the vicinity of the separation porous. Transpiration can then be used to control the shock/boundary layer interaction (SBLI). A passive control technique consists of placing a porous surface over a plemun chamber in the interaction region. The higher pressure downstream of the shock forces fluid into the cavity and out ahead of the shock.

Nagamatsu et al. [94] studied a supercritical aerofoil with a uniform perforated surface. A porosity of 2.8 % of the total area surface resulted in a drag decrease of 46 % for $M_o = 0.84$.

Next, we discuss the application of perturbation methods to the description of the interaction between shock waves and transpired turbulent boundary layers.

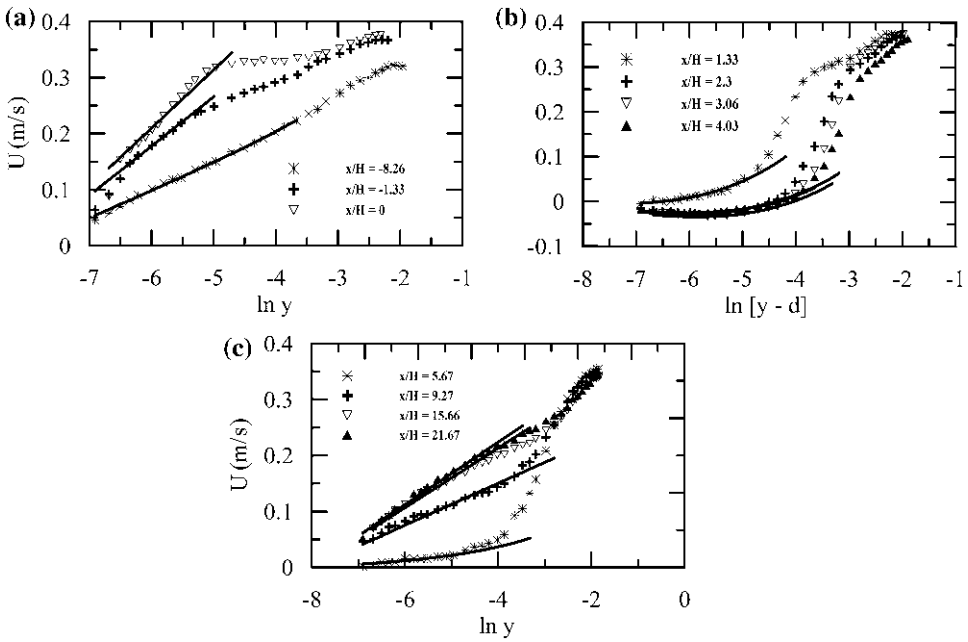

Fig. 21 Turbulent boundary layer flow over a steep hill, Loureiro et al. [90, 91]. Flow conditions RSB. x is referred to the center of the hill, H denotes the height of the hill. **a** Upstream flow, **b** reverse flow, **c** downstream flow

6.15.1 Matched asymptotic expansions analysis

An important attempt at developing a rational theory to explain the interaction problem between a shock wave and a turbulent boundary layer was made by Lighthill in 1953. Lighthill [95] identified the physical mechanisms of the interaction and recognized that in most of the boundary layer the stream-wise pressure gradient is large compared to the shear stress so that the local interaction can be described by the inviscid flow equations. Most of the details in Lighthill's theory are correct for laminar flow. However, for turbulent flow modifications need to be made to render the theory compatible with the asymptotic structure of the boundary layer.

The three basic parameters of the problem are the free stream Mach number (M_o), the non-dimensional friction velocity ($u^*_{\tau o} = u_\tau/u_o$) and the Reynolds number (R_e). The last two parameters are correlated through $u^*_{\tau o} = \mathrm{ord}(\ln R_e)^{-1}$. Melnik [96] classified the structure of the interacting field according to the order of magnitude of the parameter

$$\chi_\tau = \frac{M_o^2 - 1}{u^*_{\tau o}} \tag{172}$$

Four distinct cases were listed:

1. very weak shock wave, $\chi_\tau \to 0$,
2. weak shock wave, $\chi_\tau = \mathrm{ord}(1)$,
3. moderate shock wave, $\chi_\tau \to \infty$, $M_o \to 1$,
4. strong shock wave, $\chi_\tau \to \infty$, M_o fixed.

The present account discusses the case of a moderate shock wave.

Following previous studies of the problem by Messiter [97] and Silva Freire [49], in the interaction region we separate the asymptotic expansions for the solution into rotational and irrotational parts. The asymptotic structure of the flow is shown in Fig. 22.

We introduce the two small parameters

$$\epsilon^* = \frac{u_o}{a^*} - 1, \tag{173}$$

and

$$u^*_\tau = \frac{1}{a^*}\sqrt{\frac{\tau_w}{\rho_w}}, \tag{174}$$

where a^* is the critical sound speed in the external flow just ahead of the shock, τ_w is the shear stress at the wall, and ρ_w is the density at the wall.

The solution in the defect layer is shown by Messiter [97] to be governed by inviscid effects. The complete

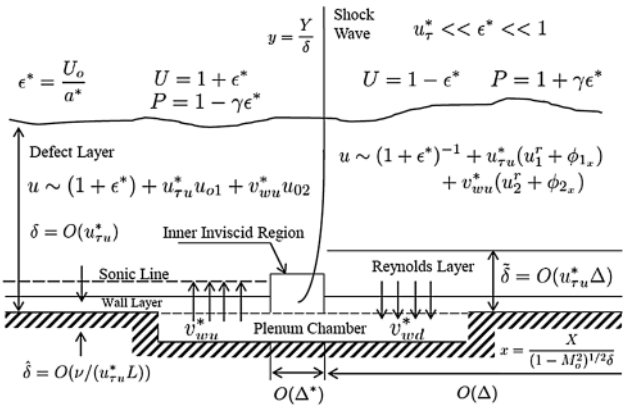

Fig. 22 Flow structure for the interaction of shock waves and transpired turbulent boundary layers

analysis is presented by Silva Freire [49]. Here, only the solution for the pressure at the wall is shown, that is,

$$\begin{aligned}\frac{p_w(x)}{p_e} &= 1 + \gamma\left[2\epsilon^* + (2\gamma - 1)\epsilon^{*2}\right] \\ &\quad - \gamma\left[1 + \gamma\epsilon^* + \epsilon^{*2}[(\gamma-1)^2 + 2^{-1}(7\gamma - 7)]\right] \\ &\quad \times \left[u^*_{\tau u}\varphi_{1x}(x,0) + v^*_{wu}\varphi_{2x}(x,0)\right]\end{aligned} \tag{175}$$

where the subscript u indicates an upstream quantity,

$$p_e = 1 - \gamma\epsilon^* + 2^{-1}\gamma\epsilon^{*2} \tag{176}$$

and

$$\begin{aligned}\varphi_{ix}(x,y) &= -\frac{4}{\pi}\left[1 + (\gamma-1)\epsilon^*\right. \\ &\quad \left. + \left[\gamma\left[\gamma - 0.5\right] + 3\right]\epsilon^{*2}\right] \\ &\quad \times \int_0^\infty \frac{x u_{oi}(y)}{x^2 + (y-\eta)^2}\mathrm{d}\eta\end{aligned} \tag{177}$$

with $u_{oi}(y) =$ mean velocity profiles in the defect layer.

The intermediate layer (*Reynolds layer*) is governed by the standard boundary layer equations. Analytical solutions to all flow parameters can be found through consideration of the mixing length closure hypothesis. The resulting equations and respective solutions, unfortunately, are too complicate and long to be shown here. The solutions in the intermediate layer must satisfy seven local equations and match with the inner solutions, which add eleven extra constraints to the problem.

The wall layer is solved by assuming $\hat{u}(x,\hat{y})$ to be decomposed as

$$\hat{u}(x,\hat{y}) = u^*_{\tau u}\hat{u}_{01}(\hat{y}) + v^*_{wu}\hat{u}_{02}(\hat{y}) + v_{wd}\hat{u}_{03}(\hat{y}) \tag{178}$$

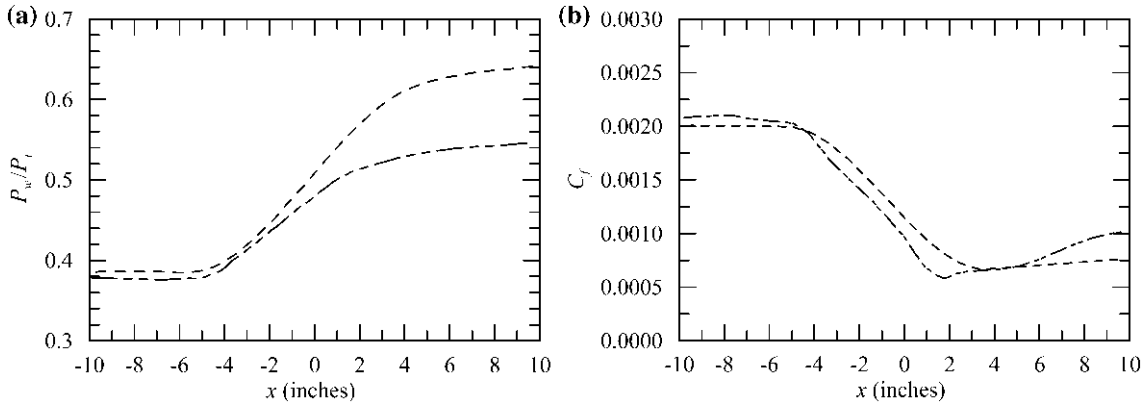

Fig. 23 Solid wall. Predictions of pressure and skin-friction for the interaction of a shock wave and a turbulent boundary layer at Mach number 1.27. — - - — experiment; – – – theory

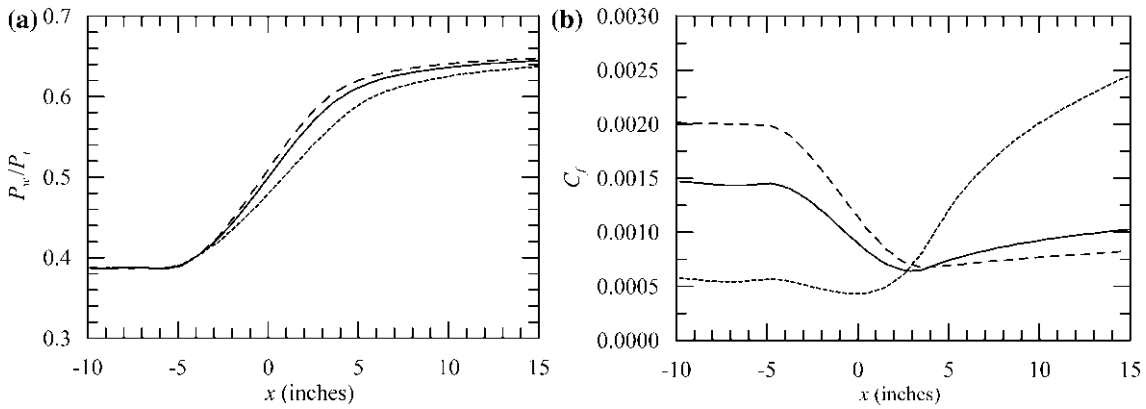

Fig. 24 Porous wall. Predictions of pressure and skin-friction for the interaction of a shock wave and a turbulent boundary layer at Mach number 1.27 for three porosities $\sigma = 0.0, 0.005, 0.02$

where the hat is used to denote a wall solution, the subscript d to denote a downstream quantity, and, in general, $u^*_{\tau d}$ is a function of x, ϵ^*, $u^*_{\tau u}$, v^*_{wu}, v^*_{wd} and $\hat{u}_{0i}$ represents the mean velocity profiles that are to be matched to the intermediate layer solution.

The wall solution gives rise to a skin-friction equation that can be written as

$$u^*_{\tau u}(x) = u^*_{\tau u}\Bigg[1 + a_1\epsilon^* + a_2\epsilon^{*2} + u^*_{\tau u}u_1(x) + \epsilon^* u^*_{\tau u}\frac{1}{\varkappa}\ln\frac{\delta}{\hat{\delta}}u_{1l}(x) + \epsilon^* u^*_{\tau u}u_{11}(x)\Bigg] + \Bigg[v^*_{wu}u_2(x) + \epsilon^* v^*_{wu}\ln^2\frac{\delta}{\hat{\delta}}u_{2l}(x) + \epsilon^* v^*_{wu}\ln\frac{\delta}{\hat{\delta}}u_{2m}(x) + v^*_{wu}\epsilon^* u_{22}(x)\Bigg] \quad (179)$$

where a_1, a_2, $u_1(x)$, $u_{1l}(x)$, $u_{11}(x)$, $u_2(x)$, $u_{2l}(x)$, $u_{2m}(x)$ and $u_{22}(x)$ are defined in Silva Freire [49].

Results provided by Eqs. (175) and (179) for the experimental flow conditions of Sawyer and Long [98] for $M_o = 1.27$ are shown in Fig. 23.

The effects of wall transpiration are illustrated in Fig. 24 for porosities that result in weak ($\sigma = 0.005$, $F = (\rho_w v_w)/(\rho a^*) = 0.001$) and moderate ($\sigma = 0.02$, $F = 0.004$) injection rates. The increase in porosity results in an overall decrease the distributed pressure, a decrease of C_f upstream of the shock wave and a sharp increase of C_f downstream of the shock.

6.15.2 Double limits for the interaction problem

To find the asymptotic structure of the flow in the interaction region through Kaplun limits, we consider the following stretching transformation,

$$x_\Delta = \frac{x}{\Delta(\epsilon^*)},$$
$$y_\eta = \frac{y}{\eta(\epsilon^*)}, \qquad \hat{u}_i(x_\Delta, y_\eta) = u_i(x, y), \tag{180}$$

with $\Delta(\epsilon^*)$ and $\eta(\epsilon^*)$ defined on Ξ.

The flow velocity components are described through

$$u = 1 + \epsilon^* u_\alpha(x, y) + u_\tau^* u_\beta(y), \tag{181}$$

$$v = \epsilon^{*3/2} v_\alpha(x, y), \tag{182}$$

where u_α and u_β represent, respectively, the irrotational and the rotational parts of the flow.

Upon substitution of Eqs. (181) and (182) into the equations of motion, and passage of the η-limit process onto the resulting equations, we get for the x-momentum equation:

$$\text{ord } \eta = 1 : \frac{\partial}{\partial x_\Delta}\left(\rho \hat{u}_\alpha \hat{u}_\alpha\right) + \frac{\partial}{\partial y_\eta}\left(\rho \hat{u}_\alpha \hat{v}_\alpha\right) = -\frac{\partial \hat{p}_\alpha}{\partial x_\Delta}, \tag{183}$$

$$\text{ord } u_\tau^{*2} < \text{ord } \eta < 1 : \frac{\partial}{\partial x_\Delta}\left(\rho \hat{u}_\alpha \hat{u}_\alpha\right) + \frac{\partial}{\partial y_\eta}\left(\rho \hat{u}_\alpha \hat{v}_\alpha\right) = -\frac{\partial \hat{p}_\alpha}{\partial x_\Delta}, \tag{184}$$

$$\text{ord } \eta = \text{ord } u_\tau^{*2} : \frac{\partial}{\partial x_\Delta}\left(\rho \hat{u}_\alpha \hat{u}_\alpha\right) + \frac{\partial}{\partial y_\eta}\left(\rho \hat{u}_\alpha \hat{v}_\alpha\right) = -\frac{\partial \hat{p}_\alpha}{\partial x_\Delta} + \frac{\partial}{\partial y_\eta}\left(-\overline{\rho \hat{u}'_\alpha \hat{v}'_\alpha}\right), \tag{185}$$

$$\text{ord } 1/R_e u_\tau^* < \text{ord } \eta < \text{ord } u_\tau^{*2} : \frac{\partial}{\partial y_\eta}\left(-\overline{\rho \hat{u}'_\alpha \hat{v}'_\alpha}\right) = 0, \tag{186}$$

$$\text{ord } \eta = \text{ord } 1/R_e u_\tau^* : \frac{\partial}{\partial y_\eta}\left(-\overline{\rho \hat{u}'_\alpha \hat{v}'_\alpha}\right) + \frac{\partial^2 \hat{u}_\beta}{\partial y_\eta^2} = 0, \tag{187}$$

$$\text{ord } \eta < \text{ord } 1/R_e u_\tau^* : \frac{\partial^2 \hat{u}_\beta}{\partial y_\eta^2} = 0. \tag{188}$$

Since we are considering the flow in the interaction region, in passing the η-limit we have taken $\text{ord}(\Delta) = \text{ord}(\epsilon^*)$. The other equations, continuity, energy and state, do not give any contribution to the asymptotic structure. In fact, Silva Freire [51] has shown that if the full energy equation is considered, and the concepts of section two are applied to the full set of equations, then the overlap domains of the velocity field and of the temperature field will coincide.

The continuity equation simply implies that

$$\text{ord}(v) = \frac{\eta}{\Delta}\text{ord}(u). \tag{189}$$

The classical two-deck structure of the turbulent boundary layer is then clearly seen from Eqs. (183)–(188). Note that Eqs. (185) and (187) are the principal equations; their overlap domain is identical to the overlap domain determined for the incompressible flow case.

In the vicinity of the shock wave, however, the asymptotic structure must change. The strong pressure gradient imparted to the boundary layer by the shock wave alters the balance of terms in the equations of motion, giving rise to a new structure where for most of the boundary layer the problem becomes an inviscid one. The need for the establishment of an inviscid rotational flow model for the description of the interaction has been recognized since Lighthill [95] proposed his linearized solution for the laminar problem. The result is that all recent theories advanced for the turbulent problem must somehow accommodate the inviscid rotational interaction model without contradicting the features of the turbulent flow. To overcome this difficulty, the theories of Melnik and Grossmann [53], Adamson and Feo [54], Messiter [97] and Liou and Adamson [48] consider the introduction of a blending region in the interaction region. The blending layer is, in fact, nothing else but the turbulent region defined by the overlap domain and derived by our asymptotic analysis of the problem. The absence of an equation similar to Eq. (186) in the matched asymptotic expansions method is the main reason for the difficulties this method presents. Likewise, this is the reason why the structure depicted by Eqs. (185)–(188) can deal with the interaction problem.

To take into account for the presence of the shock wave, we pass the Δ-limit process onto Eqs. (183)–(188). The result is:

$$\text{ord } \Delta = \text{ord } \epsilon^* : \frac{\partial}{\partial x_\Delta}\left(\rho \hat{u}_\alpha \hat{u}_\alpha\right) + \frac{\partial}{\partial y_\eta}\left(\rho \hat{u}_\alpha \hat{v}_\alpha\right) = -\frac{\partial \hat{p}_\alpha}{\partial x_\Delta}, \tag{190}$$

$$\text{ord } \epsilon^*/R_e u_\tau^{*3} < \text{ord } \Delta < \text{ord } \epsilon\eta/u_\tau^{*2} : \frac{\partial}{\partial x_\Delta}\left(\rho \hat{u}_\alpha \hat{u}_\alpha\right) + \frac{\partial}{\partial y_\eta}\left(\rho \hat{u}_\alpha \hat{v}_\alpha\right) = -\frac{\partial \hat{p}_\alpha}{\partial x_\Delta}, \tag{191}$$

$$\text{ord}\ \Delta = \text{ord}\ \epsilon^*/R_e u_\tau^{*3} : \frac{\partial}{\partial x_\Delta}\left(\rho \hat{u}_\alpha \hat{u}_\alpha\right) + \frac{\partial}{\partial y_\eta}\left(\rho \hat{u}_\alpha \hat{v}_\alpha\right) = -\frac{\partial \hat{p}_\alpha}{\partial x_\Delta} + \frac{\partial}{\partial y_\eta}\left(-\overline{\rho \hat{u}'_\alpha \hat{v}'_\alpha}\right) + \frac{\partial^2 \hat{u}_\beta}{\partial y_\eta^2}, \tag{192}$$

$$\text{ord}\ \Delta < \text{ord}\ \epsilon^*/R_e u_\tau^{*3} : \frac{\partial^2 \hat{u}_\beta}{\partial y_\eta^2} = 0. \tag{193}$$

The change in the asymptotic structure of the flow in the interaction region is noticeable from the above equations. In particular, we note that as the shock is approached, that is, as the order of magnitude of Δ increases, the validity domain of the outer principal equation changes position until the two principal equations merge at $(\Delta, \eta) = (\epsilon^*/(u_\tau^{*3} R_e), 1/(u_\tau^* R_e))$. Indeed, as shown by the calculations, at the beginning of the interaction the outer principal equation is positioned at $(\Delta, \eta) = (\epsilon^*, u_\tau^2)$. However, as the order of magnitude of η varies from u_τ^{*2} to $1/u_\tau^* R_e$, this equation moves along the path $(\epsilon^* \eta/u_\tau^{*2}, \eta)$ until reaching the point $(\epsilon^*/(u_\tau^{*3} R_e), 1/(u_\tau^* R_e))$. The flow structure is then shown to reduce from a classical two-deck structure to a one deck structure near to the foot of the shock wave. According to these results, there is a region at the foot of the shock where the full boundary layer equations are recovered.

The flow diagram defined by the above analysis is shown in Fig. 25. A comparison with the experimental data of Sawyer and Long [98] for Mach numbers 1.37 is shown in Fig. 26.

Figure 26 reproduces, from the experimental data, a map which indicates the dominant region of every term in the equations of motion. The meaning of the shades in gray is clear. Thus, the farthest from the wall tone corresponds to the inertia and pressure gradient terms, the intermediate tone to the turbulent terms and the remaining tone to the viscous terms. The shock wave is located at $x = 0$. Note, as predicted by the asymptotic theory, the complete dominance of the inertia and pressure terms in the vicinity of the shock. The consequence is that the phenomenon is, for most of the interaction region, and, to a leading order, governed by inviscid equations.

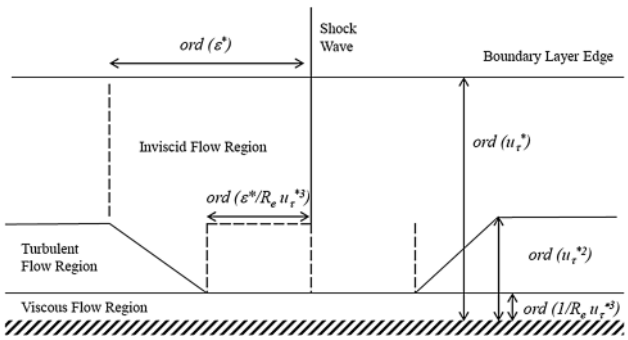

Fig. 25 Flow diagram for the interaction of a shock wave and a turbulent boundary layer

6.16 Unsteady wall layer model for the velocity profile in turbulent flows

Attempts to incorporate the structure of organized motions into near wall analytical models were given important contributions by Bark [99], Hatziavramidis and Hanratty [100], Chapman and Kuhn [101], Walker et al. [102] and Landahl [103]. These authors advanced modeling theories based on very different arguments between each other that were completely original at the time they were proposed. Walker et al. strived to develop an analytical solution for the time-dependent

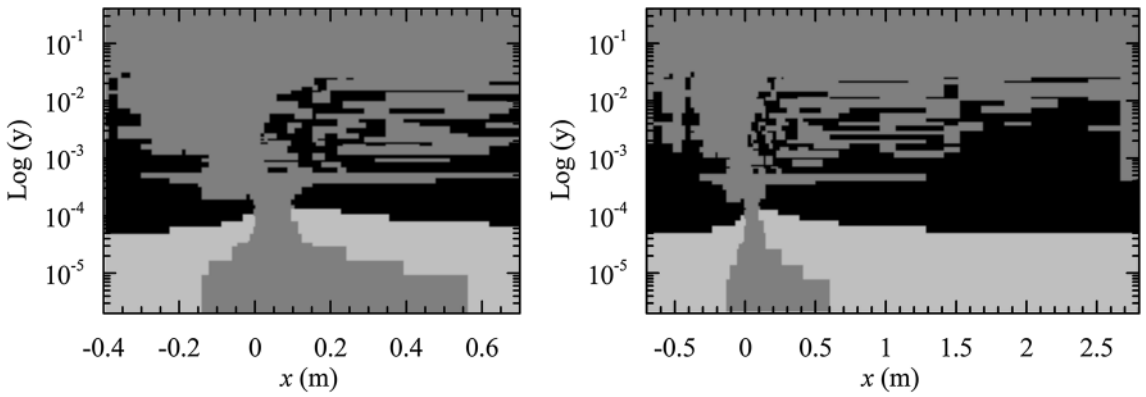

Fig. 26 Experimental validation for the flow diagram representing the interaction of a shock wave and a turbulent boundary layer. Data of Sawyer and Long [98]. Mach number 1.37. *Left* local view. *Right* global view of interaction

velocity profile from asymptotic arguments and similarity solutions of a non-homogeneous diffusion equation.

The model of Walker et al. [102] was formulated in terms of the dynamics of the time-dependent wall layer flow. A simplified set of the Navier–Stokes (N.-S.) equations was obtained to describe the unsteady flow in the wall layer during a quiescent period. Following the description generally found in the literature, the flow dynamics is considered to be dominated by two features: wall layer streaks and the bursting phenomenon. The streaks are elongated in the flow direction, typically have a length of the order of $1000\nu/u_\tau$ and can be observed over a large characteristic time, the quiescent period. To determine the mean velocity profile in the wall layer, a time average of the leading order instantaneous velocity was performed over the average period between bursts, which is considered to be approximately equal to the duration of the quiescent period.

Mikhailov and Silva Freire [104] reviewed the physical and mathematical validity domain of the model of Walker et al. [102]. The definitions of the instantaneous and mean velocity profiles, as introduced by Walker et al., depend on the determination of four unknowns, the average period between bursts (T_B^+), the origin of time (t_0^+), a constant of integration of the time-dependent equation (A_0) and the local pressure gradient (p^+). Once one of the parameters is specified, say, p^+, a set of three non-linear equations must be solved to furnish T_B^+, t_0^+ and A_0. These parameters must be real and satisfy $T_B^+ > t_0^+$. In Walker et al. [102] no comments were made regarding any possible limitation on the value of p^+. The attempts of Mikhailov and Silva Freire [104] to find a feasible domain $p^+_{\min} \le p^+ \le p^+_{\max}$ from the expressions shown in Walker et al. [102] failed. In fact, it was discovered that two terms are missing in Eq. (63) of Walker et al. [102].

The work of Mikhailov and Silva Freire [104] discusses in detail all similarity solutions for the homogeneous diffusion differential partial equation presented in Walker et al. [102]. Also, a new treatment is introduced whereby the pressure term is included as a non-homogeneous contribution. To permit fast computations, interpolation functions were generated from initial and boundary value problems, to represent the special function Ξ (Walker et al. [102]) and its derivatives (see Mikhailov and Silva Freire [105]), based on original identities for the hypergeometric functions ${}_1F_1$ and ${}_pF_p$. An explicit parameterization is presented for T_B^+, t_0^+ and A_0 in terms of p^+.

The time-mean structure of the flow in Walker et al. [102] is based on the classical two-layered asymptotic analyses of large Reynolds number turbulent boundary layer flow. Solutions are then developed in terms of the two small parameters, R_e^{-1} and u_τ^* $(=u_\tau/u_o)$.

The full details of the analysis of Walker et al. are omitted here; they can be found in Mikhailov and Silva Freire [104] or in the original paper. The leading order governing equations of the unsteady flow in the wall layer during a quiescent period were shown by Walker et al. [102] to be given by

$$\frac{\partial u_0}{\partial t^+} = -p^+ + \frac{\partial^2 u_0}{\partial y^{+2}} + M(y^+, t^+) \tag{194}$$

with

$$M = -\frac{\partial p_0}{\partial \tilde{x}} - \frac{\pi}{\lambda^+}\sum_{n=1}^{\infty} m \frac{\partial (u_m f_m)}{\partial y^+} \tag{195}$$

Equation (194) appears in Walker et al. (as Eq. 27) with an obvious typographical error. The term $\partial u_0/\partial t^+$ was misprinted as $\partial u_0/\partial y^+$. In fact, the time dependency on Walker et al.'s model is only accounted for by the term $\partial u_0/\partial t^+$.

The set of Eqs. (194) and (195) is a coupled system of non-linear equations that has to be solved numerically. The forcing function M depends on a pressure term and must be determined from the time-dependent motions in the outer layer and on further terms arising from the evolution of the other modes. Mikhailov and Silva Freire [104] shown that under the appropriate boundary conditions, Eqs. (194) and (195) can be solved to give

$$\begin{aligned} u_0 = {} & [(a_0/4)\log\tau + A_0]\operatorname{erf}\eta \\ & + (2a_0/\pi)\,\Xi(\eta) - p^+\tau \\ & \times \left[1 - \frac{8}{\sqrt{\pi}} e^{-\eta^2}\,\text{HermiteH}(-3,\eta)\right] \end{aligned} \tag{196}$$

This expression depends on four unknown parameters—a_0, A_0, t_0^+ and T_B^+—which must be specified for prescribed pressure gradients, p^+. Walker et al. [102] proposed to determine these parameters by computing the time average of u_0 and forcing the asymptotic form of the resulting expression in the limit of high y^+ to follow a logarithmic behavior so that

$$a_0 = \frac{2}{\varkappa} \tag{197}$$

$$A_0 = C_i + p^+ t_0^+ + \frac{1}{2}p^+ T_B^+ - \frac{\gamma_0}{2\varkappa} + \frac{\ln 2}{\varkappa} \tag{198}$$

$$\begin{aligned} 4p^+\varkappa((t_0^+)^{3/2} - (t_0^+ + T_B^+)^{3/2}) + 3(-\sqrt{\pi}\varkappa T_B^+ \\ - \sqrt{t_0^+}(-2 + 2A_0\varkappa + \ln(t_0^+)) \\ + \sqrt{t_0^+ + T_B^+}(-2 + 2A_0\varkappa \\ + \ln(t_0^+ + T_B^+))) = 0 \end{aligned} \tag{199}$$

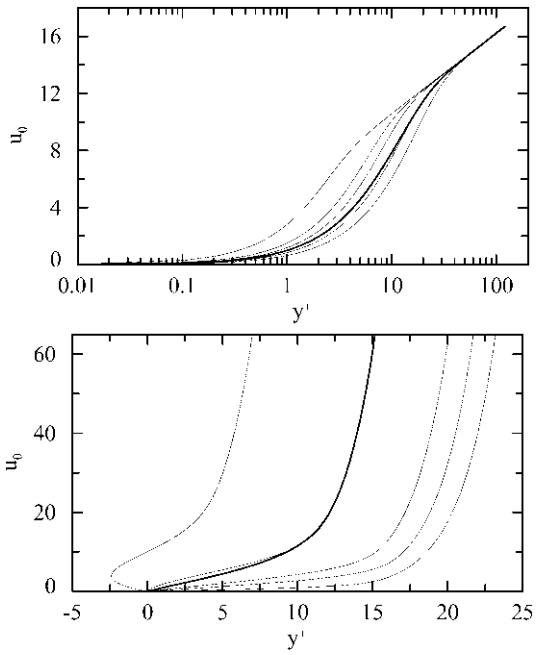

Fig. 27 Mean (*thick line*) and instantaneous velocity profiles for $p^+ = 0$ and 0.5 ($t^+/T_B^+ = 0.01, 0.1, 0.2, 0.5, 1$)

$$\left(A_0 - \frac{2}{\varkappa}\right)\left(\frac{1}{\sqrt{t_0^+ + T_B^+}} - \frac{1}{\sqrt{t_0^+}}\right) + 2p^+\left(\sqrt{t_0^+} - \sqrt{t_0^+ + T_B^+}\right) + \frac{1}{2\kappa}\left(\frac{\ln(t_0^+ + T_B^+)}{\sqrt{t_0^+ + T_B^+}} - \frac{\ln t_0^+}{\sqrt{t_0^+}}\right) = 0 \tag{200}$$

Equations (198), (199) and (200) can be solved to yield A_0, t_0^+ and T_B^+. They specify a system of transcendental non-linear algebraic equations that needs to be solved numerically.

The mean and instantaneous velocity profiles for $p^+ = 0$ and 0.5 are shown in Fig. 27. The logarithmic behavior of all profiles for large y^+ must be observed. Since all instantaneous profiles are required to tend to the same steady solution for large y^+, their average is objectively that solution. For small values of y^+ solutions are dominated by the error function, *erf*, for large y^+ solutions are dominated by the special function, Ξ.

To find parameters A_0, t_0^+ and T_B^+ the software Mathematica^{TM} was used. Solutions were found with 25 precision digits. Given the physical and mathematical constrains, the feasible domain of Walker et al.'s model was found to be $p^+ \in [-0.025, 41.886]$. However, if as a further requirement, the model of Walker et al. [102] is asked to furnish only positive derivatives at the wall for the instantaneous velocity, the feasible domain is reduced to $p^+ \in [-0.025, 0.104996]$.

Provided a flow representation is required in the interval $p^+ \in [-0.010, 0.104996]$, the following parameterization can be used:

$$A_0 = A_{03}(p^+)^3 + A_{02}(p^+)^2 + A_{01}p^+ + A_{00} \tag{201}$$

with $A_{03} = 260.0$, $A_{02=-177.7}$, $A_{01} = 51.3$, $A_{00} = 6.0$ and a maximum relative error of 0.5 %;

$$T_B^+ = T_{B2}(p^+)^2 + T_{B1}p^+ + T_{B0} \tag{202}$$

with $T_{B2} = 719.0$, $T_{B1} = -383.7$, $T_{B0} = 103.1$ and a maximum relative error of 1.5 %;

$$t_0^+ = \frac{t_{01}}{(t_{02} + (p^+))^2} + t_{00} \tag{203}$$

with $t_{01} = 0.000646$, $t_{02} = 0.0319$, $t_{00} = -0.0231$.

The set of Eqs. (196) and (201) through (203) permits a straightforward implementation of the model of Walker et al. [102] in a domain that is physically and mathematically meaningful.

6.17 Logarithmic solutions for non-Newtonian purely viscous fluids

The turbulent flow of non-Newtonian power-law fluids over smooth walls was studied by Metzner and Reed [106] and Dodge and Metzner [107]. The analysis leads to the introduction of a generalized Reynolds number defined by

$$N_R = \frac{D^n U^{2-n}\rho}{K}, \tag{204}$$

where D = pipe diameter, U = mean flow velocity, ρ = fluid density, and K and n express the relationship between shear stress and shear rate, that is,

$$\tau = K\left(\frac{-\mathrm{d}u}{\mathrm{d}r}\right)^n = K\left(\frac{-\mathrm{d}u}{\mathrm{d}r}\right)^{n-1} \times \left(\frac{-\mathrm{d}u}{\mathrm{d}r}\right) = \mu\left(\frac{-\mathrm{d}u}{\mathrm{d}r}\right). \tag{205}$$

The viscous layer solution for a power-law fluid can be found from a simple integration of the viscous layer approximate equation,

$$\frac{\partial \tau}{\partial y} = \frac{\partial}{\partial y}\left(K\left(\frac{\mathrm{d}u}{\mathrm{d}y}\right)^n\right) = 0, \tag{206}$$

so that,

$$\frac{u}{u_\tau} = \frac{y}{\left(Ku_\tau^{n-2}/\rho\right)^{1/n}}, \tag{207}$$

or else, using the usual notation,

$$u^+ = y^+. \tag{208}$$

Thus, it is follows from Eq. (207) that the viscous layer relevant length scale is

$$\ell = \left(K u_\tau^{n-2}/\rho\right)^{1/n}. \tag{209}$$

Dodge and Metzner [107] instead defined in their work $u^+ = (y^+)^{1/n}$, implying that $y^+ = y^n (u_\tau)^{2-n}\rho/K$. In the present work, we use the definition provided by Eq. (207).

If there is to be a logarithmic solution in the inner regions of a flow and, if this region is to comply to similitude conditions, then it is clear that the characteristic length and velocity scales must be ℓ and u_τ as implied by Eq. (207).

Therefore, a log-solution should be written as

$$\frac{u}{u_\tau} = A_n \ln\left(\frac{y}{\ell}\right) + B_n - g_1(yR^{-1}, n), \tag{210}$$

where g_1 is a function that must accommodate the external flow behavior and A_n and B_n need to be determined experimentally.

The implication is that the slope of the log-term in Eq. (210) should vary with the inverse of n. This fact was noticed by Clapp [108] and Bogue and Metzner [109], who proposed mean velocity profile formulations with A_n varying according to the reciprocal of n.

In Loureiro and Silva Freire [110], the asymptotic structure of the turbulent boundary layer of a non-Newtonian power-law fluid is discussed. The application of double limits to the equations of motion shows that the turbulent boundary layer exhibits a canonical two-layered structure defined by two principal equations. The viscosity of the fluid defines the thickness of the viscous region through $\epsilon\hat{\epsilon} = (\epsilon^{n-2}/R_e)^{1/n}$, where

$$\epsilon = \frac{u_\tau}{u_o}, \quad \epsilon^2\hat{\epsilon}^n = \frac{1}{R_e}, \quad R_e = \frac{\rho u_o^{2-n} L^n}{K}, \tag{211}$$

the influence of the non-Newtonian turbulence term is shown to be very restrict, limited to domain $\mathrm{ord}(\eta) \leq \mathrm{ord}(\epsilon\hat{\epsilon})$. The turbulence dominated region (defined by $\mathrm{ord}(\epsilon\hat{\epsilon}) < \mathrm{ord}(\eta) < \mathrm{ord}(\epsilon^2)$) is governed by turbulence originated from the inertial terms in the equations of motion. No contribution arises from the averaging of the non-linear viscous terms. In fact, the analysis shows that in the fully turbulent region, $\mathrm{ord}(\epsilon\hat{\epsilon}) < \mathrm{ord}(\eta) < \mathrm{ord}(\epsilon^2)$,

$$\mathrm{ord}\left(\frac{\partial \overline{u'v'}}{\partial y}\right) > \mathrm{ord}\left(\frac{\partial}{\partial y}\left(\left(\frac{\partial \overline{u}}{\partial y}\right)^{n-2}\overline{\left(\frac{\partial u'}{\partial y}\right)^2}\right)\right). \tag{212}$$

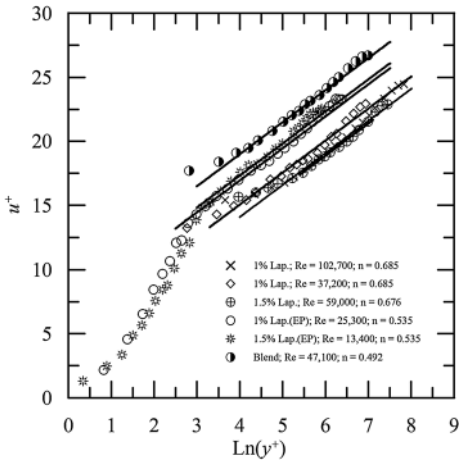

Fig. 28 Mean velocity profiles in wall coordinates according to the data of Pereira and Pinho [112] and Escudier and Presti [111]

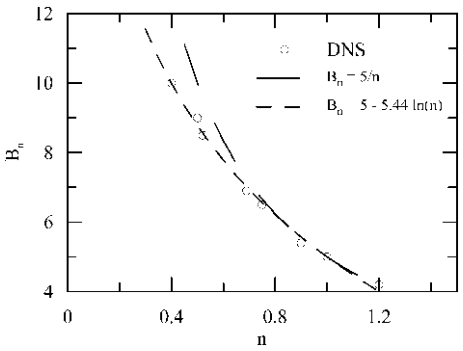

Fig. 29 The behavior of B for n ranging from 0.4 to 1.2

The two relevant length scales of the flow are:

- Turbulent layer thickness, $\tilde{\delta} = (u_\tau^2/u_o^2)L$
- Viscous sub-layer thickness, $\hat{\delta} = (K u_\tau^{n-2}/\rho)^{1/n}$

- The obvious conclusion is that for $n < 1$ the viscous sub-layer thickness decreases (in relation to that of a Newtonian fluid, $n = 1$), whereas for $n > 1$, $\hat{\delta}$ increases. Mean velocity profiles obtained by Escudier and Presti [111] and Pereira and Pinho [112] are shown in Fig. 28 for different types of shear-thinning fluids. Provided they are plotted in terms of $y^+ = y/\ell$ they all present the same slope ($=\varkappa^{-1}$) and different levels. A decrease in the value of n pushes the level up as expected.

The above results suggest $A = \varkappa^{-1}$ and $B = 5/n$.

However, the DNS results of Anbarlooei et al. [113] show that $B = 5n^{-1}$ only works well for the limited range flow indices 0.5–0.75 (Fig. 29). A detailed inspections of the results for the index range $n = 0.5$, 0.69, 0.75, 0.9, 1, 1.2 show that the following correlation must be used

$$u^+ = 2.5 \ln y^+ + 5.0 - 5.44 \ln n \tag{213}$$

The asymptotic structure of the turbulent boundary layer for a Carreau fluid is also analyzed in Loureiro and Silva Freire [110]. For a Carreau fluid, the viscosity and local shear rate are related according to

$$\mu = \mu_\infty + (\mu_0 - \mu_\infty)\left(1 + \left(\theta \frac{\partial u}{\partial y}\right)^2\right)^{\frac{n-1}{2}}, \tag{214}$$

where μ_∞ and μ_0 are the limiting viscosity levels, θ is the relaxation time and n the power-law index.

An application of double limits to the equations of motion shows that for a Carreau fluid, the morphological structure of the turbulent boundary layer is more complex: three principal equations appear in the analysis, characterizing a three-layered structure.

The analysis considers the following definitions

$$\begin{aligned} &\epsilon = \frac{u_\tau}{u_o}, \quad \epsilon^2 \tilde{\epsilon}^n = \frac{\alpha\beta}{R_e}, \\ &R_e = \frac{\rho u_o L}{\mu_o}, \quad \alpha = ((\mu_0/\mu_o) - 1), \\ &\beta = ((u_o/L)\theta)^{n-1}, \quad \tilde{\epsilon} = \hat{\epsilon}^n, \end{aligned} \tag{215}$$

and the leading order velocity fluctuations are considered to be of the order of the friction velocity.

The contribution of the viscous terms is of leading order in region ord $\epsilon\tilde{\epsilon} >$ ord η. The power-law viscosity contribution prevails in domain ord $\epsilon\tilde{\epsilon} >$ ord $\eta >$ ord $\epsilon\tilde{\epsilon}\hat{\epsilon}$. In the innermost sub-layer, ord $\epsilon\tilde{\epsilon}\hat{\epsilon} >$ ord η, the flow behavior is exactly that of a Newtonian fluid.

Thus, for a Carreau fluid, the relevant characteristic lengths in the wall region are:

- Turbulent layer thickness, $\delta = (u_\tau^2/u_o^2)L$
- Power-law sub-layer thickness, $\tilde{\delta} = (Ku_\tau^{n-2}/\rho)^{1/n}$, with $K = (\mu_0 - \mu_o)\theta^{n-1}$
- Newtonian sub-layer thickness, $\hat{\delta} = [((\mu_0 - \mu_o)/\mu_o)\theta^{n-1}u_\tau^{n-1}]^{1/(n-1)}$.
- The behavior of a Carreau fluid was illustrated in Loureiro and Silva Freire [110] through the data of Japper-Jaafar et al. [114] for a Carreau–Yasuda fluid with power-law indexes ranging from 0.3 to 0.9. Figure 30 shows the mean velocity data in terms of the inner flow variables $y_w^+ = yu_\tau/\nu_w$ and $y_o^+ = yu_\tau/\nu_o$.

6.18 Wall layer velocity profile for an impinging jet

For an impinging jet, Özdemir and Whitelaw [115] have shown that a Weibull distribution represents well some of the global features of the profile, such as the position of the maximum velocity and of the outer inflection point, but is not an adequate approximation for the near wall region. For this region, they showed that a semi-logarithmic relation can be used to model the inner equilibrium layer, so that one can write

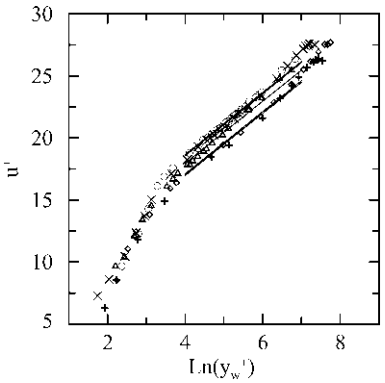

Fig. 30 Mean velocity profiles for the data of Japper-Jaafar et al. [114]; $y_w^+ = yu_\tau/\nu_w$

$$\frac{u}{u_\tau} = \frac{1}{\varkappa} \ln\left(\frac{yu_\tau}{\nu}\right) + A, \tag{216}$$

with

$$A = A_1 \frac{u_{\max}}{u_\tau} - A_2, \tag{217}$$

and where $\varkappa = 0.4$, u_τ denotes the friction velocity and A_1 and A_2 must be experimentally determined. The experimental data of Loureiro and Silva Freire [116] imply that $A_1 = 0.962$ and $A_2 = 9$.

The main contribution of Özdemir and Whitelaw [115] was to show that, for the impinging jet, the inner layer appears to constitute a considerable part of the inner boundary layer, and, if the outer edge of the equilibrium layer is attached to the point of maximum velocity, which is very close to the wall, then, this maximum, $u_{\max}$, should be an appropriate velocity scale. The conclusion, therefore, is that parameter A is not invariant, but changes with a deviation function.

Wygnanski et al. [117] remarked that, for a turbulent wall jet, the velocity profile cannot be universally represented in wall coordinates, as it can in the boundary layer. That is due to large variations in the additive constant in the law of the wall. In fact, depending on the jet Reynolds number, logarithmic fits can be found to their data in regions defined by specific limits. These fitted straight lines have levels varying from 5.5 to 9.5. The existence of a well-defined logarithmic region is particularly important for the determination of the skin-friction. Wygnanski et al. further remark that in previous experiments the skin-friction was either directly assessed through floating drag balances or indirectly by wall heat transfer devices or by impact probes like Stanton probes or Preston tubes. Since these devices are calibrated taking as reference the universal law

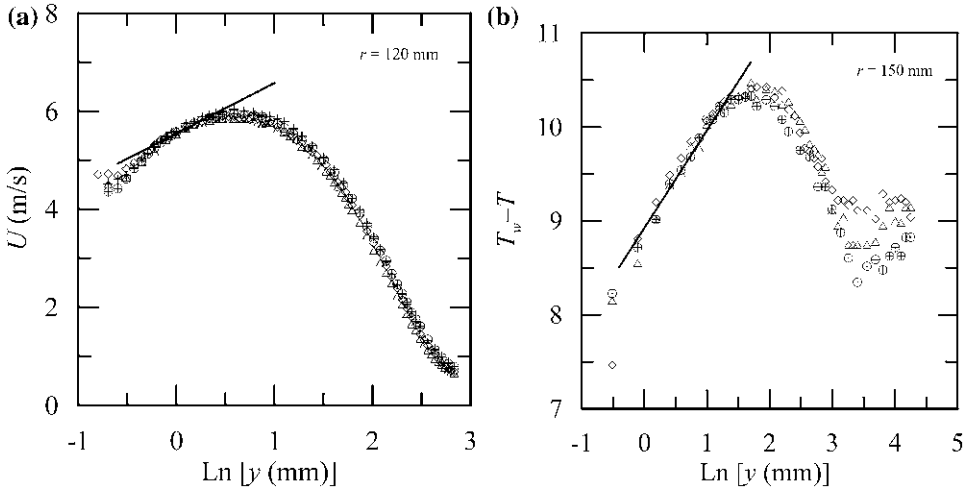

Fig. 31 Impinging jet mean velocity and temperature profiles. Data of Guerra et al. [118]

of the wall, they cannot be reliably used in regions where the existence of the law of the wall can be questioned. Wygnanski et al. estimated the skin-friction through three different techniques: a momentum integral method, the mean velocity gradient in the viscous sub-layer, and by use of a Preston tube.

The establishment of the above concepts for the velocity field clearly raises some questions for the temperature field. An immediate question concerns the existence of an appropriate temperature scale at the outer edge of the equilibrium layer. At the point of velocity maximum ($u_{\max}$), the temperature profiles reach a minimum ($T_{\min}$) (Guerra et al. [118]). Thus, drawing an analogy to the velocity analyses of Narasimha et al. [119] and of Özdemir and Whitelaw [115], one would expect the appropriate scaling temperature parameter to be this minimum temperature.

The inner temperature profile was shown by Guerra et al. [118] to follow a logarithmic solution, that is,

$$\frac{T_w - T}{t_\tau} = \frac{1}{\varkappa_t} \ln\left(\frac{y u_\tau}{\nu}\right) + B, \tag{218}$$

with

$$B = B_1 \left(\frac{T_w - T_{min}}{t_\tau}\right) - B_2, \tag{219}$$

where $B_1 = 1.003$ and $B_2 = 9.462$.

In the above equation, t_τ is the friction temperature ($=q_w/(\rho c_p u_\tau)$), u_τ is the friction velocity ($=\sqrt{\tau_w/\rho}$) and $\varkappa_t = 0.44$.

The logarithmic behavior of the inner regions of an impinging jet is shown in Fig. 31.

7 Final remarks

The present paper has attempted to show how simple arguments based on similitude, mixing theories and limit processes can be used to develop useful approximate solutions to very intricate configurations of the turbulent boundary layer. After a short review of eleven proposals for the near wall description of the mean velocity profile for incompressible zero-pressure-gradient turbulent boundary layer, different formulations for problems involving compressibility, wall transpiration, heat transfer, roughness, flow separation, shock waves and a combination of these effects were introduced.

But, the previous content is not exhaustive. Further cases of interest were not included in the review. Silva Freire [37, 38] showed how Kaplun limits can be used to find an analytical solution for the model equation defined by

$$f\frac{\partial f}{\partial x} - \frac{\partial}{\partial y}\left(\nu \frac{\partial f}{\partial y}\right) - \epsilon \frac{\partial^2 f}{\partial y^2} = 0, \tag{220}$$

$$\nu = \begin{cases} \varkappa^2 y^2 \frac{\partial f}{\partial y} & \text{if } y < y_1, \\ \alpha \epsilon x f_0 f & \text{if } y \geq y_1; \end{cases} \tag{221}$$

subject to the boundary conditions

$$\begin{aligned} &x = 0, \quad f = 1; \quad y = 0, \quad f = 0; \\ &y \longrightarrow \infty, \quad f = 1 \end{aligned} \tag{222}$$

and where $y_1 =$ point where continuity of f, $\partial f/\partial y$ and ν must be ensured, $\epsilon = 10^{-6}$, $\alpha = 0.02$, $\varkappa = 0.4$, and $f_0(x) = \partial f(x,0)/\partial y$.

Equation (220) mimics turbulent flow past over a flat surface, retaining most of the features of the real problem. The developed analytical solution is instrumental in elucidating the flow structure, making clear that the problem consists of two characteristic layers defined by two principal equations.

Su and Silva Freire [120] show how logarithmic velocity and temperature profiles can be used to develop a simple

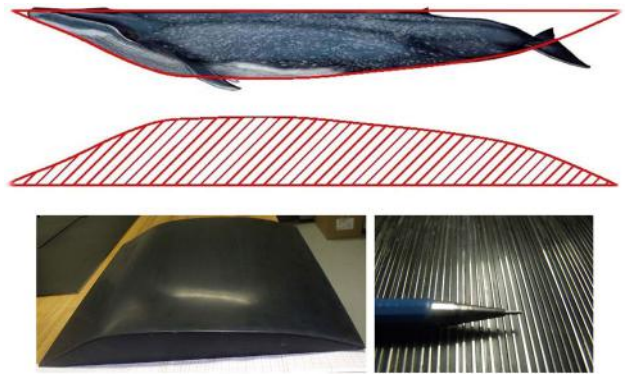

Fig. 32 Model shape and geometry of riblets

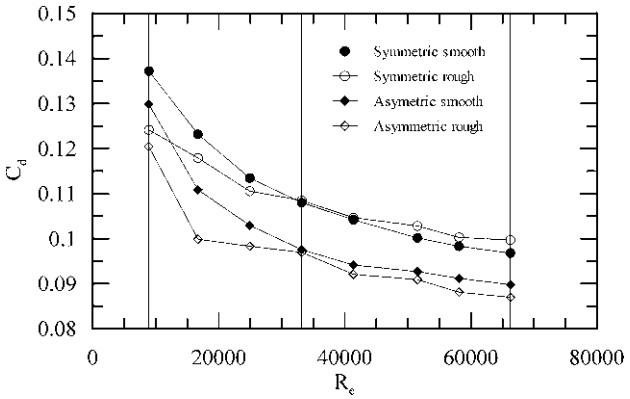

Fig. 33 Drag coefficient for the four tested surfaces. The three vertical lines correspond to $R_e = 8,900, 33,150$ and 66,260

analytical method for the prediction of friction factors and Nusselt numbers of turbulent forced convection in rod bundles with smooth and rough surfaces.

In Brasil et al. [121], an inverse problem is solved for the estimation of upstream velocity profiles in an incompressible turbulent boundary layer over a smooth flat plate. The inverse analysis is based on the boundary layer morphology, making use of the law of the wall and the law of the wake to estimate boundary layer parameters from measured velocity histories.

The effects of flow stability conditions on the properties of boundary layers subjected to steep surface elevations were discussed in Loureiro and Silva Freire [122]. The results discuss the effects of the stratification on the speed-up factor, i.e., the maximum acceleration of the flow on hilltop, and on the heat up/down factor. The numerical simulation of turbulent flow over steep hills has been discussed in Loureiro et al. [123].

The mechanics of turbulent drag reduction over curved surfaces by riblets was studied in Loureiro and Silva Freire [124]. Four types of two-dimensional surfaces were studied based on the morphometric parameters that describe the body of a blue whale (Fig. 32). In general, for the whole range of Reynolds number that was considered, the riblet surfaces were shown to perform better than the smooth surfaces. For the higher R_e's, a higher C_d for the symmetric riblet surface (as compared to the smooth surface) was consistently observed (Fig. 33).

The above discussion on the logarithmic law is strongly biased by my own experience on the subject. In preparing the paper, I took the decision of supporting most of the arguments on results obtained by one particular research group. Thus, the above review must not be seen as a ample review on the fundamentals of the logarithmic law, but rather on the results obtained by a small group of people that have dedicated part of their time to the investigation of wall turbulence.

This text has been specially prepared for the 35th anniversary issue of the Journal of the Brazilian Society of Mechanical Sciences and Engineering. The history of turbulent research in Brazil from 1971 to 1996—another previously commissioned article by JBSMSE—can be found in Silva Freire et al. [125].

Acknowledgments Many people have contributed to the results discussed in the present work. Their relative importance is easily recognized through a casual inspection of the list of references. To these people—most of them my former students—I owe my gratitude. Specifically, most of the figures shown in this review have been prepared by Dr. J.B.R. Loureiro. Thank you for this particular effort. APSF is grateful to the Brazilian National Research Council (CNPq) for the award of a Research Fellowship (Grant No. 305338/2014-5). The work was financially supported by CNPq through Grants No. 477293/2011-5 and by the Rio de Janeiro Research Foundation (FAPERJ) through Grant E-26/102.937/2011.

References

1. Taylor GI (1916) Conditions at a surface of a hot body exposed to the wind. Brit Aeronaut Res Comm R & M 272
2. Prandtl L (1925) Über die Ausgebildete Turbulenz. ZaMM 5:136
3. Von Karman T (1930) Mechanische Ähnlichkeit u. Turbulenz. Nachr Ges der Wiss Göttingen. Math Phys Klasse 58
4. Von Karman T (1939) The analogy between fluid friction and heat transfer. Trans ASME 61:705–710
5. Millikan CB (1939) A critical discussion of turbulent flow in channels and tubes. In: Proceedings of 5th international congress on applied mechanics. J Wiley, NY
6. Townsend AA (1961) Equilibrium layers and wall turbulence. J Fluid Mech 11:97–120
7. Stratford BS (1959) An experimental flow with zero skin-friction throughout its region of pressure rise. J Fluid Mech 5:17–35
8. Launder BE, Spalding DB (1974) The numerical computation of turbulent flow. Comput Methods Appl Mech Eng 3:269–289
9. Craft TJ, Gerasimov AV, Iacovides H, Launder BE (2002) Progress in the generalization of wall-function treatments. Int J Heat Fluid Flow 23:148–160

10. Popovac M, Hanjalic K (2007) Compound wall treatment for RANS computation of complex turbulent flows and heat transfer. Flow Turbul Combust 78:177–202
11. Fontoura Rodrigues JLA, Gontijo RG, Soares DV (2013) A new algorithm for the implementation of wall-functions in high Reynolds number simulations. J Braz Soc Mech Sci Eng 35:391–406
12. Andersen PS, Kays WM, Moffat RJ (1972) The turbulent boundary layer on a porous plate: an experimental study of the fluid mechanics for adverse free-stream pressure gradients. HMT Report No 15 Stanford University
13. Purtell LP, Klebanoff PS, Buckley FT (1981) Turbulent boundary layer at low Reynolds number. Phys Fluids 24:802–811
14. Yajnik KS (1970) Asymptotic theory of turbulent shear flow. J Fluid Mech 42:411–427
15. Sychev VV, Sychev VV (1987) On turbulent boundary layer structure. PMM USSR 51:462–467
16. Cebeci T, Smith AMO (1974) Analysis of turbulent boundary layers. Academic Press, New York
17. Coles D (1956) The law of the wake in turbulent boundary layers. J Fluid Mech 1:191–226
18. Reichardt H (1940) Die Wärmeübertragung in Turbulenten Reibungschichten. ZaMM 20:297
19. Rotta J (1950) Das in Wandnahe giiltige Geschwindigkeitsgesetz turbulenter Stromungen. J Ing-Arch 18:277–280
20. Van Driest ER (1956) On turbulent flow near a wall. J Aeronaut Sci 23:1007
21. Rannie WD (1956) Heat transfer in turbulent shear flow. J Aeronaut Sci 23:485
22. Spalding DB (1961) A single formula for the law of the wall. J Appl Mech 83:455–458
23. Rasmussen ML (1975) On compressible turbulent boundary layers in the presence of favorable pressure gradients. ASME paper 75-WA/HT-53
24. Musker AJ (1979) Explicit expression for the smooth wall velocity distribution in a turbulent boundary layer. AIAA J 17:655–657
25. Kline SJ, Reynolds WC, Schraub FA, Rundstadler PW (1967) The structure of turbulent boundary layers. J Fluid Mech 30:41–72
26. Kovasznay LSG (1967) Structure of the turbulent boundary layer. Phys Fluids Suppl S25–S30
27. Haritonidis JH (1989) A model for near wall turbulence. Phys Fluids A 1:302–306
28. Yakhot A, Khait VD, Orszag SA (1993) Analytic expression for the universal logarithmic velocity law. J Fluids Eng 115:532–534
29. Barenblatt GI (1993) Scaling laws for fully developed turbulent shear flows. Part 1. Basic hypotheses and analysis. J Fluid Mech 248:513–520
30. Nikuradze J (1932) Gesetzmässigkeiten der turbulenten Strömung in glatten Rohren. Forschung ad Geb Ing, No 356
31. Eckhaus W (1994) Fundamental concepts of matching. SIAM Rev 36:431–439
32. Eckhaus W (1973) Asymptotic analysis of singular perturbations. North-Holland, Amsterdam
33. Kaplun S (1967) Fluid mechanics and singular perturbations. Academic Press, New York
34. Lagerstrom PA, Casten RG (1972) Basic concepts underlying singular perturbation techniques. SIAM Rev 14:63–120
35. Lagerstrom PA (1988) Matched asymptotic expansions. Springer Verlag, Heidelberg
36. Silva Freire AP, Hirata MH (1990) Approximate solutions to singular perturbation problems: the intermediate variable technique. J Math Anal Appl 145:241–253
37. Silva Freire AP (1996) On Kaplun limits and the asymptotic structure of the turbulent boundary layers. J Braz Soc Mech Sci (RBCM) 18:80–87
38. Silva Freire AP (1999) On Kaplun limits and the multi-layered asymptotic structure of the turbulent boundary layer. Hybrid Met Eng 1:185–216
39. Mellor GL (1972) The large Reynolds number asymptotic theory of turbulent boundary layers. Int J Eng Sci 10:851–873
40. Bush WB, Fendell FE (1972) Asymptotic analysis of turbulent channel and boundary layer flows. J Fluid Mech 56:657–681
41. Deriat E, Guiraud JP (1986) On the asymptotic description of turbulent boundary layers. J Theor Appl Mech Special Issue 109–140
42. Meyer RE (1967) On the approximation of double limits by single limits and the Kaplun extension theorem. J Inst Math Appl 3:245–249
43. Kaplun S, Lagerstrom PA (1957) Asymptotic expansions of Navier–Stokes solutions for small Reynolds numbers. J Math Mech 6:585–593
44. Cruz DOA, Silva Freire AP (1998) On single limits and the asymptotic behavior of separating turbulent boundary layers. Int J Heat Mass Transf 41:2097–2111
45. Kistler AL (1959) Fluctuation measurements in a supersonic turbulent boundary layer. Phys Fluids 2:290–296
46. Kistler AL, Chen WS (1963) A fluctuating pressure field in a supersonic turbulent boundary layer. J Fluid Mech 16:41–64
47. Loureiro JBR, Silva Freire AP (2011) Scaling of turbulent separating flows. Int J Eng Sci 49:397–410
48. Liou MS, Adamson TC (1980) Interaction between a normal shock wave and a turbulent boundary layer at high transonic speeds. Part II: wall shear stress. ZaMP 31:227–246
49. Silva Freire AP (1988) An asymptotic approach for shock-wave/transpired turbulent boundary layer interactions. ZaMP 39:478–503
50. Silva Freire AP (1989) A detailed review of a solution procedure for shock-wave transpired turbulent boundary layer interaction problems. J Braz Soc Mech Sci (RBCM) 11:211–246
51. Silva Freire AP (1989) On the matching conditions for a two-deck compressible turbulent boundary layer model. ZaMM 69:100–104
52. Afzal N (1973) A higher order theory for compressible turbulent boundary layers at moderately large Reynolds number. J Fluid Mech 57:1–27
53. Melnik RE, Grossman B (1974) Analysis of the interaction of a weak normal shock wave with a turbulent boundary layer. AIAA paper No 74-598
54. Adamson TC, Feo A (1975) Interaction between a shock wave and a turbulent boundary layer at transonic speeds. SIAM J Appl Math 29:121–145
55. Morkovin MV (1962) Effects of compressibility on turbulent flows. International symposium on "Mecanique de la turbulence" 1962
56. Crocco L (1963) Transformations of the compressible turbulent boundary layer with heat exchange. AIAA J 1:2723–2731
57. van Driest ER (1951) Turbulent boundary layer in compressible fluid. J Aeronaut Sci 18:145–160
58. Maise G, McDonald H (1968) Mixing length and kinematic eddy viscosity in a compressible boundary layer. AIAA J 6:73–80
59. Silva Freire AP (1988) An asymptotic solution for transpired incompressible turbulent boundary layers. Int J Heat Mass Transf 31(5):1011–1021
60. Loureiro JBR, Silva Freire AP (2011) Slug flow in horizontal pipes with transpiration at the wall. J Phys Conf Ser 318:022014–022024

61. Bandeira FJS, Loureiro JBR, Silva Freire AP (2015) Pressure drop and turbulence statistics in transpired pipe fow. In: 15th European turbulence conference, August, Delft, 2015
62. Squire LC (1969) A law of the wall for compressible turbulent boundary layers with air injection. J Fluid Mech 37:449–456
63. Silva Freire AP (1988) An extension of the transpired skin-friction equation to compressible turbulent boundary layers. Int J Heat Mass Transf 31(11):2395–2398
64. Avelino M, Su J, Silva Freire AP (1999) An analytical near wall solution for the κ–ϵ model for transpired boundary layer flows. Int J Heat Mass Transf 42:3085–3096
65. Medeiros MAF, Silva Freire AP (1992) The transfer of heat in turbulent boundary layers with injection or suction: universal laws and Stanton number equations. Int J Heat Mass Transf 35(4):991–992
66. Whitten DG, Kays WM, Moffat RJ (1967) The turbulent boundary layer on a porous plate: experimental heat transfer with variable suction, blowing and surface temperature. Stanford University Report No. HMT-3
67. Silva Freire AP, Cruz DOA, Pellegrini CC (1995) Velocity and temperature distributions in compressible turbulent boundary layers with heat and mass transfer. Int J Heat Mass Transf 38(13):2507–2515
68. Danberg JE (1967) Characteristics of the turbulent boundary layer with heat and mass transfer: data tabulation. NOLTR 675-6
69. Squire LC (1970) Further experimental investigations of compressible turbulent boundary layers with air injection. ARC R&M No. 3627
70. Mabey DG, Meier HV, Sawyer WG (1974) Experimental and theoretical studies of the boundary layer on a flat plate at Mach numbers from 2.5 to 4.5. RAE TR 74127
71. Winter KG, Gaudet L (1973) Turbulent boundary layer studies at high Reynolds numbers at Mach numbers between 0.2 and 2.8. ARC R&M No. 3712
72. Schlichting H (1979) Boundary layer theory. McGraw Hill, New York
73. Perry AE, Schofield WH, Joubert PN (1969) Rough-wall turbulent boundary layers. J Fluid Mech 37:383–413
74. Perry AE, Joubert PN (1963) Rough-wall boundary layers in adverse pressure gradients. J Fluid Mech 17:193–211
75. Antonia RA, Luxton RE (1971) The response of a turbulent boundary layer to a step change in surface roughness. Part 1. Smooth to rough. J Fluid Mech 48:721–761
76. Avelino M, Silva Freire AP (2002) On the displacement in origin for turbulent boundary layers subjected to sudden changes in wall temperature and roughness. Int J Heat Mass Transf 45:3143–3153
77. Loureiro JBR, Silva Freire AP (2014) Transient thermal boundary layers over rough surfaces. Int J Heat Mass Transf 71:217–227
78. Loureiro JBR, Sousa FBCC, Zotin JLZ, Silva Freire AP (2010) The distribution of wall shear stress downstream of a change in roughness. Int J Heat Fluid Flow 31:785–793
79. Owen PR, Thomson WR (1963) Heat transfer across rough surfaces. J Fluid Mech 15:321–334
80. Malhi Y (1996) The behaviour of the roughness length for the temperature over heterogeneous surfaces. Q J R Meteorol Soc 122:1095–1125
81. Sun J (1999) Diurnal variations of thermal roughness height over a grassland. Boundary-Layer Meteorol 92:407–427
82. Raupach MR (1979) Anomalies in flux-gradient relationships over forest. Boundary-Layer Meteorol 16:467–486
83. Jackson PS (1981) On the displacement height in the logarithmic velocity profile. J Fluid Mech 111:15–25
84. Loureiro JBR, Soares DV, Fontoura Rodrigues JLA, Pinho FT, Silva Freire AP (2007) Water tank and numerical model studies of flow over steep smooth two-dimensional hills. Boundary-Layer Meteorol 122:343–365
85. Loureiro JBR, Pinho FT, Silva Freire AP (2007) Near wall characterization of the flow over a two-dimensional steep smooth hill. Exp Fluids 42:441–457
86. Na Y, Moin P (1998) Direct numerical simulation of a separated turbulent boundary layer. J Fluid Mech 374:379–405
87. Cruz DOA, Silva Freire AP (2002) Note on a thermal law of the wall for separating and recirculating flows. Int J Heat Mass Transf 45:1459–1465
88. Mellor GL (1966) The effects of pressure gradients on turbulent flow near a smooth wall. J Fluid Mech 24:255–274
89. Nakayama A, Koyama H (1984) A wall law for turbulent boundary layers in adverse pressure gradients. AIAA J 22:1386–1389
90. Loureiro JBR, Monteiro AS, Pinho FT, Silva Freire AP (2008) Water tank studies of separating flow over rough hills. Boundary-Layer Meteorol 129:289–308
91. Loureiro JBR, Monteiro AS, Pinho FT, Silva Freire AP (2009) The effect of roughness on separating flow over two-dimensional hills. Exp Fluids 46:577–596
92. Loureiro JBR, Silva Freire AP (2009) Note on a parametric relation for separating flow over a rough hill. Boundary-Layer Meteorol 131:309–318
93. Nieuwland GY, Spee BM (1973) Transonic airfoils: recent developments in the theory, experiment and design. Ann Rev Fluid Mech 5:118–150
94. Nagamatsu HT, Ficarra RV, Dyer R (1985) Supercritical airfoli drag reduction by passive shock wave/boundary layer control in the Mach number range 0.75 to 0.90. AIAA paper 85-0207
95. Lighthill MJ (1953) On boundary layer upstream influence. Part II: supersonic flow without separation. Proc R Soc Lond A 217:478–507
96. Melnik RE (1981) Turbulent interactions on airfoils at transonic speeds: recent developments. In: Symposium on computation of viscous-inviscid flows. Paper 10, 1981
97. Messiter AF (1980) Interaction between a normal shock wave and a turbulent boundary layer at high transonic speeds. Part I: pressure distribution. ZaMP 31:204–227
98. Sawyer WG, Long, CJ (1982) A study of normal shock-wave turbulent boundary layer interactions at Mach numbers 1.3, 1.4 and 1.5. RAE TR No 82099
99. Bark FH (1975) On the wave structure of the wall region of a turbulent boundary layer. J Fluid Mech 70:229–250
100. Hatziavramidis DT, Hanratty TJ (1979) The representation of the viscous wall region by a regular eddy pattern. J Fluid Mech 95:655–679
101. Chapman DR, Kuhn GD (1986) The limiting behaviour of turbulence near a wall. J Fluid Mech 170:265–292
102. Walker JDA, Abbott DE, Scharnhorst RK, Weigand GG (1989) Wall-layer model for the velocity profile in turbulent flow. AIAA J 27:140–149
103. Landahl MY (1990) On sublayer streaks. J Fluid Mech 212:593–614
104. Mikhailov MD, Silva Freire AP (2014) Feasible domain of Walker's unsteady wall-layer model for the velocity profile in turbulent flows. Ann Braz Acad Sci 86(4):2121–2135
105. Mikhailov MD, Silva Freire AP (2012) The Walker function. Math J 14:1–9
106. Metzner AB, Reed JC (1955) Flow on non-Newtonian fluids—correlation of the laminar, transition and turbulent-flow regimes. AIChE J 1:434–440
107. Dodge DW, Metzner AB (1959) Turbulent flow of non-Newtonian systems. AIChE J 5:189–204

108. Clapp RM (1961) Turbulent heat transfer in pseudoplastic non-Newtonian fluids. Int Dev Heat Transf, Part III, ASME, New York, pp 652–661
109. Bogue DC, Metzner AB (1963) Velocity profiles in turbulent pipe flow. Ind Eng Chem (Fundam) 2:143–149
110. Loureiro JBR, Silva Freire AP (2013) Asymptotic analysis of turbulent boundary-layer flow of purely viscous non-Newtonian fluids. J Non-Newton Fluid Mech 199:20–28
111. Escudier MP, Presti F (1996) Pipe flow of a thixotropic fluid. J Non-Newton Fluid Mech 62:291–306
112. Pereira AS, Pinho FT (2002) Turbulent pipe flow of thixotropic fluids. Int J Heat Fluid Flow 23:36–51
113. Anbarlooei HR, Cruz DOA, Silva Freire AP (2015) Fully turbulent mean velocity profile for purely viscous non-Newtonian fluids. In: 15th European turbulence conference, August, Delft, 2015
114. Japper-Jaafar A, Escudier MP, Poole RJ (2009) Turbulent pipe flow of a drag-reducing rigid "rod-like" polymer solution. J Non-Newton Fluid Mech 161:86–93
115. Özdemir IB, Whitelaw JH (1992) Impingement of an axisymmetric jet on unheated and heated flat plates. J Fluid Mech 24:503–532
116. Loureiro JBR, Silva Freire AP (2012) Wall shear stress measurements and parametric analysis of impinging wall jets. Int J Heat Mass Transf 55:6400–6409
117. Wygnanski I, Katz Y, Horev E (1992) On the applicability of various scaling laws to the turbulent wall jet. J Fluid Mech 234:669–690
118. Guerra DRS, Su J, Silva Freire AP (2005) The near wall behaviour of an impinging jet. Int J Heat Mass Transf 48:2829–2840
119. Narasimha R, Narayan KY, Pathasarathy SP (1973) Parametric analysis of turbulent wall jets in still air. Aeronaut J 77:335–339
120. Su J, Silva Freire AP (2002) Analytical prediction of friction factors and Nusselt numbers of turbulent forced convection in rod bundles with smooth and rough surfaces. Nucl Eng Des 217:111–127
121. Brasil W, Su J, Silva Freire AP (2004) An inverse problem for the estimation of upstream velocity profiles in an incompressible turbulent boundary layer. Int J Heat Mass Transf 47:1267–1274
122. Loureiro JBR, Silva Freire AP (2005) Experimental investigation of turbulent boundary layers over steep two-dimensional elevations. J Braz Soc Mech Sci Eng 27:329–344
123. Loureiro JBR, Alho A, Silva Freire AP (2008) The numerical computation of near-wall turbulent flow over a steep hill. J Wind Eng Ind Aerodyn 96:540–561
124. Loureiro JBR, Silva Freire AP (2011) Flow over riblet curved surfaces. J Phys Conf Ser 318:022035–022045
125. Silva Freire AP, Avelino MR, Santos LCC (1998) The state of the art in turbulence modelling in Brazil. J Braz Soc Mech Sci (RBCM) 20(1):1–38